DETERMINISTIC MODELS TO EXPLAIN THE PHENOMENON OF INTERFACIAL MIXING IN REFINED PRODUCTS PIPELINES

By

PATRACHARI, ANIRUDH RAMANUJAN

Bachelor of Engineering in Chemical Engineering
University of Mumbai
Mumbai, India
2006

Master of Science in Chemical Engineering
Oklahoma State University
Stillwater, Oklahoma
2008

Submitted to the Faculty of the
Graduate College of the
Oklahoma State University
in partial fulfillment of
the requirements for
the Degree of
DOCTOR OF PHILOSOPHY
December, 2012

DETERMINISTIC MODELS TO EXPLAIN THE PHENOMENON OF INTERFACIAL MIXING IN REFINED PRODUCTS PIPELINES

Dissertation Approved:

Dr. Arland H. Johannes

Dissertation Adviser

Dr. Martin S. High

Dr. Sundararajan V. Madihally

Dr. Frank W. Chambers

Outside Committee Member

Dr. Sheryl A. Tucker

Dean of the Graduate College

.

TABLE OF CONTENTS

Chapter Page

LIST OF TABLES

LIST OF FIGURES

Figure Page

Figure Page

NOMENCLATURE

$\%AAD$	percent absolute average deviation
$\%D$	percent deviation
a, b	arbitrary constants
A_b	effective area of a single burst
A_d	cross-sectional area of the pipe
a_δ	viscous contributions to effective dispersion
A_δ	cross-sectional area of the pipe occupied by viscous region
C	concentration
C	concentration of the contaminant
c	dimensionless constant, function of the Reynolds number
C_z	concentration profile in the axial direction
d	pipe diameter
D	molecular diffusion coefficient
D_E	effective diffusion/dispersion coefficient
$e_{f,B}$	friction losses in bent regions of a system

$F(Re)$	proportionality factor in the Park and Gomezplata model
$f(z)$	dimensionless velocity profile
f, f_{SP}	Fanning friction factor
f_B	friction factor representing the friction losses in bent regions of a system
$G(Re)$	monotonically decreasing function of Reynolds number
h	channel height
h_1	viscous sublayer thickness in a channel
h_b	height of turbulent burst
h_b^+	dimensionless height of a turbulent ejection
j	plug number/location in Moving plug model
k	length exponent in Scraper and wash-off model
k'	interface cut-off multiplier in Equation (3.25)
k''	dimensionless constant based on turbulent burst parameters
K, K_∞, K_E, K_{SP}	steady state effective dispersion coefficient in a straight pipe
K_1, K_i, K_d	empirical constants in Darby equation to estimate the loss coefficient for a bend
K_B	axial dispersion coefficient for flow through a bend
$K_{E,B}$	effective axial dispersion coefficient for systems with bends

$K_{f,B}$	loss coefficient for the bend
K_T	turbulent axial dispersion coefficient in a straight pipe
K_V	viscous axial dispersion coefficient
l	characteristic dimension
L, L_{SP}	straight pipe length
l_b	length of turbulent burst
L_B	length of the straight pipe being affected by the bend
$L_{B,Eq}$	equivalent straight pipe length to represent a pipe bend
l_b^+	dimensionless length of a turbulent ejection
m	number of time steps in Moving plug model
n	exponent in Prandtl's power law velocity profile; number of repeating sections in a system with bends
Pe	Peclet number
Q	total transport of contaminant across the pipe cross-section
r	radial distance
R	pipe radius
Re, Re_d	Reynolds number based on pipe diameter
Re_C	critical Reynolds number, Austin and Palfrey model

Re_{Cr}	critical Reynolds number, Scraper and wash-off model
Re_{High}	Reynolds number of thinner, lighter liquid
Re_t	Reynolds number based on friction velocity
S	contaminated transmix length
t	time, residence time of interface in the pipe
T	time required for axial dispersion to reach steady state
t_B	time spent by the interface in the bend region
T_b^+	dimensionless average time between two bursts
$\overline{T}$	average time between two turbulent bursts
t_T	total time spent by the interface in the system
u	local velocity at a radius "r"
U, $\bar{U}$	average flow velocity
u^+	dimensionless local velocity in the axial direction
u_0	maximum or centerline velocity
u_δ	velocity at the boundary of the viscous region
$u_{\delta,\, corr}$	corrected velocity at boundary of the viscous region
u_τ	friction velocity
v	volume occupied by viscous sublayer in mixed plug

V	volume of mixed plug in moving plug model
$V_{Annulus}$	annular volume occupied by the viscous sublayer
w_b	width of turbulent burst
w_b^+	dimensionless width of a turbulent ejection
x	longitudinal distance
x^+	dimensionless distance in the axial direction
x_1, x_2	volume fraction of leading and trailing fluids in mixed plug
y^+	dimensionless distance away from the wall
z	dimensionless radial distance
z_V	dimensionless radial distance of the viscous sublayer from pipe center

Greek Letters

α	proportionality constant in Taylor's turbulent axial dispersion equation
β	empirically determined proportionality constant for axial dispersion in pipe bends
δ	viscous region thickness
δ_V	viscous sublayer thickness in a pipe
ΔP	pressure drop
e_r	radial turbulent eddy diffusivity

l_x	turbulent burst spacing/wavelength in the axial direction
l_z	turbulent burst spacing/wavelength in the transverse direction
l_x^+	dimensionless turbulent burst spacing in the transverse direction
l_z^+	dimensionless turbulent burst spacing in the axial direction
v	kinematic viscosity
ρ	fluid density
ρ_1 , ρ_2	density of leading and trailing plugs in Moving plug flow model
ρ_{MIX}	density more mixed plug in Moving plug model
σ^2	variance
τ_W	wall shear stress
$\phi(z)$	integral of the dimensionless velocity profile function
$\chi(z)$	integral of the dimensionless velocity profile function
$\psi(z)$	integral of the dimensionless velocity profile function

CHAPTER I

INTRODUCTION

Pipelines are the primary means of transporting crude and refined petroleum products in the United States. Pipelines accounted for 83% of all crude oil transportation and 62% of all refined product transported in 2008 (AOPL 2011). They are also used for transporting other type of goods in the country and account for around 17% of all cargo transportations, while amounting to just over 2% of the transportation bills (Rabinow 2004). As an illustration of the cost effectiveness of pipelines, AOPL (2011) reported a transportation cost of less than 3¢ for moving a gallon of gasoline from Houston, Texas to New York Harbor. In addition to being cost effective and efficient, pipelines are also recognized as one of the safest modes of transportation in the oil and gas industry.

The refined oil pipeline network in the United States spans over 200,000 miles in length across all 50 states, transporting over 14 billion barrels (600 billion gallons) of product every year (Trench 2001). Pipelines may be small (8~12" diameter) or large, up to 48" in diameter (Trans-Alaska Pipeline System, TAPS) and ranging over a 1000 miles in length extending across multiple states in the country. Some of the well-known oil transportation lines in the country include the Plantation pipeline (6~30", 3100 miles), Colonial pipelines (36~40", 5500 miles), Centennial pipeline (24~26", 795 miles), and Calnev pipeline (8~14", 550 miles).

The process of batching is one of the main reasons why pipelines are highly efficient and cost effective. Batching consists of transporting different types of products or different grades of the same product in batches in the pipe. A typical large pipeline in the United States carries on an average 30~50 different products or grades of products in each transport cycle (10~15 days) and has the capability to handle up to 100~120 product batches per cycle (Rabinow 2004). The size of each batch being transported depends on the logistics and demand of the product at the distributor's end downstream. Batching enables the refineries to quickly and efficiently transport the products to local distributors and helps meet the increasing energy demands of the nation. While batching makes pipelines a highly cost effective method of transportation, it also results in loss of product or product quality due to contamination by product mixing. Once contaminated, the product can either be passed off as a lower grade product (downgraded) if possible, or be re-refined to recover the pure products. This results in inflation in the final retail price of the product in the market. The financial losses because of product contamination are enormous considering that over 600 billion gallons of oil is transported in at least 26 transport cycles in a year. As an illustration, Kinder Morgan L.P., reported lost revenues amounting to around $1.5 billion per year because of product contamination, while another source (Bennett Jr. and Taylor III 2000) reported lost revenues of around $1 million per month for a southern Texas pipeline.

Oil pipeline operation

The pipelines that move oil from the refineries to the final consumer are not individual lines that transport oil from one particular refinery to a particular location. The oil transportation industry consists of a network of pipelines that are connected by nodes referred to as logistic hubs. These logistic hubs serve as the intermediate connection points and are often accompanied by extensive storage capabilities. The initial part of the transportation process consists of moving refined petroleum products from refineries to major hubs in the network. These logistic hubs then supply the products to other smaller (sub-) hubs through pipelines and also to the local

distributors over short distances by means of rails and trucks. This system of hub-to-hub progression provides the oil transportation industry the flexibility to increase or decrease the amount of oil transported to a specific location based on the changing price-levels and demands. Examples of major logistic hubs include the New York Harbor, NY, which supplies many distributors in the northeast, northwest and west, and the hub at Chicago, IL that supplies the Midwest.

The oil is generally moved through the extensive length of pipes by pumping stations that are located at every 20 to 100 mile intervals (Trench 2001). Centrifugal pumps are employed for moving liquids, while compressors are used for moving gases. Depending on the topology, pipe design and construction, and the characteristics of the fluid being transported, transportation speeds of 3~8 miles per hour are common in refined products pipelines (Trench 2001). Most of the products pipelines are operated throughout the year and are continuously monitored for changes in process conditions such as pipe pressures, flow rates, transportation speed, and product qualities.

Maintaining product quality, and reducing contamination and spillage losses are the most important and difficult problems encountered in the oil transportation industry. Product quality is the most important specification in the oil industry. Even the slightest of contaminations can reduce the product's resale value or, in the worst case render the product commercially unviable. Loss in product quality might occur because of various reasons including improper switching of valves when segregating the products arriving from the pipelines into separate storage tanks, environmental contaminations, and interfacial mixing in the pipelines. Interfacial mixing in particular has been an unavoidable problem in the industry as it is a direct consequence of batching, a process that makes transportation using pipelines efficient. Various techniques have been tested for reducing the extent of contamination such as, use of solid/rigid separators at the products interface, liquid/gel/flexible separators at the interface, advanced scheduling algorithms

that determine the best combination for the pumping sequence of the products based on a set of predefined heuristics, and advanced batch cutting techniques. These methods have only been marginally successful at alleviating interfacial contamination or have resulted in unnecessary secondary problems.

Batching

Batching basically involves transporting batches of different grades (or types) of products one after the other, sequentially through a pipeline. Each batch is regularly dissimilar to the immediately preceding and the following batches. The products mix at the interface between successive batches when no separating mediums are employed, resulting in loss of a portion of the products forming the interface. This interface is a mixture of the products in the two batches and is commonly referred to as transmix, and it grows in volume as the products moves downstream.

Transmix is a product that is off specification because, with respect to quality, it matches neither the leading batch nor the trailing one. It is therefore downgraded and mixed with the batch having the lower grade product (when the two batches are different grades of the same product) or is isolated into a separate tank and shipped back for reprocessing. Both the above-mentioned cases result in a decrease in the revenue of the shipper, with the latter being of higher concern. The problem of interfacial mixing increases considerably in case of large capacity pipelines that transport huge batches and wide variety of products. Such lines result in a large number of interfaces being formed and therefore higher loss of valuable product.

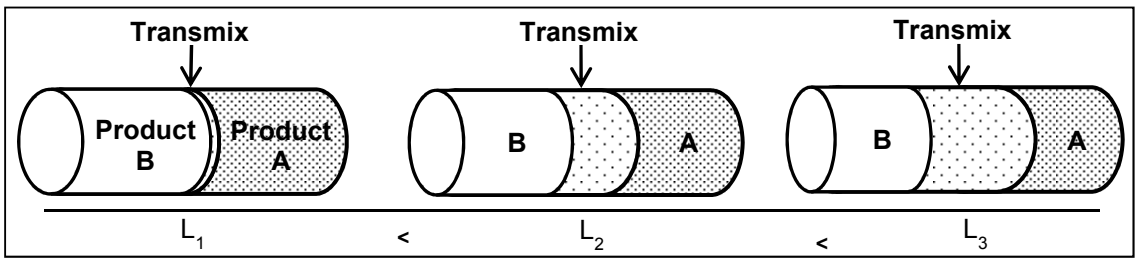

Figure 1.1: Transmix growth in a products pipeline as the interface travels downstream.

Figure 1.1 illustrates the process of batching in a uniform, constant diameter products pipeline without bends or fittings. Consider a batch of product-A being pumped into the pipeline followed by product-B. A contaminated/mixed interface forms between the two products as soon as product B enters the pipeline and this interface travels downstream with the products. The extent of mixing (volume or length of contamination) is low at the beginning and it increases as the interface travels farther downstream. The contamination volume (also termed as transmix volume) can be visualized as a section of the mixed product that gradually varies in concentration as we proceed from one edge of the interface to the other. As a general rule of thumb contamination volume is directly proportional to the square root of the pipe length.

The problem of interfacial mixing becomes particularly acute when laws and regulations concerning additives in the products change. One of the earliest occurrences of such a situation was during the 1980s when leaded gasoline was being phased out from production and the pipeline operators had to pay close attention to the intermixing process between leaded and unleaded products. In recent years, the focus has shifted to eliminating sulfur-based fuels as they result in lower gas mileage and other environmental issues. The Environmental Protection Agency (EPA) issued a regulation in the early 2000s that required a reduction in the amount of sulfur from 50 ppm to 30 ppm in some petroleum fuels. The products therefore had to be segregated based on their sulfur content before transportation, in order to reduce mixing of the low sulfur content batches and the high sulfur content batches. This issue has become more

important ever since the introduction of the Ultra-Low Sulfur Diesel (ULSD) regulation by the EPA and the amount of transmix is expected to increase specifically for interfaces involving diesel.

Interfacial mixing of petroleum products in pipelines has been a long standing and an economically significant issue in the oil transportation industry. It influences the design considerations for pipeline constructions, as well as the scheduling for pipeline operation. Faulty design and operation of a pipeline might result in higher degree of product loss through interfacial mixing. An improperly designed pipeline would add to the expenses of lost products in addition to other operation costs. Parameters such as pipe dimensions, flow regimes, and valve switching are of high importance, and operators and designers need to know the effect of these parameters on transmix volume. This causes major economic damage to the industry by increasing the cost of the products. It is therefore important to estimate and minimize the amount of mixing that occurs between two products in order to improve the economics of batching.

A timeline of investigators

The earliest investigations (Fowler and Brown 1943; Birge 1947; Smith and Sulze 1948; Smith and Sulze 1948) on longitudinal contamination of petroleum fluids were predominantly empirical in nature. The observed growth in the contaminated region was characterized as a function of various system parameters. Pipe volume, fluid properties (density and viscosity), and flow velocity were reported as major parameters influencing longitudinal contamination in pipelines. Observations reveal higher contaminations in longer pipes at lower flow rates. The contamination length has been reported to be directly proportional to the pipe length and inversely proportional to the flow velocity and therefore the Reynolds number. Most of these investigations were system specific owing to their empirical background. The model parameters from one such investigation would therefore not be applicable to a different investigation. All

investigations however reported numbers similar enough to provide a glimpse of the theories involved. Many investigators tried to provide explanations to such observations and connect it to the theoretically known diffusion equations.

One of the earliest theoretical analysis of axial dispersion, a term synonymous with Taylor (1953) and Aris (1956), was first reported in 1922 (Taylor 1922). The term axial dispersion denotes the longitudinal spreading of a contaminant due to the convective and diffusive effects prevalent in the flow. It has been widely suggested as the phenomenon governing the process of interfacial mixing in petroleum pipelines. Axial contamination was first thought of being a consequence of just the convective transport of the contaminant due to turbulent velocity fluctuations in the system (Taylor 1922). The contamination growth equation (Equation 1.1) was represented in terms of the flow velocity and a correlation coefficient for the velocity at a particular point with time.

$$\frac{d^2\left[X^2\right]}{dt^2} = 2\left[u^2\right]R_\xi \tag{1.1}$$

Where X is the distance travelled by a particle in a particular amount of time, u is the particle velocity and R_ξ is the correlation coefficient for the particle velocity (u) at any time t to the particle velocity after an interval of time ξ.

The period between the mid-1940s and the mid-1960s was especially productive in terms of developments in the area of longitudinal mixing. The first major breakthrough on the theoretical aspect of this topic was reported by Taylor (1953) for mixing under laminar flow conditions, followed by a separate analysis for turbulent flow (Taylor 1954). Taylor (1953; 1954) modeled the system as a transient molecular diffusion process, with the diffusion coefficient for the model being estimated as a combination of both diffusive mixing (molecular for laminar and eddy for turbulent flow) and convective mixing due to the velocity profiles inherent in the two

flow regimes. Taylor's analyses reveal that the axial dispersion coefficient normalized by the pipe diameter and flow velocity would decrease with Reynolds number in the turbulent regime as opposed to an increasing trend observed in the laminar flow regime. The concepts introduced by Taylor (1922; 1953; 1954) have been extensively examined in the following years and have been used as a starting point in most of the axial dispersion studies since, including this work.

Most investigators since have stuck to the idea of obtaining independent equations for the laminar and turbulent flows. Such independent analyses for the laminar and turbulent flow regime would require a sudden shift from purely laminar flow to complete turbulence. An abrupt shift does not make sense as turbulent flows are characterized by near plug flow type velocity profiles as opposed to the parabolic velocity profiles in the laminar flow regime. Experimental data show that the dispersion coefficient in its dimensionless form attains a maximum at the cusp of the laminar-turbulent transition and reduces gradually in a hyperbolic manner to a lower asymptotic value at higher Reynolds numbers. A sudden switch from laminar to turbulent flow at a specific Reynolds number in the models would suggest an accompanying discontinuity in the predictions for axial dispersion coefficient. This is not observed in the experimental data. In addition to the disagreement with the experimental data, the models also overlook a fundamental concept that the transition from laminar to turbulent regime does not necessarily occur at one particular Reynolds number but over a range of Reynolds numbers.

Further investigations on Taylor's turbulent dispersion analysis have shown that molecular diffusivity (Aris 1956) and Schmidt number (Levenspiel 1958; Flint and Eisenklam 1969; Flint and Eisenklam 1970) also play an important role for specific systems such as gases and other low density systems, where the Schmidt number could be considerably less than 1. Other investigators have questioned the validity of the velocity profile employed by Taylor (1954) in his models (Tichacek, Barkelew et al. 1957; Flint and Eisenklam 1969; Chatwin 1971; Krantz and Wasan 1974; Maron 1978; Rachid, Araujo et al. 2002) as well as the applicability of

the Reynolds analogy (Sjenitzer 1958; Flint and Eisenklam 1969) to certain situations; suggesting that a more accurate velocity profile would improve the dispersion coefficient predictions. Attempts have also been made to improve the model rangeability by accounting for anisotropy in the diffusion coefficient due to progressive mixing (Krantz and Wasan 1974; Rachid, Araujo et al. 2002; Ekambara and Joshi 2003); thus adding to model complexity without adequate improvement in the predictions.

Most subsequent investigations (Gill 1966; Gill and Sankarasubramanian 1970; Soltanieh and Sadraei 1991) on axial dispersions have been directed towards axial dispersion in short pipes for which Taylor's equations (Taylor 1953; Taylor 1954) are not valid. In addition to transient dispersion conditions, dispersion in the presence of strong centrifugal forces on the flow field has also been extensively investigated (Aunicky 1970; Johnson and Kamm 1986; Castelain, Mokrani et al. 1997; Zhao and Bau 2007). Such scenarios are common for flow through helical tubes and closely stacked pipe bends or fittings.

Austin and Palfrey (1964) published one of the major developments in axial dispersion investigations. They assembled experimental data on axial dispersion available in the open literature and proposed the existence of two distinct mechanisms that would contribute to dispersion in turbulent flow. This suggests that the dispersion regions can be divided into three sections namely the laminar, the low Reynolds number turbulent, and the high Reynolds number turbulent dispersion regions. Other investigators (Chatwin 1973; Chikwendu and Ojiakor 1985; Smith 1987) have proposed models that incorporate the above observations by dividing the flow cross-section into multiple sections and using varied velocity profiles and diffusion characteristics in each region. Modeling the flow field as multiple layers each with its own characteristics is fundamentally consistent with the theories of fluid dynamics. The general trend of such investigations has been to obtain regressed values for the various parameters describing a collection of systems. As a consequence, these models only apply to specific cases. It is

extremely important that the models associate the characteristics of each layer to that observed in theory, as opposed to obtaining regressed values for these parameters that fit the observed experimental data.

In line with the above observations, this study hypothesizes that the viscous sublayer plays a vital role in the phenomenon of axial dispersion and can be used to adequately quantify the extent of transmix growth. Incorporating the viscous sublayer as one of the parameters in the model will ensure smooth transition between the two dispersion regimes reported for turbulent flows in the literature (Austin and Palfrey 1964) and thus result in more reliable turbulent dispersion models. Additionally, developing a model based on commonly observed phenomena in turbulent flows will provide a theoretical basis to the model, which is lacking in the models currently available in open literature.

Scope of this work

Convective-diffusion has been the most commonly used framework to describe the phenomena of axial dispersion in both the laminar and turbulent flow regimes. The present work couples the fundamental equations of bulk transport with the concepts of viscous boundary layer theory to provide an improved model for transmix predictions. The model employs the commonly accepted linear near-wall velocity profile for the viscous sub-layer. A standard version of the universal velocity profile employed by Taylor (1954) is used to model the turbulent core. The steady state thickness of the viscous sublayer (Schlichting and Gersten 2000) is then used to estimate the contributions of the viscous sublayer and the turbulent core to effective contamination rate.

The current investigation analyzes the models available in the literature and explains the reasons for their failure to accurately estimate the axial dispersion coefficient at low to moderate turbulent Reynolds numbers ($Re \leq 70{,}000$). The model developed in this investigation is based

on Taylor's theory (1954) for the turbulent axial dispersion coefficient. It includes modifications that would allow Taylor's equations to be employed through all Reynolds numbers in the turbulent flow regime. The improvement in the prediction accuracy and the applicability would be especially discernible in the lower Reynolds number turbulent flow region.

This investigation attempts to provide explanations for the various unanswered questions in the development of Taylor's turbulent axial dispersion model, such as the validity of using Reynolds analogy for the estimations. Furthermore, this study aims to examine the effects of the turbulent bursting phenomena (commonly observed in the near wall region of turbulent flows) on axial dispersion in liquids. A mechanistic term explaining the physical occurrences in transport pipelines is developed based on the theory of turbulent bursts. The effect of turbulent bursts on the overall mass transfer rates is captured and used as a parameter to determine the dispersion coefficient.

The presence of bends and other auxiliary units in a pipeline is known to increase longitudinal dispersion effects (Smith and Sulze 1948; Davidson, Farquharson et al. 1955; Carter and Bir 1962; Aunicky 1968; Cassell and Perona 1969; Park and Gomezplata 1971). At the same time, flows through helical coils resulting in secondary flows have also been known to reduce longitudinal dispersion (Koutsky and Adler 1964; Cassell and Perona 1969). An analysis of the available literature on flow through bends will be performed and a model/methodology will be proposed to incorporate the effects of bends, elbows and other such units on transmix growth.

The scientific contributions from this work include – (a) understanding the importance of the near-wall region in bulk transport, (b) a methodology to combine the convective-diffusion equations with boundary layer theory, (c) comprehending the effects of turbulent bursts on axial dispersion, and (d) a methodology to capture the effects of auxiliary units such as bends and elbows in the model. The analysis presented provides a physical backing to Taylor's theory

(1953; 1954) while providing new conceptual visualizations of the processes governing axial dispersions. Furthermore, this research could also be used in identifying techniques to help reduce axial dispersion in straight pipes. This investigation will also benefit the oil pipeline companies as every gallon of product that can be saved equates to higher revenue. Apart from resolving the aforementioned issues, the results of this study would also help in optimizing pipeline capacities and scheduling; thereby help improve the overall pipeline infrastructure.

CHAPTER II

STUDIES ON AXIAL DISPERSION

Axial dispersion is a compound phenomenon that depends on various parameters such as the types of fluids involved, the hydrodynamic conditions, dimensions of the pipe, the pipe network geometry, etc. Some of these parameters are known to have considerable influence on the extent of dispersion, while not enough information is available to discern the effect of some of the other parameters. The experimental data available in literature is diverse and data from different sources seem to indicate conflicting observations. The varied nature of the experimental observations has led to the application of different types of modeling techniques to describe the process of axial dispersion.

There are a number of models available in the literature aimed at approximating the extent of interfacial mixing. Empirical models have been by far the preferred method to tackle this problem. Models relating the various system parameters such as pipe length, diameter, fluid properties and transmix volume, have been proposed using data obtained from laboratory and field experiments. These models however vary in their predictions and have a very narrow scope of applicability. In addition to this, most of the empirically fit equations have been focusing on parameters that are known to directly affect transmix volume, while neglecting other parameters that influence transmix growth, such as velocity, concentration, and pressure gradients, etc. Most

of the parameters neglected are ones that define the flow pattern and the physical chaotic mixing characteristics observed in flowing liquids. Hence, these models are unable to explain certain characteristic observations seen in petroleum transportation pipelines. Some questions that arise in this context are: Which model to use? What are the predictive capabilities of the model? Does the model explain the phenomenon properly? Unfortunately, none of the theories or models available in literature is able to completely describe this phenomenon or provide a proven methodology that would be applicable for predicting axial dispersion in all transport systems.

This chapter provides a review of the experimental data and the accompanying observations that have been reported by previous investigators. In addition, Taylor's theories (1953; 1954) and models on axial dispersion, which have been considered as a fundamental base by most researchers, are also discussed. Furthermore, this section also presents a comprehensive survey of the other modeling techniques that have been employed in transmix estimations. Aspects such as, the dependence of transmix growth on various system parameters, and the theoretical frameworks that have been employed have been included in the discussion. An analysis of the research gaps in current literature and an approach strategy are also presented.

Published data on axial dispersion

A large amount of experimental data on axial dispersion is available in the literature. This includes data from lab-scale, pilot-scale, and field experiments (Fowler and Brown 1943; Birge 1947; Smith and Sulze 1948; Smith and Sulze 1948; Hull and Kent 1952; Taylor 1954; Sjenitzer 1958; Austin and Palfrey 1964). The data consists of axial dispersion measurement for pipes 0.124" to 40" in diameter and 0.8 ft. to 2270000 ft. in length using water-water (with solute), kerosene-gasoline, and gasoline-fuel oil interfaces. There are more data available in the literature pertaining to experiments with gases, helical pipes, short pipe lengths or pipes with small length to diameter ratios, etc. These have not been considered as the current research

focuses on investigating axial dispersion in liquids flowing through systems of circular cross-sections with large length to diameter ratios. A small number of experimental data consisting of results obtained in pipe systems with bends or pipes with small length to diameter ratios have been included in the current investigation. Such data have been included to obtain an estimate for the accuracy (or inaccuracy) of the proposed model and other models from published literature for these systems. Table 2.1 lists the various sources for the experimental data and the variety of the system conditions used in the current investigation. The data assembled covers an extensive breadth of information. It consists of axial dispersion results from experiments using a wide range of pipe lengths and diameters. The experimental data encompasses Reynolds numbers spread over what is generally accepted as transition region for practical purposes to fully turbulent flows, and with different types of fluid combinations.

Empirical studies and key parameters

Empirical modeling has been a popular and effective mode of analysis in transmix research. Investigators employing such techniques have identified a list of parameters that affect axial dispersion and put forth equations based on the extent to which each of these parameters influenced the process. The empirical coefficients for the models are then regressed from experimental data, which usually is in the form of transmix growth rate (length or volume basis). Appendix-A contains a list of empirical correlations that are currently available in open literature. Empirical models, though system specific, provide essential knowledge of transmix growth as an independent or combined function of the system parameters. The experimental observations and results reported in open literature reveal distinct trends when analyzed individually, thus providing useful insights on the dynamics of axial dispersion. The parameters commonly listed in literature are discussed in this section.

Table 2.1: Experimental data matrix.

Source	Diameter (in.)	Pipe Length (ft.)	Reynolds Number	# of Data Points
Austin and Palfrey (1964)	20 – 40	355 – 1,230,000	128,000 – 970,000	12
[a]Fowler and Brown (1943)	0.124 – 0.313	5 – 105.6	2,220 – 19,800	27
[a]Birge (1947)	4 – 12	140,000 – 227,000	67,000 – 538,000	8
[a]Hull and Kent (1952)	8 – 10	72,000 – 970,000	24,000 – 300,000	6
Smith and Schulze (1948)	2 – 12	2,500 – 2,033,803	14,160 – 591,000	62
[a]Sjenitzer (1958)	8 – 10	3,000 – 246,000	8,000 – 52,000	7
Taylor (1954)	0.375	0.8 – 5.35	11,800 – 19,300	4

[a]Part of the data taken from Austin and Palfrey

Pipe length: The residence time of a fluid interface in a pipe, which is equivalent to the length of the pipe, is an important parameter governing transmix growth. Transmix volume or length is known to be higher in longer pipes as compared to shorter pipes. Experimental evidence reveals that transmix growth is a non-linear function of the pipe length. This dependence is commonly expressed in the form of a power law equation, with the values of the exponent varying between 0.3 and 0.62 based on the experimental data employed for regression (Birge 1947; Smith and Sulze 1948; Smith and Sulze 1948; Sjenitzer 1958). This information supports the theoretically estimated value of 0.5 for the exponent (Taylor 1922; Fowler and Brown 1943; Hull and Kent 1952; Taylor 1953; Taylor 1954; Levenspiel and Smith 1957; Levenspiel 1958; Austin and Palfrey 1964; Aunicky 1970). The variation in the pipe length exponent can be attributed to researchers overlooking certain parameters such as system geometry, entrance effects, and other unavoidable errors in the experiments. The structure of an experimental setup has considerable influence on the axial dispersion data. It can be inferred through intuition that the presence of bends, elbows and other kinds of pipe fittings would enhance the mixing characteristics of the systems and therefore intensify axial dispersion. Similar observations have also been reported in the literature (Smith and Sulze 1948; Smith and Sulze 1948), suggesting a higher value for the pipe length exponent for flow through such systems. Nonetheless, all experimental results confirm that a plot of the transmix growth (in an ideal straight pipe) against pipe length would be a straight line with a slope of around 0.5 on a semi-log graph.

Pipe diameter: Most of the experiments on axial dispersion that are reported in the literature were performed using setups with pipes of fixed cross-sectional area. The pipe diameter is therefore a less common feature in most empirical models. Some empirical models do account for the effect of pipe diameters, either directly or indirectly in the form of pipe volume. The effect of pipe diameter has also been included in the form of Reynolds number in

some of the studies. Most of these correlations have the diameter manipulated using complex non-linear relationships, thus making it difficult to separate out its effect on transmix growth (Fowler and Brown 1943; Sjenitzer 1958; Austin and Palfrey 1964). Some empirical investigations also indicate a near square root dependence of the transmix growth rate on pipe diameter. Austin and Palfrey (1964) analyzed experimental data for turbulent dispersion from various sources and concluded that the transmix growth rate is more sensitive to the variations in the pipe diameter at lower Reynolds number as compared to higher Reynolds numbers. Other researchers have (Taylor 1954; Sjenitzer 1958; Aunicky 1970) also reported similar observations through separate theoretical and regression analyses.

Reynolds number and flow regime: The flow hydraulics of a system has a defining impact on the extent of axial dispersion. Conventionally, turbulence is known to enhance the mixing characteristics. The effect of Reynolds number and therefore the flow regime on axial dispersion though is rather contrary to this convention. Turbulence, especially at higher Reynolds numbers, is known to diminish axial dispersion. The empirical equations for axial dispersion use either the Reynolds number or the flow velocity to account for the effects of the flow regime. Similar to the formulations using pipe length and diameters, most empirical equations employ a power law term for the Reynolds number. The power law formulations using the Reynolds number however provide reasonable estimations only at higher Reynolds number. Some investigators (Austin and Palfrey 1964; Flint and Eisenklam 1969; Udoetok and Nguyen 2009) have proposed more complicated formulations to improve the prediction accuracy at lower Reynolds numbers. The experimental evidence indicates that transmix growth is relatively slow in the turbulent flow regime as compared to laminar flow, with all the other parameters remaining constant (Fowler and Brown 1943; Flint and Eisenklam 1969; Aunicky 1970; Flint and Eisenklam 1970). The exact dependence of transmix growth on Reynolds number is however, yet to be established.

Secondary parameters: The three parameters discussed earlier are known to directly affect axial dispersion as compared to other parameters such as fluid properties, pressure gradient, friction, etc. These parameters have therefore been explored in less detail as compared to pipe diameter, length and the flow Reynolds number. It could be argued that some of these secondary parameters have been indirectly included in the equation through the Reynolds numbers. However, some investigators (Birge 1947; Levenspiel 1958) suggest a need to incorporate them as primary parameters in the axial dispersion equations.

Experimental data as well as theoretical analysis of axial dispersion imply that friction factor and consequently pressure drop will play an important role in transmix predictions. Friction factor decreases with increasing Reynolds number and exhibits a distinct discontinuity when plotted against the Reynolds number. Friction factor has therefore been attributed as a possible explanation for the discontinuity observed in the transmix length vs. Reynolds number curves (Austin and Palfrey 1964). Aunicky (1970) and Austin and Palfrey (1964) suggested the use of two separate equations, one on either side of the discontinuity to model this observation.

Axial dispersion data from some field experiments also seem to indicate some variations in the extent of axial mixing for different fluid combinations (Birge 1947; Weyer 1962). Investigations have reported higher intermixing for systems comprised of lower density fluids (Birge 1947), while viscosity has been reported to have an opposite effect. Birge (1947) and Weyer (1962) from their independent investigations suggest that differences in the specific gravities of the fluids forming the interface would also have a significant effect on transmix growth rate. However, no experimental evidences are provided to support this theory. Other parameters such as fluid sequence and presence of bends have also been studied by a few researchers. Such studies however have been mostly ignored with the assumption that these parameters do not contribute significantly to transmix growth.

Austin and Palfrey empirical model

The Austin and Palfrey empirical model (Austin and Palfrey 1964) for estimating transmix length is one of the more robust models available in the literature. The equations proposed by the investigators are based on their analysis of a large database consisting of laboratory scale, pilot scale and field data that were available in open literature. The application of this model is therefore not restricted to a select set of systems and can be considered comprehensive and reliable for predicting transmix length over a wide range of conditions.

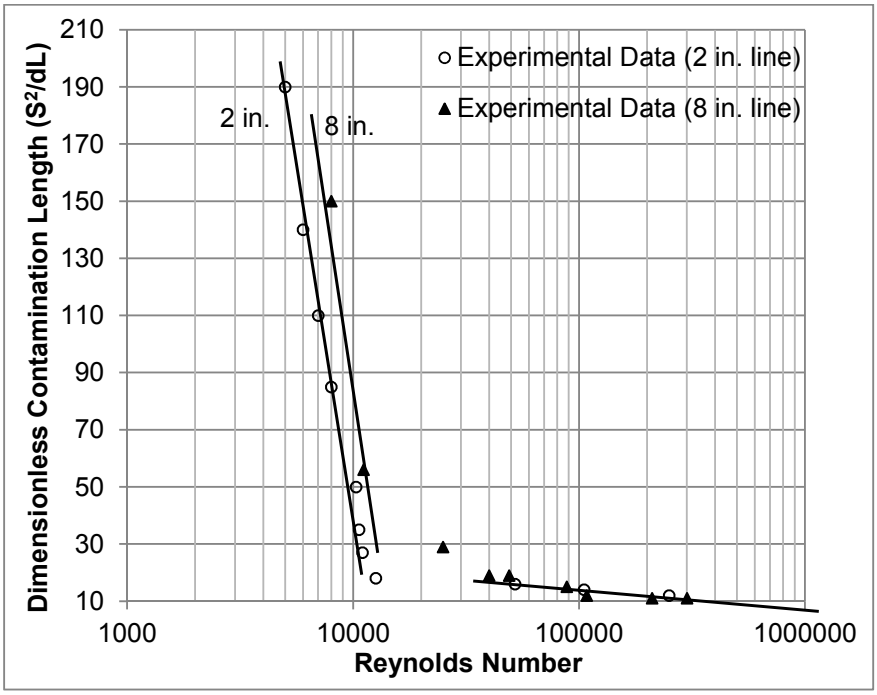

Figure 2.1: Dimensionless contamination length vs. Reynolds number for 2" and 8" diameter pipes. Adapted from Austin and Palfrey (1964).

Austin and Palfrey noted that the empirically estimated constants in their equations bore a remarkable resemblance to the constants commonly used in momentum transport equations. They suggested that viscous effects, which are dominant in the near-wall regions, play a significant role in axial dispersion. Austin and Palfrey identified two distinct dispersion curves for Reynolds numbers in the turbulent regime (Figure 2.1). In the low Reynolds number region, the rate of

axial dispersion decreases rapidly with increasing Reynolds number and beyond a certain critical value it flattens out and appears to be only slightly dependent on variations in the Reynolds number. Based on this observation, they proposed the existence of two distinct mechanisms in the turbulent regime and suggested viscous dispersion to be one of the mechanisms.

Their model for estimating contamination length consisted of two separate equations, Equation (2.2) for Reynolds numbers below a critical value (Equation 2.1) and Equation (2.3) for transmix length estimations at higher Reynolds numbers. Their analysis of the experimental data suggested the critical Reynolds number to be a function of the pipe diameter.

$$\mathrm{Re}_C = 10,000 e^{1.52\sqrt{d}} \tag{2.1}$$

$$S = 18,420\sqrt{d \cdot L}\,\mathrm{Re}^{-0.9}\, e^{1.21\sqrt{d}} \tag{2.2}$$

$$S = 11.75\sqrt{d \cdot L}\,\mathrm{Re}^{-0.1} \tag{2.3}$$

The empirical constants used in the above equations were determined based on the calculations of contamination length (S) defined as the distance between two points in the interface along which the mixture composition varies from 1% to 99% of either product. They point to the similarity between a popular equation for estimating the viscous sublayer thickness (Equation 2.4) and the proposed empirical relation for axial dispersion in turbulent flow (Equation 2.2) to support their claim. They also argued the significance of viscous effects by pointing out experimental results showing an increase in contamination length with increasing pipe diameters at the same Reynolds number.

$$\delta_V \propto d\,\mathrm{Re}_d^{-0.875} \tag{2.4}$$

The similarities between the two phenomena are clearly discernible. There are however no other evidences or theories explaining the change in slope of the curves at the so called critical

Reynolds number. Austin and Palfrey's supposition of the viscous sub-layer being an important parameter in the process seems reasonable as the viscous sub-layer thickness also displays a similar trend with increasing Reynolds numbers.

Theoretical developments on axial dispersion

Danckwerts (1953) was among the earliest investigators to conduct theoretical studies on longitudinal dispersion. He suggested the application of age- and time-distribution functions for solving such estimations. Danckwerts (1953) recognized that the assumption of plug flow for such systems would be incorrect and argued that the velocity profile and consequently the near-wall dynamics will affect longitudinal dispersion. Klinkenberg and Sjenitzer (1956), Lee (1960), Levenspeil and Smith (1957) and Bischoff and Levenspiel (1962; 1962) have elaborated on this theory and pointed out the existence of an error function profile type skew in the distribution curves as opposed to the more common standard Gaussian profiles to represent the contamination distribution. Klinkenberg and Sjenitzer (1956) investigated the mechanisms proposed by previous researchers and based on statistical reasoning suggested that the effects of multiple mechanisms contributing to longitudinal dispersion will be additive. This effect in axial dispersion is very similar to the additive nature of the pressure drops through packed beds as observed by Darcy and expanded by Forchheimer and later Ergun (1952). Levenspiel and Smith (1957) suggested the use of Peclet numbers as a similarity criterion for fluid self-mixing and conducted statistical analysis of tracer studies. They proposed the use of Equation (2.5) to estimate longitudinal dispersion coefficient based on measured spread of the contaminant.

$$Pe = \frac{D_E}{uL} = \frac{1}{8}\left(\sqrt{8\sigma^2 + 1} - 1\right) \tag{2.5}$$

Levenspiel and Smith (1957) also discussed the effect of flow parameters, geometry parameters, and axial dispersion coefficient on distribution functions. They noted that shorter

residence times and higher axial dispersion coefficients skew the normal distribution functions observed for such systems, with the distributions approaching Gaussian error curves for higher axial dispersion coefficient values. It is important to notice that the dispersion coefficients are assumed to be uniform across the flow cross-sectional area and that such an assumption will only be valid at high Reynolds numbers i.e. at high flow rates.

Taylor's theory of axial dispersion

Taylor (1953; 1954) suggested that velocity profile plays a significant role in the dispersion of matter in the axial direction and proposed a model similar to the conventional diffusion equation to determine the extent of axial dispersion. Taylor (1953; 1954) performed separate theoretical analysis on flow through pipes in laminar and turbulent regimes, and conceptualized a parameter referred to as the axial dispersion coefficient. The axial dispersion coefficient is similar to the conventional diffusion coefficient used in the one-dimensional transient diffusion equation (Equation 2.6). It governs the rate of spreading of a contaminant in the longitudinal direction.

$$\frac{\partial C}{\partial t} = K \frac{\partial^2 C}{\partial x^2} \tag{2.6}$$

Taylor (1953) visualized axial dispersion to be a two-step process. The first step consists of the contaminant concentration profile being skewed into a parabolic shape (in laminar flow) due to the velocity gradient, with diffusion across the cross-section smoothing out the radial concentration variations in the second step (Figure 2.2).

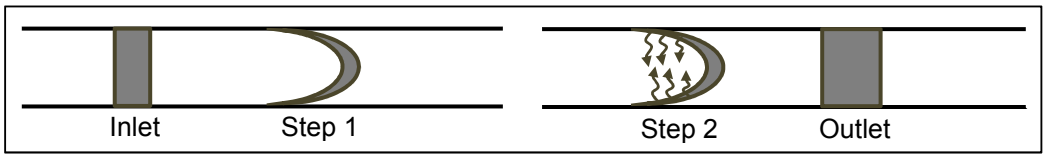

Figure 2.2: Taylor's proposed diffusion mechanism.

Taylor (1953; 1954) solved the convective-diffusion equation (Equation 2.7) using the velocity profile across the flow cross section and obtained an estimate for the longitudinal dispersion coefficient to be used in a transient diffusion model (Equation 2.6). Taylor (1953; 1954) conducted independent analysis for the laminar and turbulent flow conditions and reported separate equations to estimate axial dispersion coefficients in the two flow regimes.

$$\frac{\partial C}{\partial t}+\left(u-\bar{U}\right)\frac{\partial C}{\partial x}=D\left[\frac{\partial^2 C}{\partial x^2}+\frac{1}{r}\frac{\partial}{\partial r}\left(r\frac{\partial C}{\partial r}\right)\right] \tag{2.7}$$

Axial dispersion in laminar flow

A parabolic velocity profile (Equation 2.8) was employed for solving the convective-diffusion equation in the laminar flow regime. In such flows, the longitudinal dispersion can be considered to occur entirely due to the velocity differences between streamlines, and the resulting radial molecular diffusion. Taylor solved the convective-diffusion equation assuming instantaneous radial diffusion and a concentration independent diffusion coefficient to obtain the axial concentration gradient (∂C/∂x). The axial concentration gradient was integrated across the flow cross-section to reflect the rate of transport of contaminant across the cross section and therefore the axial dispersion coefficient (Equation 2.9).

$$u=u_0\left[1-\left(\frac{r}{R}\right)^2\right] \tag{2.8}$$

$$K_L=\frac{R^2u_0^2}{192D}=\frac{R^2\bar{U}^2}{48D} \tag{2.9}$$

Axial dispersion in turbulent flow

The turbulent axial dispersion coefficient was estimated using a universal velocity profile for the velocity term in the convective-diffusion equation (Equation 2.7). The universal velocity profile in its dimensionless form is given as

$$f(z) = \frac{u_0 - u_\tau}{u_\tau} \tag{2.10}$$

where, $z = \frac{r}{R}$ and $u_\tau = \sqrt{\tau_W / \rho}$ (2.11)

with *f(z)* being the dimensionless velocity and τ_W is the wall shear stress. The values for the dimensionless velocity function (Figure 2.3) were determined from a mean curve using data reported by Stanton and Pannell, and Nikuradse (Taylor 1954).

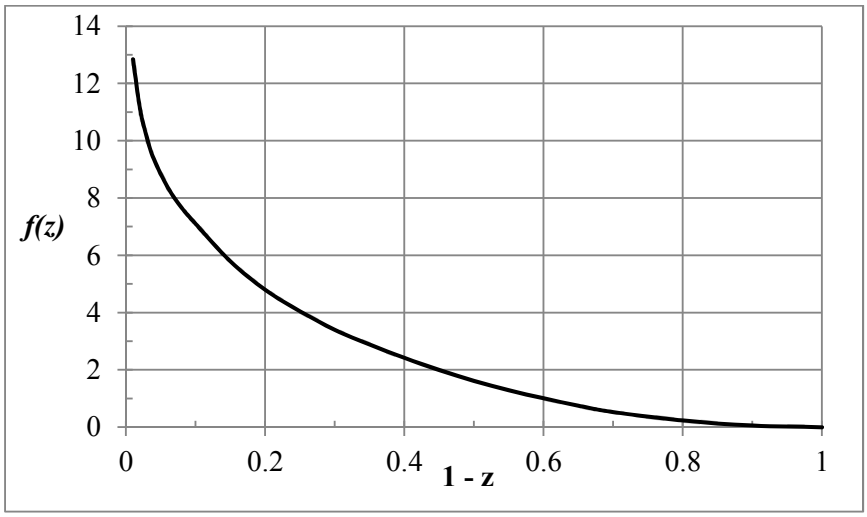

Figure 2.3: Velocity profile as a function of distance away from the wall, used in Taylor's estimation of the turbulent axial dispersion coefficient.

Assuming Reynolds theory of the analogous nature of mass, momentum and heat transfer, Taylor expressed the radial eddy diffusivity in terms of the shear and velocity profiles across the cross-section of the flow field. Replacing the diffusion coefficient (D) in the

convective-diffusion equation with eddy diffusivity, and solving Equation (2.7) in the same manner as for laminar dispersion gives the final expression for the axial dispersion coefficient.

$$K_T = 10.1 R u_\tau \tag{2.12}$$

Taylor (1953; 1954) conducted the axial dispersion analyses assuming an equilibrium between the axial convective and radial diffusive transport. Such a condition requires the interface to reside in the pipe for a certain amount of time as specified by Equation (2.13) for laminar flow systems (Taylor 1953). Therefore, Taylor's equations (Equation 2.9, Equation 2.12) yield asymptotic values for the axial dispersion coefficient. Equation (2.9) and Equation (2.12) are only applicable in cases where the interface has resided in the pipe for a sufficiently long period of time and therefore cannot be applied to short pipes. A similar argument can be proposed for axial dispersion in turbulent flow. It is assumed that Equation (2.13) also holds for turbulent flow, albeit with the diffusion coefficient being replaced with eddy diffusivity (ε).

$$\frac{L}{u_0} >> \frac{R^2}{3.8^2 D} \tag{2.13}$$

Taylor's results for axial dispersion estimations (Equations 2.9 and Equation 2.12) are excellent in predicting the general trends observed in the process. The magnitudes of the predictions are however consistently lower than the experimental results (Figure 2.4). Austin and Palfrey (1964) showed through quantitative analysis that Taylor's expression for turbulent flow (Equation 2.12) under-predicts axial dispersion coefficient by a huge extent (order of magnitude differences) at low Reynolds numbers ($\leq$ 5000). Similar comparisons at higher Reynolds number ($\geq$ 100000) showed better agreement with experimental data, though Taylor's analysis (Equation 2.12) still under-predicts the extent of contamination. Austin and Palfrey (1964) suggested the inadequacies of Taylor's analysis (1954) in incorporating "tailing" effects as the reason for the slight deviation at high Reynolds numbers.

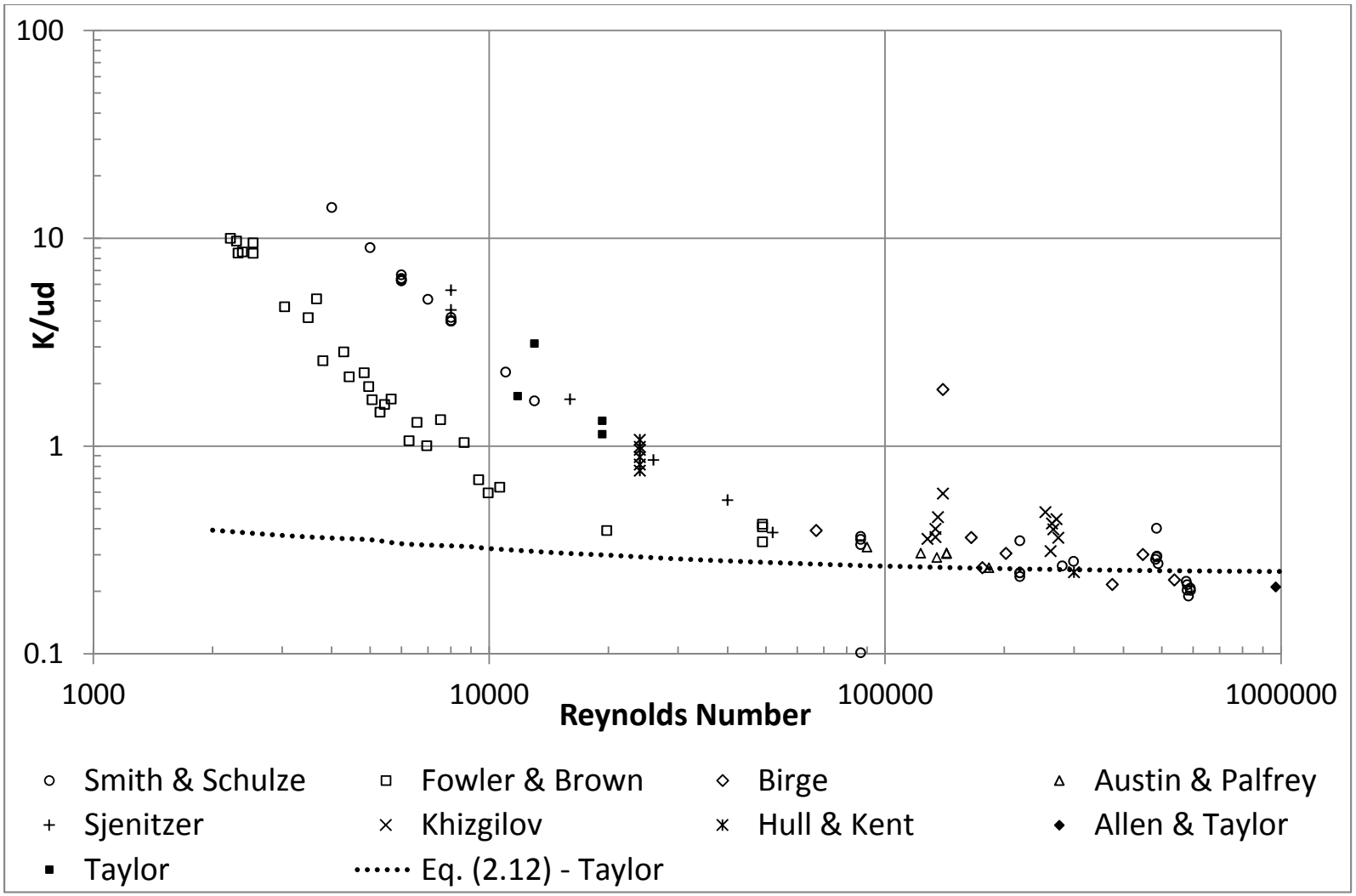

Figure 2.4: Performance of Taylor's turbulent dispersion equation (Equation 2.12).

Aris (1956) pointed out that Taylor's expressions were obtained assuming Reynolds analogy for mass and momentum transport, and hence, are only valid for systems with a Schmidt number of one. Aris (1956) then corrected Taylor's expression (Equation 2.9) by adding molecular diffusivity to the axial dispersion coefficient and improved the predictions for low Schmidt number systems (gases) and laminar flow conditions. For Schmidt numbers higher than one, which is the case with liquids, the effect of molecular diffusivity is negligible and can therefore be ignored. This was shown to be true at higher Reynolds numbers using the data assembled by Levenspiel (1958), and Flint and Eisenklam (1969; 1970). Many researchers (Tichacek, Barkelew et al. 1957; Flint and Eisenklam 1969; Atesman, Baldwin et al. 1971; Chatwin 1971; Krantz and Wasan 1974; Maron 1978; Rachid, Araujo et al. 2002) also suggest Taylor's (1954) use of the universal velocity profile and concentration independent diffusion coefficients as reasons for this eccentricity. Tichacek et al. (1957) evaluated the convective-diffusion equation with different velocity profiles and showed that even a 3% variation in the velocity profile resulted in a deviation of around 50% in the dispersion coefficient. Flint and Eisenklam (1969) reworked Taylor's analysis (1954) for turbulent axial dispersion in gases and reported similar observations.

Multilayer models

The deviation of Taylor's turbulent dispersion predictions at lower Reynolds numbers is well documented. Investigators have proposed various techniques to overcome this ambiguity. One technique (Chatwin 1971; Chatwin 1973; Chikwendu and Ojiakor 1985; Smith 1987) to model such variations would be by splitting the flow cross-section into multiple regions (concentric cylinders for pipes and layers for open channel flow), and modeling each region with the characteristics specific to those observed in the actual processes. This technique is based on the premise that velocity is not constant across the entire cross-section of the flow. Accounting

for these variations should result in better dispersion models, especially for low Reynolds number turbulent flows.

Chikwendu and Ojiakor (1985) proposed a multilayer model for flow in open channels, with each layer having different diffusion characteristics and velocity profiles (Figure 2.5). The convective-diffusion equation (Equation 2.7) was applied separately to the regions and an empirically estimated lateral diffusion coefficient was employed to model the transport of material between the two layers. The concentration distribution functions obtained from the separate solutions for the two layers were then superimposed to give the effective distribution expected in the system. Employing more than two layers would improve the model accuracy (Smith 1987); though, this would also increase the number of empirical constants in the model, making the equations significantly more complex.

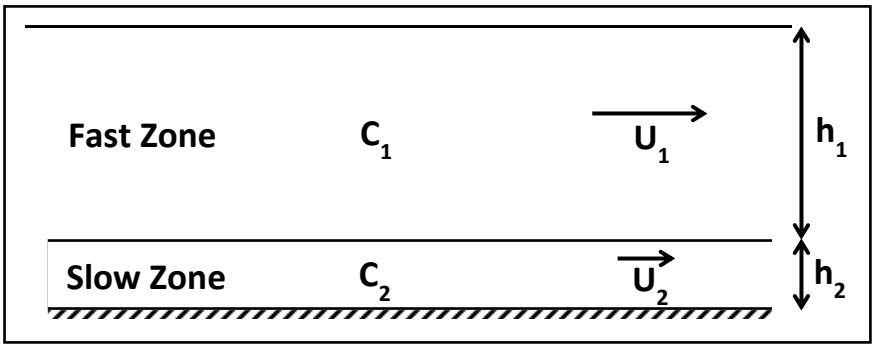

Figure 2.5: Multilayer model schematic. Adapted from Chikwendu and Ojiakor (1985).

Chatwin (1971; 1973) had proposed similar multilayer concepts prior to Chikwendu and Ojiakor (1985) and suggested to model a two layer system with the viscous sub-layer and the turbulent core as the two layers. Chatwin (1971) solved the convective-diffusion equation using a linear velocity profile for the viscous sub-layer region (non-dimensional wall units, $y^+ \leq 5$) and the log law profile in the turbulent core region to obtain a 20% increase in the dispersion coefficient calculated using Taylor's turbulent dispersion equation. However, the equations still under-predict the overall dispersion coefficient and Chatwin (1971) attributed this to the

incompetency in modeling the viscous effects. Chatwin (1973) later reported a detailed analysis for open channel flows and obtained an expression for the effective dispersion coefficient (Equation 2.14) as a function of the height of the viscous sub-layer, using a linear velocity profile across the flow cross-section.

$$D_E = \frac{u_0 h^2}{30}\left\{\frac{10\left(h_1/h\right)^2}{D_1} + \frac{1}{D_2}\right\} \tag{2.14}$$

where, D_1 and D_2 represent the radial diffusion coefficients in the viscous sub-layer and the turbulent layer, h_1 and h indicate the thickness of the viscous sub-layer and the total channel height respectively, and u_0 is the maximum flow velocity (open surface).

Research strategy and timeline

The available literature reveals that further research is necessary to effectively describe the phenomenon of axial dispersion in liquid petroleum pipelines. Most of the models currently available in the literature are empirical; they do not have an established theoretical basis, are accurate only for select systems and therefore lack generality. Taylor (1953; 1954) proposed robust theoretical concepts for axial dispersion, the resulting model equations though are only applicable for asymptotic conditions of high Reynolds number turbulent flows. Subsequent investigations on Taylor's theories have led to some developments in the field. The improved theoretical models however exhibit similar inconsistencies in accurately predicting the experimental results, as observed in the original.

Apart from Taylor's analysis (1953; 1954), almost all other studies involve solving complex equations using numerical simulation techniques. The models have been developed assuming a uniform flow field and are solved by considering either the laminar flow regime or the turbulent flow regime as the controlling factor. These models therefore tend to be erroneous for

conditions when both the viscous and the turbulent effects are significant. The models that employ improved velocity profiles fare slightly better, but the discrepancies still exist. The various theoretical and empirical models discussed earlier are known to predict transmix growth with less than 20% deviation for systems that are similar to the study conditions. The same models however also differ by over 200% for cases that were not included for developing the model. The empirical model proposed by Austin and Palfrey (Equations 2.1-2.3) is obtained from the analysis of experimental data from many different investigations and hence is more generalized as compared to the other empirical models. This model has also been used to successfully predict transmix volume for other independent experimental investigations (Shaker and Mansour 1999). The Austin and Palfrey model however fails to provide insights on the phenomenon governing axial dispersion.

The above discussion clearly indicates the need for a theoretical model for transmix growth predictions. The new theoretical models would most likely build on Taylor's theories of axial dispersion and provide explanations on the divergence of Taylor's model equation (Equation 2.12) from experimental observations in the low Reynolds number turbulent regime. Furthermore, the models should also be able to describe the role of turbulence mechanics in axial dispersion studies. Such models would provide a vision to what could be happening in the system during the process of pipeline transport and help identify techniques to help reduce axial dispersion. The most important aspect though, would be to develop a generalized model with better accuracy than the ones currently available in literature.

A theory that has been suggested to explain the deviations in Taylor's analysis (Taylor 1954) for low Reynolds number turbulent flow is the inattention to viscous effects in the near wall region. Austin and Palfrey (1964) and Chatwin (1973) were among the first to investigate this hypothesis and report encouraging observations. The experimental data reported by other investigators also validates this theory. The extent of longitudinal contamination depends upon

the operating flow rate or Reynolds number (Figure 2.6A). At Reynolds numbers approaching zero, the system approaches stagnation and in this region axial dispersion coefficient approaches the molecular diffusivity and convection is no longer a significant factor. Reynolds number seems to have an opposite effect on axial dispersion in the turbulent regime. The dimensionless axial dispersion coefficient seems to decrease rapidly with increasing Reynolds number at lower values of turbulent Reynolds numbers. This then changes to a gradual reduction beyond a certain higher Reynolds number, approaching an asymptote to the turbulent eddy diffusivity. The above observation can be explained by considering the effects of the viscous boundary layer. For fully developed laminar flow, the viscous boundary layer covers the entire cross section of the pipe. This changes as the flow enters into transition and then turbulence. The viscous layer thickness decreases as a hyperbolic function of the Reynolds number (Figure 2.6B), with the pipe diameter as an asymptote for the Reynolds number at onset of turbulence, and zero as the other asymptote at infinite Reynolds number. The values for the dimensionless viscous sub-layer thickness shown in Figure 2.6B were calculated using the equation (Schlichting and Gersten 2000)

$$\frac{\delta_V}{d} = 122 \frac{\ln(\mathrm{Re})}{\mathrm{Re} \cdot G\{\ln(\mathrm{Re})\}} \tag{2.15}$$

where G is a monotonically decreasing function of the Reynolds number, which tends to one at infinite values of the Reynolds number. This phenomenon is very similar to the observations on axial dispersion. Viscous region effects can therefore be considered as a possibly significant parameter in dispersion studies.

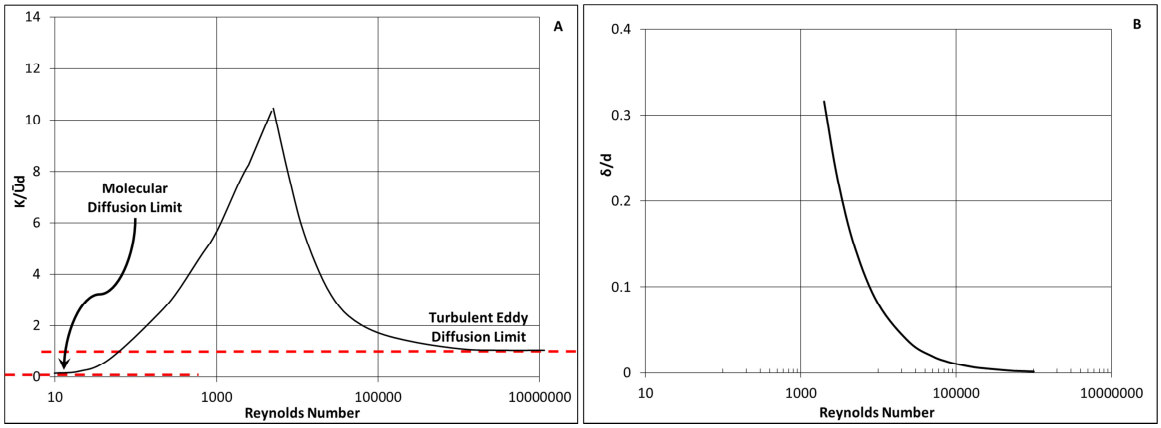

Figure 2.6: A) Dimensionless dispersion coefficient and, B) dimensionless viscous sublayer thickness, as a function of the Reynolds number.

The current work builds on this similarity observed between the axial dispersion coefficient and the viscous sub-layer variations to foster a new model for axial dispersion estimations. Initial modeling efforts concentrate on establishing a direct dependence of axial dispersion on the viscous sub-layer thickness and investigate the possibility of empirically relating the two quantities. This empirical model was analyzed to learn about any obvious correlations or equivalence to other theoretical or well-established relations in mass and momentum transport studies. The knowledge thus gathered was then applied to put together theoretical concepts that might be contributing to axial dispersion.

The definitive contribution of this work to the state-of-the-art is a model that combines Taylor's theories on axial dispersion and the theories of boundary layer flow. The concepts for this contribution were conceived and developed as a consequence of continuous work, which resulted in other intermediate models in addition to the main model. A pipe wall scraper model and a tank-in-series model were among the most promising of the various theories of solutions strategies that were investigated. The various observations, inaccuracies and inadequacies of these models helped redirect this work in subsequent path that lead to the eventual development of the combined model.

Organization

Chapter III of this report presents a detailed review of the various checkpoints encountered in this work and discusses the development of the final axial dispersion model. Chapter IV discusses the contributions of the near-wall turbulent bursting events on axial dispersion and proposes a methodology to mathematically incorporate these effects into the axial dispersion equation. Chapter IV also deliberates on the various concepts and assumptions in Taylor's analysis based on the analysis including the turbulent bursting mechanisms. The concepts discussed in the previous chapters are used to perform rigorous recalculations of the convective-diffusion equations employed by Taylor (1954) using the commonly accepted velocity profiles for turbulent flows in the contemporary world. Finally, a methodology to include the effects of pipe fittings, specifically elbows and bends is enumerated in Chapter V. Recommendations for advancing the concepts proposed in the current work to improve the axial dispersion predictions and also to other areas are discussed in concluding Chapter VI.

CHAPTER III

MODELS FOR AXIAL DISPERSION IN STRAIGHT PIPES

The viscous sublayer has been stated to be heavily involved in the process of axial dispersion and suggested to be a potentially significant factor by many investigators (Austin and Palfrey 1964; Chatwin 1971; Chatwin 1973; Dewey and Sullivan 1977; Chikwendu and Ojiakor 1985; Smith 1987; Udoetok and Nguyen 2009). Most researchers have tried to provide a phenomenological explanation of how the viscous sublayer might contribute to, or enhance axial dispersion. Various theories have been proposed and researchers have published mathematical formulations based on these theories. Though the viscous sublayer has been noted as a significant factor, the magnitudes of its contributions to axial dispersion remain relatively unknown. This is mainly because the viscous sublayer thickness is not a primary measured variable such as flow rate, pressure or temperature. Most mathematical formulations available in literature therefore do not employ the sublayer thickness as a separate parameter.

The significance of the viscous sublayer seems obvious when analyzing Taylor's theories on axial dispersion. The idea that the flow in the near-wall region is slower and results in enhanced mixing at an interface seems a logical explanation for axial dispersion. In addition to this, the success of Taylor's model equation in predicting the general trend of the process has simply bolstered this idea. This work focuses on expanding on Taylor's theories of axial mixing

and explores the hypothesis that employing the viscous sublayer thickness as a direct parameter in axial dispersion equations would improve the prediction accuracy of such models. Although having more accurate axial dispersion estimation equations is convenient, understanding the concepts governing these processes are equally, if not more vital. The objective of this work has therefore always been to put forward models and equations that reveal the functioning of the underlying physics.

The current chapter provides a chronological recount of the three axial dispersion models that were developed in this work. The three techniques described include a Scraper and wash-off model, a Tank-in-Series modeling approximation, and a combined Taylor model also referred to as the model of viscous and turbulent contributions. Each model in the order of their progression played a significant part in the conceptualization and realization of all subsequent models.

Scraper and wash-off model

The scraper and wash-off model is an empirical formulation that was realized during the efforts to confirm the dependence of axial dispersion on the near-wall viscous region thickness. This model has been developed based on the assumption that any mixing in the axial direction is solely an effect of the slow moving liquid in the near-wall region of the flow. The liquid adjacent to the pipe walls move slower than the bulk flow and therefore lag behind the interface and into the trailing liquid. The trailing liquid then washes off this thin layer of the leading liquid from the pipe walls, resulting in a mixed region in-between the two pure liquids. The length of the mixing region would be dependent on the rate at which the trailing liquid is able to clear the pipe wall off the layer left behind by the leading liquid.

A schematic visualization of the scraper and wash-off concept is shown in Figure 3.1. The schematic shows the heavier, more viscous of the two liquids involved in the interface as the leading liquid and the lighter, less viscous liquid as the trailing liquid. Based on fundamental

knowledge, the heavier, thicker (more viscous) liquid would have a thicker viscous region as compared to the thinner (less viscous) and lighter liquid. The exact opposite would be true for the central turbulent core in the two regions. It is theorized that the central core of the trailing liquid being broader, would only allow a certain part of the annular region left behind by the leading liquid into the trailing liquid region. This annular region forms a part of the mixed interface that results between the two liquids. The amount of leading liquid that would be available to form the contaminated interface would therefore be defined by the viscous sublayer thickness for the thinner, lighter liquid. The same logic also applies for the case when the lighter, thinner liquid is followed by the heavier, thicker liquid. In such a case, the annular region left behind by the leading liquid would be thinner than the one from the trailing liquid. The extent of mixing would therefore still be defined based on the viscous sublayer thickness of the thinner, lighter liquid.

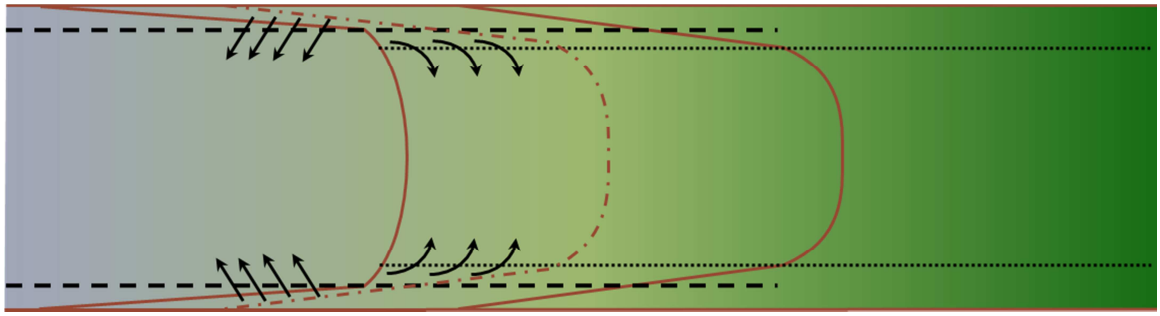

Figure 3.1: Process schematic for the scraper and wash-off model.

Preliminary model equations

The annular region would be as thick as the viscous sublayer of the thinner, lighter fluid. The volume of the leading liquid that contributes to the mixed interface can therefore be estimated using basic geometry (Equation 3.1).

$$V_{Annulus} = \left[\pi R^2 - \pi \left(R - \delta_v \right)^2 \right] \cdot L \tag{3.1}$$

where, R and L indicate the pipe radius and length, and δ_v is the thickness of the viscous sublayer of the thinner, lighter liquid. Many different approximations are available to estimate the thickness of the viscous sublayer. The current model employs an approximate relation stated in a book by Schlichting and Gersten (2000) for this purpose (Equation 2.15).

$$\frac{\delta_V}{d} = 122\frac{\ln(\mathrm{Re})}{\mathrm{Re}\cdot G\{\ln(\mathrm{Re})\}} \tag{2.15}$$

The G in the above equation is a function of the Reynolds number and is calculated using

$$\frac{\Lambda}{G} + 2\ln\left(\frac{\Lambda}{G}\right) - \Delta = \Lambda \tag{3.2}$$

with $\Lambda = 2\cdot ln(Re)$ and $\Delta = -0.17$ for smooth pipes. The above two equations are known to be applicable for Reynolds numbers in the range $2300 \le Re \le 10^7$. The transmix length can therefore be calculated by dividing Equation (3.1) with the cross-sectional area of the pipe to give

$$S = 2\left[1-\left(1-\frac{\delta_v}{R}\right)^2\right]\cdot L \tag{3.3}$$

The annular volume calculated based on the equations listed above can be used to estimate the extent of contamination. An equi-volume mixture of this annular volume with the trailing liquid was one of the combinations investigated. Some investigators have revealed no observable trends in contamination volume when related to the properties of individual fluids. The properties of an equi-volume mixture of the fluids however does seem to have a significant effect on the contamination growth. Almost all model equations available in the literature use equi-volume properties of the two fluids to estimate the Reynolds number and therefore the extent of axial dispersion (contamination). The total contaminated volume therefore becomes twice the

volume of the annular film due to the thinner, lighter liquid. This is represented by the constant multiplying factor 2 in Equation (3.3).

Preliminary Results

The use of the viscous sublayer thickness (Equation 2.15) enables Equation (3.3) to capture the trends observed in contamination length for variations in the Reynolds number (Figure 3.2A). Equation (3.3) suggests that the total contaminated length (extent of axial dispersion) would increase with increasing pipe length. This agrees with the experimental observations reported in the literature. The equation however suggests a linear trend with respect to the pipe length, which is contradictory to the observed square root behavior, thus rendering the model incomplete.

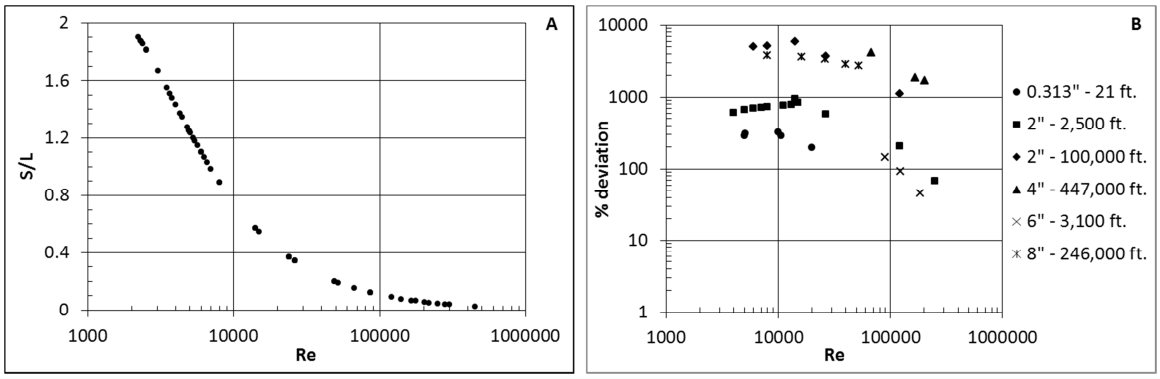

Figure 3.2: A) Transmix length predicted using Equation (3.3) as a function of *Re*, and B) percent deviations in the model predictions as a function of *Re* and pipe length.

Udoetok and Nguyen (2009) proposed a similar concept wherein they considered that the central turbulent core acted similar to a pig separator and does not allow mixing in the central region. Any contamination that occurs is solely on account of the leading liquid that lags behind the imaginary disc pig separator through an annular region adjoining the pipe wall. The thickness of the annular region was assumed to be the distance from the pipe wall where the localized flow velocity is 58.5% of the centerline velocity (empirically estimated number based on experimental

data from the Colonial Pipeline Co.). A local velocity of 58.5% of the centerline velocity lies in the vicinity of a radial distance that defines the viscous sublayer in pipe flow. They proposed the contamination volume would be equal to the ratio of the area of annular region to the total cross-sectional area of the pipe multiplied by the pipe volume (Equation A.18). This is equivalent to saying that the contamination length is directly proportional to the pipe length. The disc pig model therefore also suffers from the same problems as Equation (3.3) because of its inability to correctly capture the dependence of transmix length on pipe length.

The trend in percent deviation of the model predictions (Equation 3.3) from the experimentally generated contamination lengths reported in the literature are presented in Figure 3.2B. The model tends to show comparatively better accuracy for shorter pipe lengths and higher Reynolds numbers. The deviations though higher at lower Reynolds number ($Re \leq 15{,}000$), the accuracy gradually improves with increasing Reynolds numbers asymptotically tending to zero for infinite values of the Reynolds number. The general trend observed in Figure 3.2B suggests that the total contamination volume would be equivalent to twice the volume of the viscous sublayer at higher velocities, though this is not necessarily true for low velocity. The performance of Equation (3.3) for varying pipe lengths is shown in Figure 3.3. A near straight line on a log-log plot indicates higher dependence of contamination length on the pipe length for longer pipes, advocating the need for a power law type relation. Also, the different intercepts for these straight lines for varying Reynolds number suggests a dependence of the length exponent (k) on Reynolds number.

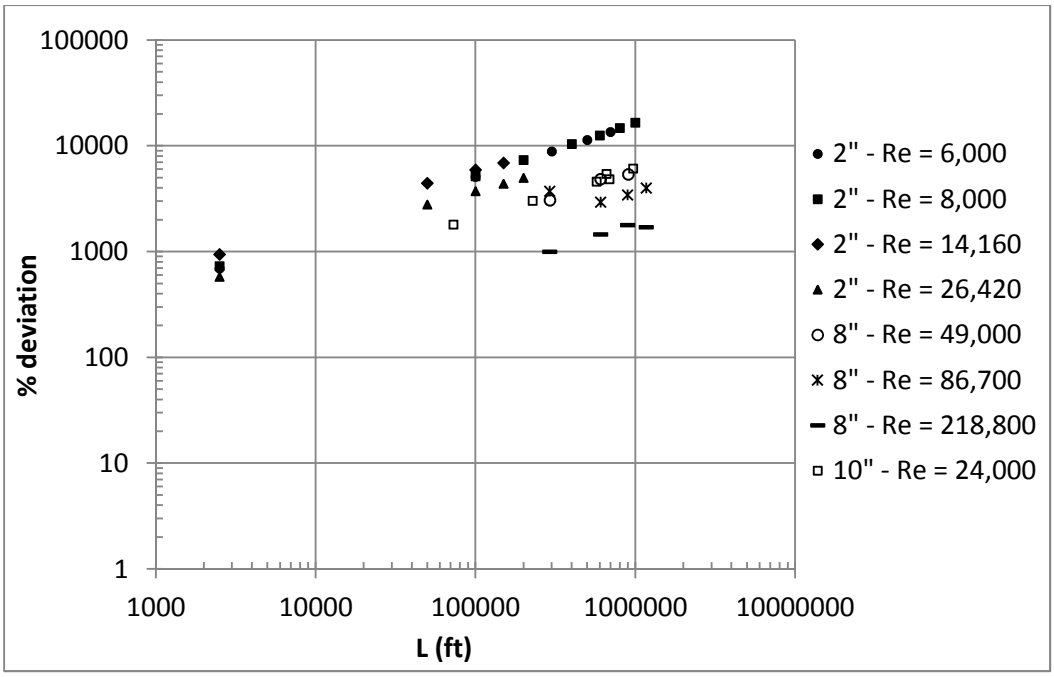

Figure 3.3: Percent deviation of the contamination lengths predicted using Equation (3.3) versus pipe length.

Modification and improved results

Based on the above observations, a power law exponent is added to the length term in Equation (3.3). The contamination length equation therefore becomes

$$S = 2\left[1-\left(1-\frac{\delta_v}{R}\right)^2\right]\cdot L^k \tag{3.4}$$

where, k is a function of the Reynolds number. The values of the length exponent (k) were back calculated from the experimental data on axial dispersion (Table 2.1). These experimentally estimated values are plotted against the Reynolds number in Figure 3.4. The values of the length exponent exhibit a trend similar to that observed for the ratio of the average velocity to centerline velocity in turbulent flow conditions against the Reynolds number (Figure 3.4B).

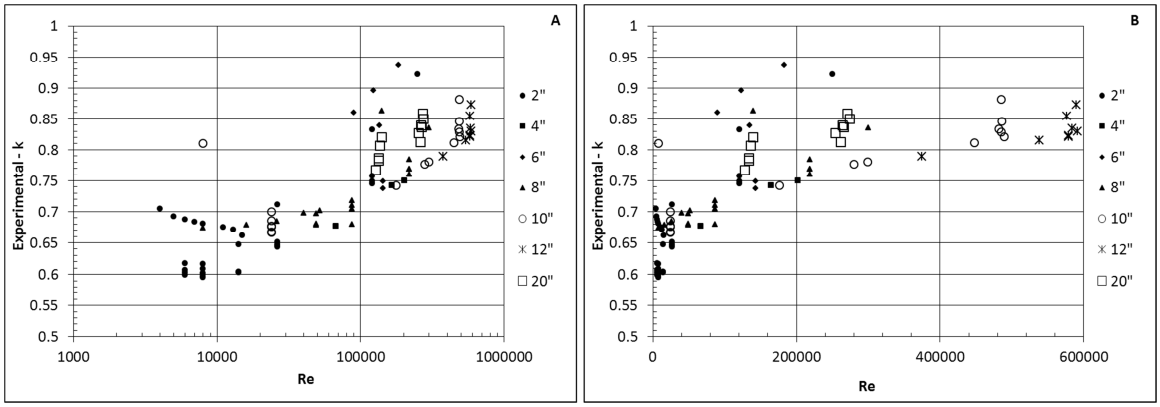

Figure 3.4: Regressed values of the length exponent (k) in Equation (3.4) as a function of the Reynolds number, A) on a semi-log plot, B) in normal scale.

The exponent values for all different pipe dimensions seem to collapse into a single line on a semi-log plot (Figure 3.4A) indicating minor or no impact of the pipe dimensions on the value of the exponent. Many different relationships for the length exponent as a function of the flow Reynolds numbers were investigated and Equation (3.5) is proposed to estimate the length exponent for the Reynolds numbers (50-50 by volume mixture) less than 1,000,000.

$$k = 0.9 \cdot \left[\frac{\bar{U}}{u_0} \cdot \frac{\ln\left(\mathrm{Re}_{High}\right)}{\ln\left(1{,}000{,}000\right)} \right], \quad \mathrm{Re}_{cr} \leq 1{,}000{,}000 \tag{3.5}$$

In the above equation, Re_{High} is the Reynolds number of the lighter, thinner liquid, 0.9 is an empirically calculated parameter, and Re_{cr} is the Reynolds number based on the properties of a 50-50 by volume mixture. The ratio of the average flow velocity to the centerline velocity in a pipe can be estimated using Prandtl's power law exponent (n) as,

$$\frac{\bar{U}}{u_0} = \frac{2n^2}{\left(n+1\right)\left(2n+1\right)} \tag{3.6}$$

with the exponent n being estimated as the inverse of the square root of the friction factor. Figure 3.5 compares the length exponent values predicted using Equation (3.5) against the expected

exponent values back calculated from the experimental data. Equation (3.5) does a commendable job in predicting the exponent value for Reynolds number greater than 20,000. The prediction accuracy however appears to drop at lower Reynolds numbers. Furthermore, the model consistently under-predicts the exponent value at these lower turbulent Reynolds numbers and can therefore be labeled to be biased for this region. The estimated absolute average deviations (*AAD*) of the model from the experimental data increases to as high as 28% at a Reynolds number of 4,000.

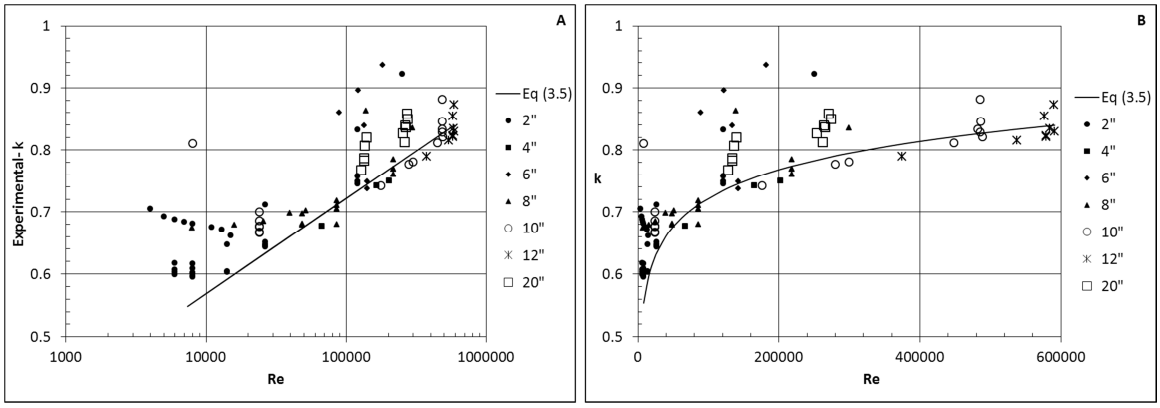

Figure 3.5: Performance of Equation (3.5) over a range of Reynolds numbers, A) on a semi-log plot, and B) in normal scale.

The bias in the predictions is rather distinct at Reynolds number less than 20,000 and there exists a very visible trend in the extent of deviation as the Reynolds number increases in this region (Figure 3.6). The prediction accuracy of Equation (3.5) gradually improves with increasing Reynolds numbers, settling down to an *AAD* of less than 5% beyond a Reynolds number of 20,000. The nature of the bias could be attributed to the inability of Equation (2.15) to accurately estimate the viscous sublayer thickness in this region. Equation (2.15) is however known to be fairly accurate for all Reynolds numbers in the range $2{,}300 \leq Re \leq 10^7$. It is hypothesized that the loss in prediction accuracy is due the inability of the equations to model the enhanced contributions of viscous stresses for Reynolds numbers less than 20,000. This is a

reasonable hypothesis considering that the contributions of the viscous stresses would be higher at lower Reynolds numbers and would gradually decrease as the Reynolds number increases, which is similar to the trend observed in Figure 3.6.

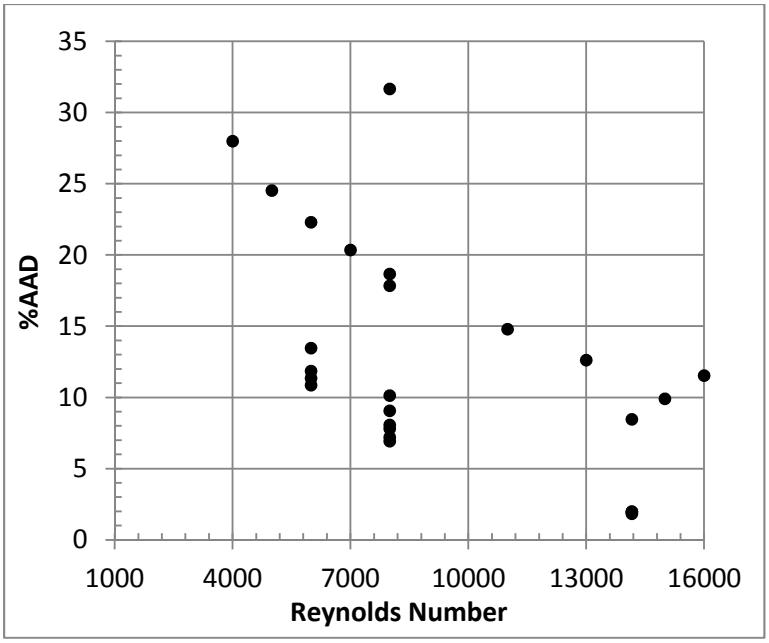

Figure 3.6: Nature of bias of the predictions from Equation (3.5) as a function of *Re*.

Figure 3.7A is a parity plot comparing the length exponent predicted using Equation (3.5) against the experimentally determined exponent values. Figure 3.7B shows the parity plot for the case when the empirical parameter in Equation (3.5) is adjusted for Reynolds numbers less than 2,000 in order to achieve a better fit. A value of one for the adjustable parameter improves the predictions at lower Reynolds numbers. The bias though reduced, still exists and follows the same trend observed in Figure 3.6. The justification for such an adjustment is an increase in the applicable Reynolds number range of Equation (3.5), which can now be employed for contamination growth estimations at all Reynolds numbers greater than 10,000.

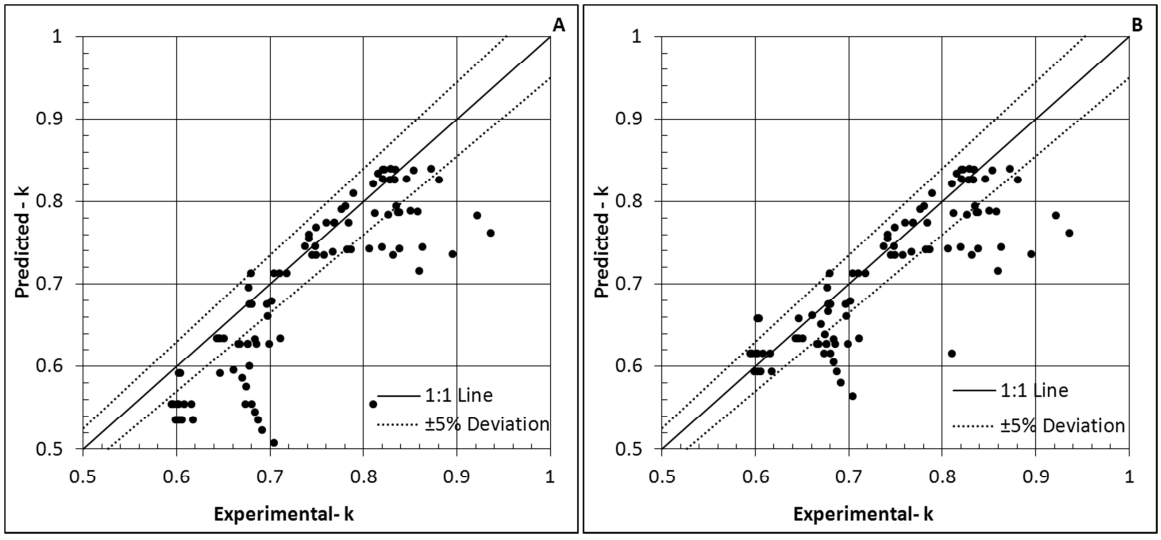

Figure 3.7: Parity plots highlighting model performance. A) Equation (3.5) before modification, and B) Equation (3.5) after modification.

Equation (3.4) in combination with Equation (3.5) provides better estimates of the contamination length (or volume) when compared with Equation (3.3) and Equation (A.18). The equation is however still unreliable considering that even a 5% uncertainty in predicting the length exponent can magnify to a 50% or even a 100% uncertainty when converted to contamination length. This is particularly a problem for estimations involving higher pipe lengths, which is almost always the case with petroleum transportations. The absolute average deviation of the predictions for contaminated length *S* using Equation (3.4) is around 30%.

Moving plug model

The deductions from the Scraper and wash-off model and other investigations in the literature indicate that transmix estimations can be improved by incorporating the contributions of viscous and turbulent regions in the flow field as independent influences. The moving plug model is a variation of the tank-in-series (T-I-S) modeling approach that is commonly employed in residence time distribution studies of plug flow reactors. The basic idea of the T-I-S approach involves dividing the plug flow reactor (pipe) into multiple sections of well mixed regions

(Continuous Stirred Tank Reactors, CSTR) placed in series, with the outlet of one being the inlet of the next. The moving plug model uses a similar concept though with a slightly different modeling perspective. A schematic of the moving plug visualization is presented in Figure 3.8.

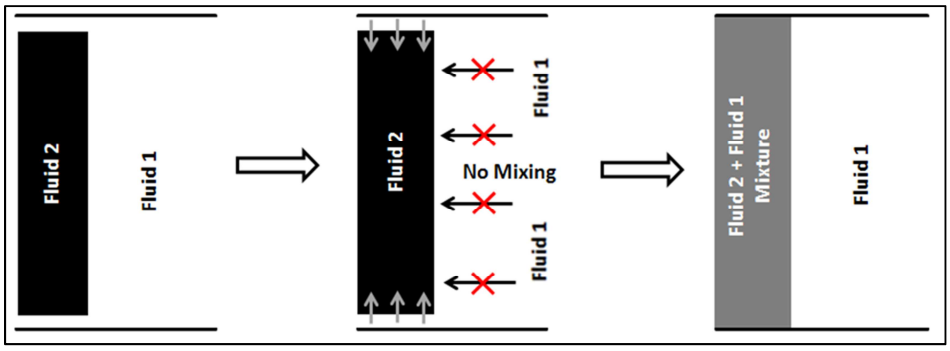

Figure 3.8: A schematic of the first step in the moving plug flow model.

The phenomenon of axial dispersion is divided into multiple steps, with each step resulting in a contaminated interface moving a short distance down the pipe. Figure 3.8 depicts the occurrences in the system at the end of the first step and before the second step commences. The objective of the model is to capture snapshots of the process at predefined time intervals as the two fluids mix and move downstream. Consider a case when the pipe is initially filled with fluid 1 moving downstream at a set velocity. At a particular time ($t = 0$), the inlet to the pipe is switched from fluid 1 to fluid 2. The process is allowed to progress for an infinitesimal period (Δt), during which time a thin, disc shaped plug of fluid 2 enters the pipe. The new fluid (fluid 2) entering the pipe instantaneously mixes with a thin annular volume of fluid 1 that had originally occupied the region. The mixing results in a mixed fluid region as shown in the middle picture of Figure 3.8. It is assumed that the two fluids do not mix through the central cylindrical region of the flow.

Model equations

The annular film of fluid 1 lagging behind the bulk flow is hypothesized to be the result of the viscous sublayer of fluid 1. The volume of this annular film would therefore be equivalent to the cross-sectional area occupied by the viscous sublayer multiplied by the length of the plug of fluid 2 that has entered the pipe. The volume of the annular region can therefore be calculated using Equation (3.1) by replacing pipe length (L) with the distance travelled by the interface in one time increment. Assuming ideal mixing rules apply, the density of the mixed region can be estimated as

$$\rho_{MIX} = \rho_1 x_1 + \rho_2 x_2 \tag{3.7}$$

where, ρ_{MIX} is the density in the mixed region, ρ_i is the density of fluid i, and x_1 is the volume fraction of the annular region and x_2 is the volume fraction of the central turbulent core. Both x_1 and x_2 are determined based on the properties of fluid 1, the leading fluid. The volume fraction of fluid 1 in the mixed region (x_1) can be estimated as the ratio of the annular volume of the mixed region to the total volume of the mixed region.

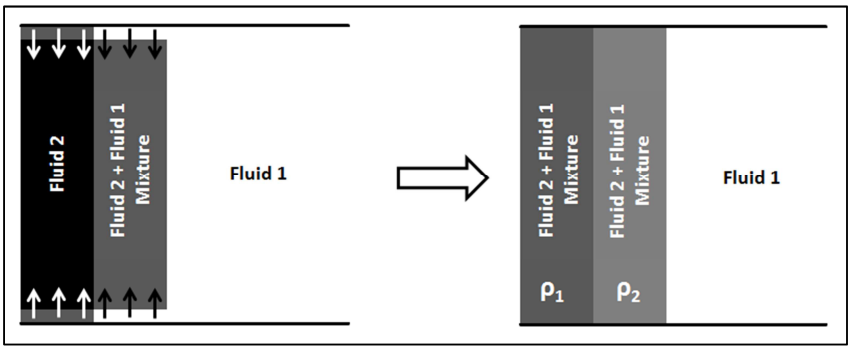

Figure 3.9: Second step of the moving plug flow visualization.

Figure 3.9 depicts the occurrences at the end of the second time step and before the start of the third step of the process. More fresh fluid 2 enters the pipe pushing the mixed fluid region from step 1 along with the uncontaminated fluid 1 farther downstream. As the mixed fluid from

step 1 moves into position, it mixes with the uncontaminated fluid 1 in the annular region, increasing the fraction of fluid 1 in this region. Fresh fluid 2 then enters the spot vacated by the mixed fluid and combines with the fluid in the annular region to form a separate mixed fluid region, concentrated with fluid 2. This process continues as the two fluids flow downstream and exit the pipe in the form of bands that vary from the composition of fluid 1 to the composition of fluid 2. The composition of each of the bands can be estimated in a manner similar to Equation (3.7). Equation (3.7) can be generalized and rewritten based only on the compositions of the leading and trailing fluid as shown below

$$\rho_j(m) = \left[1 - \frac{v}{V}\right]^m \cdot \rho_j(0) + \frac{v}{V}\left[\sum_{i=0}^{m-1}\left\{\left(1 - \frac{v}{V}\right)^i \cdot \rho_{j-1}(m-i)\right\}\right] \tag{3.8}$$

The $\rho_j(m)$ in Equation (3.8) refers to the density of the mixed fluid in the j^{th} plug after m time steps, v is the volume of the annular region left behind by the fluid in the previous plug and V is the total volume of each plug. The above equation has been formulated considering the entire pipe to be split into a series of equal volume plugs. The volume for each plug is estimated using the cross-sectional area of the pipe and the distance travelled by a plug in one time increment (Figure 3.10).

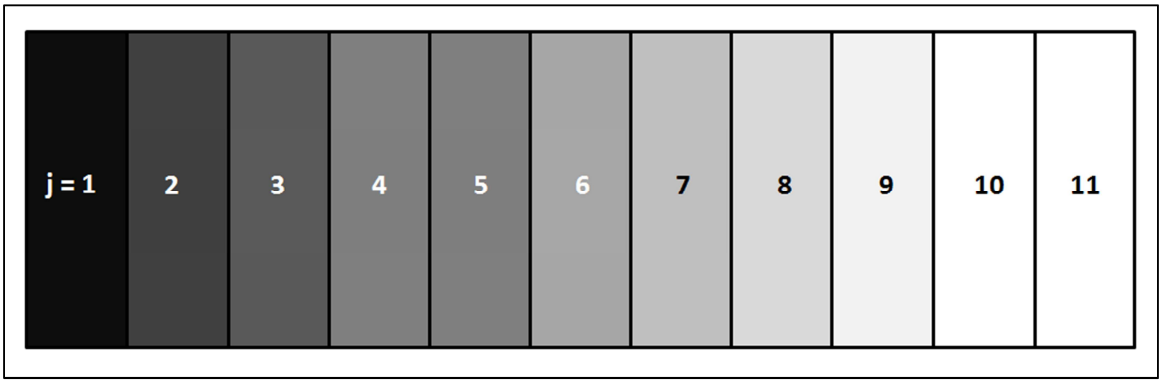

Figure 3.10: Transverse view of the pipe divided into multiple plugs.

The total number of plugs in the pipeline can be calculated from the value of the time increment to be used in the solution. The value for the time increment would ideally be equivalent to the time taken by the annular region to mix completely with the inrushing fluid in turbulent flow. Such a model would identify the exact concentration profile in the mixed region in addition to estimating the length of the contaminated region.

Discussion

The initial objective was to use this model and back calculate values of the time increment (Δt) that would give the best possible match for the experimentally observed transmix lengths (similar to the estimations for the length exponent in the Scraper and wash-off model). During the initial estimations it was observed that the value of Δt necessary to fit the experimental data was extremely small in comparison with the total residence time of the interface in the pipeline. Such an observation seems reasonable considering that Δt would be the time required for a small amount of annular liquid to be completely mixed with an incoming turbulent plug. The smaller the value of Δt, the larger the number of plugs in the pipeline and therefore more the number of calculations. It should also be noted that Equation (3.8) is for a single plug (j) at a particular time instance defined by the number of time steps (m) elapsed after the second fluid enters the pipeline. Therefore, if a particular pipeline has 1000 plugs, the total number of time steps would be much higher than 1000, making the total number of computations exceed 1 million. Applying such a model to a 1000 mile pipeline would be computationally unreasonable.

Though computationally demanding, the theory of moving plug model is extremely important because of its ability to predict the S-curve concentration profiles that are commonly observed in longitudinal mixing. Furthermore, the model builds on the idea of a slow moving near-wall region mixing with an inrushing fluid, which by most researchers is believed to be the mechanism resulting in axial dispersion. It should also be noted that the incorporation of the

viscous sublayer concept (Equation 2.15) allows the model to predict the variations in axial dispersion with changing Reynolds number. The mathematical formulation given by Equation (3.8) was rejected due to the associated extreme computational burden. The concept of the moving plug model however bolstered the hypothesis that formulating the viscous and turbulent core as separate entities can be used for axial dispersion estimations. The theories involved in the Scraper and wash-off model and the moving plug model form the base for the combined Taylor model of viscous and turbulent contributions. The two models also assist in visualizing how turbulence mechanics influence axial dispersion.

Combined Taylor model of viscous and turbulent contributions

Taylor (1953; 1954) reported independent theoretical investigations to calculate the axial dispersion coefficient in the laminar and turbulent regimes. As stated in Chapter II, these expressions perform very well for fully laminar flow and very high Reynolds number turbulent flows. Their accuracy however drops in the transitional low Reynolds numbers and moderate Reynolds number flow regimes, indicating a need for some sort of corrections in these regions. The examination of literature data and the observations from the earlier two models direct towards a combined axial dispersion model that unifies the two independent equations proposed by Taylor (1953; 1954). The resulting unified equation would collectively account for both the viscous and turbulent effects for axial dispersion estimations.

The model proposed derives inspiration from the shear stress distribution observed across a cross section in turbulent flow, and also from the pressure drop analysis proposed by Darcy and extended by Forchheimer, and later by Ergun (1952) for turbulent flow through packed beds. The shear stress for turbulent flow can be segregated into two components a) shear due to laminar or viscous effects and b) shear due to turbulent Reynolds stresses (Figure 3.11). The viscous effects entirely constitute for the total shear at the wall, and its contribution falls rapidly as one proceeds

away from the wall towards the turbulent core. In contrast, the contribution of turbulent effects to the total shear stress is zero at the wall as all fluctuations go to zero at the wall. The contributions of the turbulent effects to the total shear stress increase with increasing distance away from the boundary, farther towards the center of the pipe. Thus, the total shear stress experienced by the flow depends on both the viscous and turbulent contributions. This has been widely accepted and confirmed through many experimental investigations (Pope 2000).

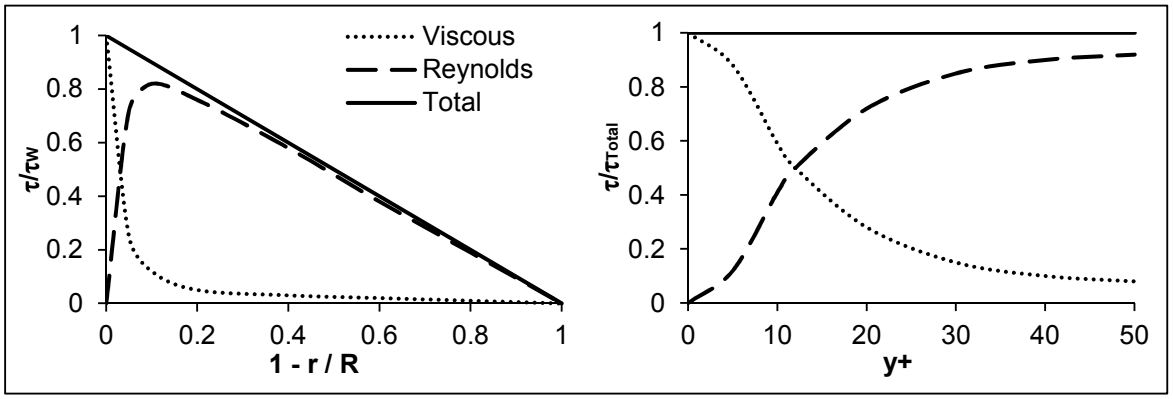

Figure 3.11: Profiles for contributions of the viscous and Reynolds shear stresses to the total stress in turbulent channel flow. Adapted from Pope (2000).

Taylor's theories (1953; 1954) indicate a clear dependence of axial dispersion on the shear stress distribution across the flow cross section. Hence, it would not be farfetched to suggest that the viscous contributions will also have a major effect on axial dispersion coefficient. The effects of viscous stresses would be pronounced in the lower Reynolds number region as the viscous sublayer would be thicker in this region. Neglecting the viscous contributions would therefore have a proportionally higher impact on calculations in this region as compared to calculations in the higher Reynolds numbers region. This behavior fits very well with the observed higher deviations of Taylor's analysis (Taylor 1954) from experimental data in the low Reynolds number turbulent regime (Austin and Palfrey 1964). Based on this analysis, Taylor's expression (Taylor 1954) can also be expected to under-predict axial dispersion coefficient for higher Reynolds number, though to a lesser extent. This also agrees with the observations

presented by other investigators (Austin and Palfrey 1964; Flint and Eisenklam 1969; Flint and Eisenklam 1970; Chatwin 1971; Chatwin 1973).

Model equations

The shortcomings in Taylor's analysis (1954) can be resolved by selectively adding the contributions of the viscous and the turbulent stresses. Similar concepts have also been employed for pressure drop calculations. Pressure drop, like axial dispersion is an outcome of the shear due to a solid wall. The shear stress distribution across the flow cross-section would therefore have a similar effect on both these quantities. Ergun (1952) proposed the concept of estimating the coefficients in the Darcy-Forchheimer equation (Equation 3.9) by considering the multiplying terms (*a* and *b*) to be a consequence of the viscous and turbulent effects in the system.

$$\frac{\Delta P}{L} = a\nu\bar{U} + b\rho\bar{U}^2 \tag{3.9}$$

The first term in Equation (3.9) represents the contribution of viscosity to the pressure drop, while the second term was explained as the pressure drop resulting due to eddy momentum transfer. On similar lines, the overall or effective axial dispersion coefficient across a cross section of the flow can be determined as

$$K_E = a_\delta K_V + \left(1 - a_\delta\right) K_T \tag{3.10}$$

In the above equation, a_δ is a constant representing the contributions of the viscous dispersion coefficient (K_V) to the overall axial dispersion coefficient (K_E). The value for a_δ being determined based on the thickness of the region where viscous effects contribute significantly to K_E. The laminar dispersion coefficient (Equation 2.9) is used to represent the contributions of viscous stresses to the effective dispersion coefficient and the turbulent axial dispersion equation (Equation 2.12) is employed to model turbulent dispersion.

$$K_V = \frac{R^2 u_0^2}{192D} \tag{2.9}$$

$$K_T = 10.1 R u_\tau = 3.57 d\bar{U}\sqrt{f} \tag{2.12}$$

The contribution coefficient (a_δ) in Equation (3.10) is the fraction of the flow area dominated by viscous characteristics, and is expressed as a ratio of the area occupied by the viscous region to the total cross-sectional area of the pipe (Equation 3.12). The viscous region occupies the annular space extending from the pipe walls to a certain thickness into the flow. The viscous layer thickness (δ) expressed in terms of the non-dimensional wall units (y^+) can be written as

$$\delta = \frac{y^+ \nu}{u_\tau} \tag{3.11}$$

$$a_\delta = \frac{A_\delta}{A_d} = \left[1 - \frac{\delta}{R}\right]^2 \tag{3.12}$$

A value of $y^+ = 5$ is commonly accepted for the viscous sublayer thickness (Pope 2000). However, the cross-sectional area denoted by this value does not necessarily cover the entire region of appreciable viscous effects (Figure 3.11). It is a commonly accepted fact that the turbulent and viscous contributions to total shear stress are nearly equal at y^+ of about 12 and the viscous contributions are known to be appreciable even at higher values of y^+ (about 30~50) (Pope 2000). Therefore, a value of $y^+ = 30$, which is generally accepted as the thickness of the buffer layer, is selected for the model (Pope 2000).

Taylor's equation for K_V (Equation 2.9) is based on the entire flow cross-section and the maximum or centerline flow velocity. This expression needs to be modified before it can be used

for calculating the extent of dispersion in the viscous region of the cross-section. Equation (2.9) can be rewritten using the maximum velocity in the viscous region to give

$$K_V = \frac{R^2 u_\delta^2}{192D} \tag{3.13}$$

where, u_δ refers to the velocity at the boundary of the viscous region ($y^+ = 30$). An approximate value for this velocity can be calculated using Prandtl's power law velocity profile (Equation 3.14). The exponent (n) in Equation (3.14) is a function of the Reynolds number and can be calculated as the inverse of the square root of the friction factor (f). A more appropriate relation to estimate this velocity at $y^+ = 30$ would be the log-law velocity profile (Buschmann and Gad-El-Hak 2003). The power law profile though less accurate at higher Reynolds numbers, is preferred as it allows a compact, single equation formulation for axial dispersion, as opposed to when using the log-law profile. The final accuracy of the axial dispersion equation would not be compromised as the power law profile is known to provide a good estimate of the local velocity in the $y^+ = 30$ region at low Reynolds numbers (Buschmann and Gad-El-Hak 2003). The deviation of the power-law profile at higher Reynolds numbers would not have a significant effect on the overall axial dispersion calculations as the contribution of viscous dispersion is negligible when compared to turbulent dispersion in this region.

$$u_\delta = u_0 \left(\frac{\delta}{R} \right)^{1/n} \tag{3.14}$$

Equation (3.13) represents the dispersion coefficient for a fluid flowing with a velocity u_δ through a pipe of diameter $2R$. This equation would therefore overestimate the value of K_V and requires modification to appropriately represent the dispersion in the annular region. This can be done by correcting the velocity from Equation (3.14) using a ratio of the boundary layer Reynolds number (Re_δ) to the overall flow Reynolds number (Re_d). Equation (3.14) can therefore be revised to give

$$\frac{u_{\delta,corr}}{u_0} = \frac{u_\delta}{u_0}\frac{\mathrm{Re}_\delta}{\mathrm{Re}_d} \tag{3.15}$$

where Re_δ refers to the Reynolds number based on the thickness of the viscous layer, and Re_d is the standard flow Reynolds number based on the pipe diameter.

$$\therefore \frac{u_{\delta,corr}}{u_0} = \frac{u_\delta}{u_0}\frac{\left(u_\delta \delta/\nu\right)}{\left(\bar{U}d/\nu\right)} \tag{3.16}$$

$$\therefore \frac{u_{\delta,corr}}{u_0} = \frac{u_\delta}{u_0}\cdot\frac{u_\delta \delta}{\bar{U}d} \tag{3.17}$$

Substituting Equation (3.14) into the above expression then yields

$$\frac{u_{\delta,corr}}{u_0} = \frac{1}{2}\left(\frac{\delta}{R}\right)^{\frac{1}{n}+1}\left(\frac{u_\delta}{\bar{U}}\right) \tag{3.18}$$

We know that the average velocity in a pipe can be related to the maximum centerline velocity using Equation (3.19).

$$\frac{\bar{U}}{u_0} = \frac{2n^2}{\left(2n+1\right)\left(n+1\right)} \tag{3.19}$$

Substituting this relation in Equation (3.18) gives

$$\frac{u_{\delta,corr}}{u_0} = \frac{1}{2}\left(\frac{\delta}{R}\right)^{\frac{1}{n}+1}\left(\frac{u_\delta}{u_0}\right)\left(\frac{\left(2n+1\right)\left(n+1\right)}{2n^2}\right) \tag{3.20}$$

Re-substituting Equation (3.14) in the above equation results in

$$\frac{u_{\delta,corr}}{u_0} = \left(\frac{\left(2n+1\right)\left(n+1\right)}{4n^2}\right)\left(\frac{\delta}{R}\right)^{\frac{2}{n}+1} \tag{3.21}$$

$$\therefore \frac{u_{\delta,corr}}{\bar{U}} = \frac{1}{2}\left(\frac{(2n+1)(n+1)}{2n^2}\right)^2 \left(\frac{\delta}{R}\right)^{1+\frac{2}{n}} \tag{3.22}$$

The u_δ in Equation (3.13) can then be replaced with $u_{\delta,corr}$ (Equation 3.22) to represent the final form of the dispersion coefficient due to viscous effects.

$$K_V = \frac{R^2 u_{\delta,corr}^2}{192D} \tag{3.23}$$

Taylor's expression (Taylor 1954) for axial dispersion in turbulent flow can be used in its original form in Equation (3.10), with the friction factor (f) being calculated using the Swamee-Jain (1976) or any other commonly employed equations. The use of the entire pipe diameter in the equation for turbulent dispersion can be argued to over-predict the turbulent contributions to the overall dispersion coefficient. This increase would however be negligible considering that the viscous region thickness (δ) is much smaller compared to the diameter and would therefore have no appreciable effect on the calculated effective dispersion coefficient. The final completed equation for the effective axial dispersion coefficient can be written as

$$\frac{K_E}{\bar{U}d} = \left(1-\frac{\delta}{R}\right)^2 \cdot \left(\frac{R^2 u_{\delta,corr}^2}{192D}\right)\frac{1}{\bar{U}d} + \left[1-\left(1-\frac{\delta}{R}\right)^2\right]\cdot\left(3.57\sqrt{f}\right) \tag{3.24}$$

Figure 3.12 depicts the contribution of each of the two terms in the above equation as a function of the Reynolds number of a 50-50 by volume mixture of the fluids forming the interface. At lower Reynolds numbers ($2{,}300 \leq Re \leq 10{,}000$) the viscous dispersion term almost entirely constitutes the effective dispersion coefficient. As the Reynolds number increases, the magnitude of the viscous term drops gradually and so does its contribution to the effective dispersion coefficient. The turbulent dispersion term then begins to dominate and almost entirely constitutes the effective axial dispersion coefficient beyond a Reynolds number of 100,000.

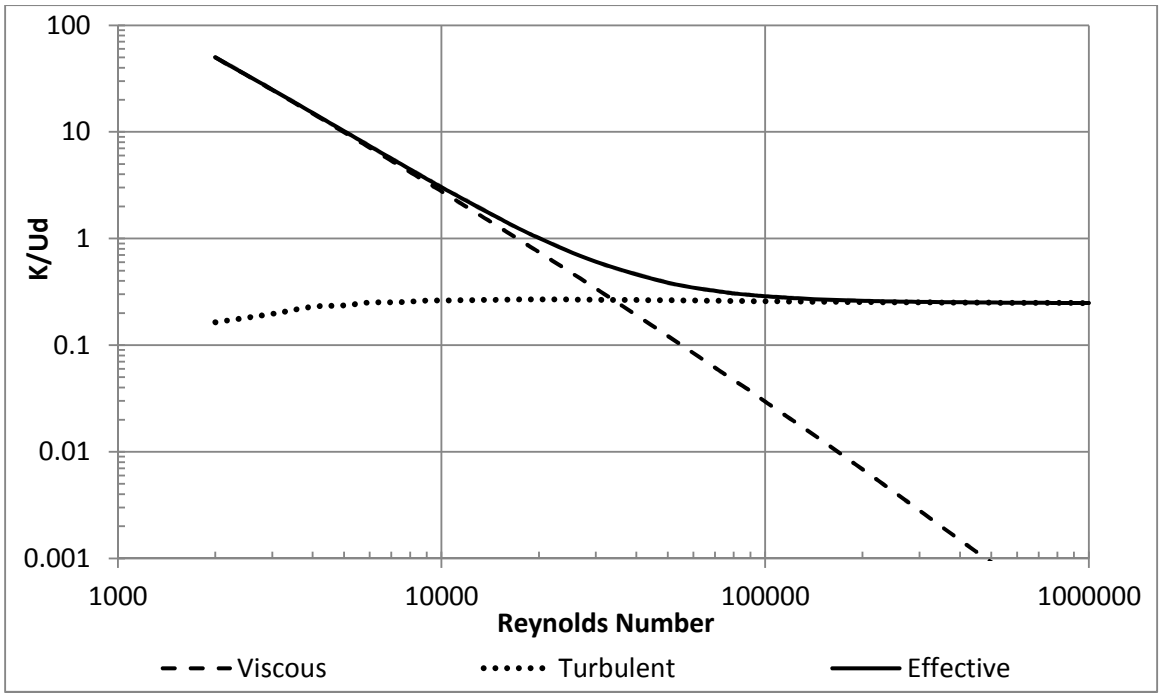

Figure 3.12: Significance of the viscous and turbulent dispersion terms in the dimensionless effective axial dispersion coefficient (Equation 3.24).

Statistical analysis and comparison to literature data

Most sources (Fowler and Brown 1943; Birge 1947; Smith and Sulze 1948; Smith and Sulze 1948; Austin and Palfrey 1964; Aunicky 1970) in the literature express the axial dispersion data in terms of measured contamination lengths at the pipe exit. The axial dispersion coefficient obtained from the proposed model is therefore translated into a contamination length form for comparison purposes. This can be done by using the effective axial dispersion coefficient (Equation 3.24) to solve the transient diffusion equation (Equation 2.6) to give

$$S = k' \sqrt{\frac{K_E L}{\bar{u}}} \tag{3.25}$$

$$\frac{\partial C}{\partial t} = K \frac{\partial^2 C}{\partial x^2} \tag{2.6}$$

where, k' is a constant multiplier dependent on the interface concentration cut-off points ($k' \approx 6.57$ if contamination length is limited to the region where the interface composition varies between 1-99% of either product). The contamination lengths reported in the literature are based on different interface concentration cut-off basis in each investigation. They therefore need to be converted to a common basis for impartial comparisons. Austin and Palfrey (1964) performed such corrections using a ratio of inverse error function of the differences in purities. Similar conversions were performed in the current investigation to translate the contamination lengths reported in the literature to a common 1-99% interface cut-off basis. The derivation of Equation (3.25) from Equation (2.6) is given in Appendix-B.

Another item of note concerns data for the 2" pipeline (Smith and Sulze 1948; Austin and Palfrey 1964). Smith and Schulze (1948) employed a loop-like facility for their experiments, which consisted of a complicated network with multiple bends and pumps. The effect of the bends and pumps in particular cannot be quantified and therefore the data obtained from this source cannot be directly used for comparison with the model calculations. However, this issue can be resolved by correcting the reported lengths to be applicable to straight pipes. Smith and Schulze (1948) provide a set of Reynolds number dependent contamination length curves standardized in terms of the pipe diameter. These contamination curves can be used to approximate the contamination lengths for shortened pipe lengths, which would be more indicative of mixing in straight pipes. In spite of this, some of the experimental results from the loop experiments were included in the analysis in order to demonstrate the effects of pumps and fittings on contamination lengths.

The values for K_E (and S) were evaluated using the model equations (Equations 3.24-3.25) for each of the 126 data points listed in Table 2.1. These values were then converted to percent deviation (*%D*) form using Equation (3.26). Owing to the large quantity of experimental data, only overall comparisons expressed in terms of percent absolute average deviation (*%AAD*)

and segregated based on pipe diameters are listed as part of the main text, while the comparison for each individual case is listed in Appendix-C.

$$\%D = \frac{Estimated - Experimental}{Experimental} \times 100 \tag{3.26}$$

$$\%AAD = \frac{1}{n}\sum |\%D| \tag{3.27}$$

where, n is the number of data point considered to estimate the *%AAD*.

Dispersion in long pipes

The physical properties of equi-volume mixtures of the leading and trailing fluids were employed for determining the Reynolds number and for subsequent calculations. Table 3.1 lists the *%AAD* values for calculations using the proposed model and the Austin and Palfrey (1964) model.

Table 3.1: Comparison of model performance for pipes of varying diameters.

d (in.)	0.124	0.313	2	4	6	8	10	12	20	40[a]
%AAD	64.2	62.5	13.4	8.9	4.1	5.4	7.7	6.3	22.2	0.6
%AAD[b]	8.3	8.2	28.8	7.2	1.8	15.0	7.9	4.1	17.3	1.7

[a]Only a single data point, [b]Austin and Palfrey model (1964)

The proposed model provides reasonable agreement with the experimental results for all diameters 2" and above, except for the 20" pipe case. Figure 3.13 compares the predictions for transmix length estimated using the proposed model (Equations 3.24-3.25) against the predictions of the Austin and Palfrey model (Equations 2.1-2.3) and Taylor's turbulent dispersion equation (Equation 2.12). Both, the proposed model and the Austin and Palfrey model predict the correct trend for the variations in axial dispersion with Reynolds numbers. The Austin and Palfrey model

exhibits a distinct discontinuity at an intermediate Reynolds number because of the use of separate equations for each region. The proposed model exhibits a more gradual curvature in comparison to the Austin and Palfrey equations. The Austin and Palfrey model suggests that the dimensionless dispersion coefficient would vary with pipes of different diameters for the same Reynolds numbers, which contradicts theory and experimental observations. The proposed model on the contrary remains fairly similar for different pipe diameters (Figure 3.13B).

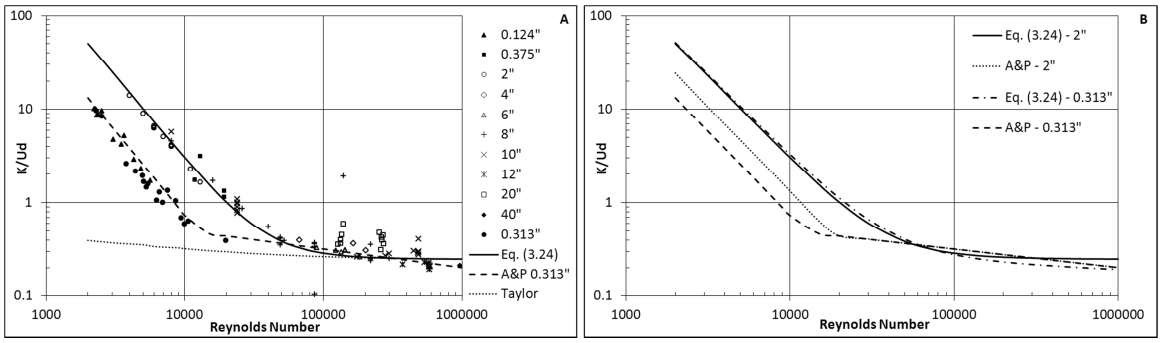

Figure 3.13: Prediction capabilities of the proposed model (Equation 3.24) in comparison with the Austin and Palfrey (1964) model and Taylor's turbulent dispersion (1954) model.

The proposed model however overestimates the amount of contamination in the 0.124" and 0.313" diameter pipelines. One possible explanation for this discrepancy might be the short pipe lengths used in the experiments for these cases. The current section will focus on discussing the results for the long pipe experiments, while the short pipe cases of 0.124" and 0.313" will be discussed in a later section titled "Dispersion in short pipes." Table 3.2 compares the performance of the proposed model against Taylor's turbulent dispersion model (Taylor 1954).

Table 3.2: Comparison of model performance against Taylor's (1954) model.

d (in.)	2	4	6	8	10	12	20	40[a]
%AAD	13.4	8.9	4.1	5.4	7.7	6.3	22.2	0.6
%AAD[b]	58.5	11.6	6.0	20.6	25.9	6.3	23.6	0.7

[a]Only a single data point, [b]Taylor's turbulent dispersion model (Equation 2.12)

The improvements are easily discernible for all the diameters under investigation. It should be noted that Taylor's model (Taylor 1954) under-predicted the axial dispersion coefficient for all the data points, with higher deviations observed at lower Reynolds number. The proposed model on the contrary is fairly unbiased over a large Reynolds number range (Figure 3.14B).

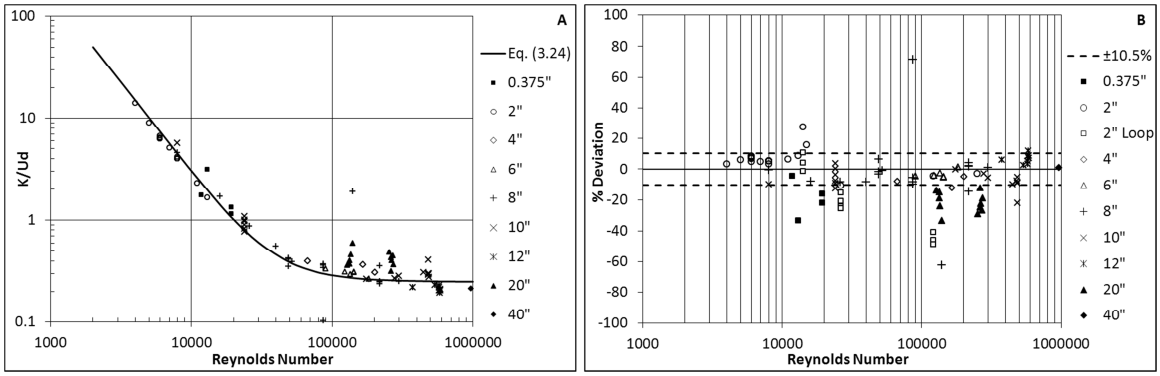

Figure 3.14: A) Dimensionless axial dispersion coefficients predicted using Equation (3.24) as a function of the *Re*, B) Bias plot for predictions using Equation (3.24) against *Re*.

The total *%AAD* for the 99 data points including the data from the loop experiments of Smith and Schulze (1948; 1948) falls around 11.5%. This drops to 10.5% when excluding the data from the loop experiments. Apart from the loop experiments, some data points in the higher Reynolds number range (around 150,000) also lay outside the 10.5 *%AAD* area. These belong to the 20" pipe experiments, indicating the poor performance of the model for this system. The proposed model performs fairly evenly through the entire range, with around 70% of the data points falling within a *%AAD* of 10% (and greater than 80% excluding loop experiment results and 20" pipe results). The model predictions for the loop experiments are represented using transparent squares (□) in Figure 3.14B. An obvious trend can be observed in the loop experiment predictions, with the model performance declining progressively as the Reynolds number deviates from about 13,000. The presence of pipe fittings in the experimental setup would result in enhanced mixing at higher Reynolds numbers.

The model consistently underperforms for the 20" experiments. An analysis of the calculations indicates that the contribution of the viscous dispersion coefficient for this system is an order of magnitude less than the turbulent coefficient, which is reasonable considering the high Reynolds numbers employed. This suggests that Taylor's predictions (Equation 2.12) for turbulent dispersion coefficient themselves are lower than those indicative of the experimental results. Likewise, the Austin and Palfrey (1964) empirical model does not improve the predictions by a significant margin. Austin and Palfrey (1964) attribute this disparity in the predictions to the presence of complicated pipe networks and valve switching at the inlet and exit. This seems a reasonable suggestion, as complicated pipe networks, fittings, pipeline debris, and valve switching tend to increase the flow friction factor, which will result in increased turbulent dispersion coefficient (Equation 2.12). This hypothesis was tested for the 20" pipe diameter case by increasing the wall roughness, which results in higher friction factors. It was found that increasing the wall roughness did result in higher turbulent dispersion coefficient and therefore higher contamination lengths, thereby reducing the percent deviation from the experimentally measured results. An equivalent roughness value of 0.36" corresponding to riveted steel reduced the *%AAD* to around 6.3%, with reduced bias.

Figure 3.15 shows a comparison of the predicted contamination lengths and the experimentally measured lengths. As discussed in the previous sections, contamination lengths increase with increasing pipe lengths. Figure 3.15 can therefore be considered as an indicator of the performance of the model with increasing pipe lengths. The data is fairly evenly distributed across the 45^{o} line (Slope ~ 0.94 for all data points) indicating that the model is reasonably impartial for increasing pipe lengths. The experimental results from the loop experiments are clearly higher than the predicted values and therefore lie outside the 10.5% deviation lines. Except for the data for the 20" pipeline (circled out in Figure 3.15) and a couple of other points (possibly outliers), most lie close to the area covered by the 10.5% deviation lines indicating the

robustness of the model. A slope less than one suggests that the model under-predicts the extent of contamination for higher pipe lengths. However, this is because of the discrepancies with the 20" pipeline data, excluding which results in a more favorable slope of 0.97.

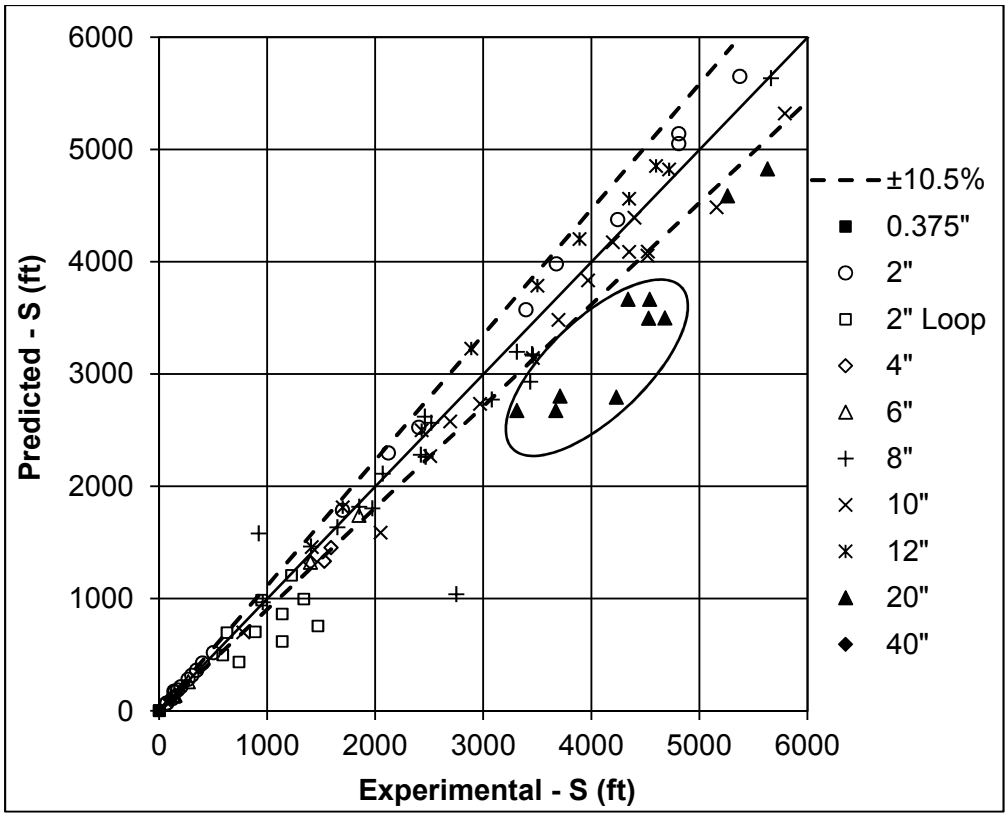

Figure 3.15: Comparison of predicted contamination lengths against experimental results.

Dispersion in short pipes

Taylor (1953; 1954) conducted the axial dispersion analysis assuming an equilibrium exists between the axial convective and radial diffusive transport. Such a condition requires the interface to reside in the pipe for a certain amount of time as specified by the equation given below (Equation 3.28) for laminar flow systems (Taylor 1953). Taylor's laminar dispersion equation (Equation 2.9) is only valid for interface residence times greater than the value of T estimated using Equation (3.28). Taylor's equations would over predict axial dispersion coefficient for all interface residence times less than this value.

$$T = \frac{R^2}{3.8^2 D} \tag{3.28}$$

Levenspiel (1958) by means of statistical analysis showed that Taylor's laminar dispersion equation over-predicts the results for Fowler and Brown's laminar flow data (Fowler and Brown 1943) because of the short pipe lengths employed in the experiments. A similar argument can be proposed for axial dispersion in turbulent flow. It is assumed that an equation similar to Equation (3.28) also holds for turbulent flow, albeit with the diffusion coefficient (D) being replaced with the radial eddy diffusivity (ε_r). It is common knowledge that eddy diffusivity increases with increasing Reynolds number and consequently the value for T would decrease with increasing Reynolds number. The proposed model is a variation on Taylor's analysis and therefore the above theory should also apply to the current model. Based on this theory, for a pipe with constant dimensions, the model prediction must improve considerably with increasing Reynolds numbers. Such a trend is observed in the model predictions for the turbulent flow data provided by Fowler and Brown (1943). Figure 3.16 shows the percent average deviation for the experimental data obtained in a 20.6 ft. long 0.313" diameter glass tubes.

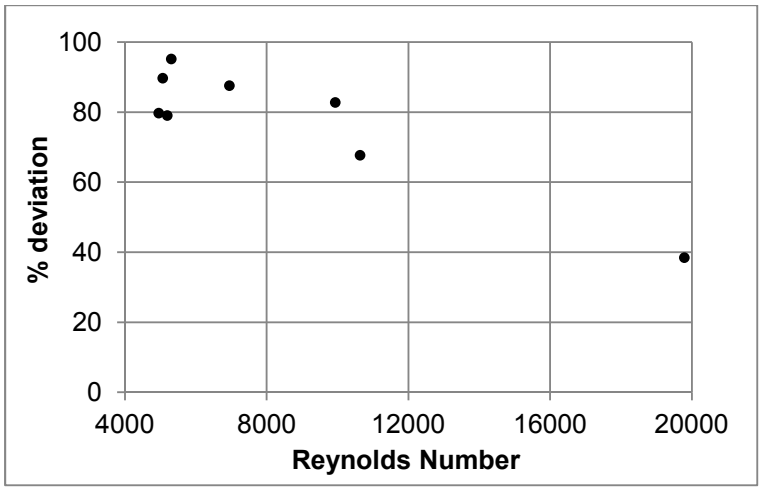

Figure 3.16: Percent deviation vs. Reynolds number for 20.6 ft. long, 0.313" diameter pipe.

It can therefore be concluded that the 0.313" experimental setups are possibly shorter than that required for the proposed model to be applicable. Similar explanation could be provided for the 0.124" lines. This however could not be quantitatively verified due to the lack of reported measurements from experiments with the same pipe length (Fowler and Brown 1943). Many investigators have proposed transient dispersion models for such scenarios (Gill 1966; Gill and Sankarasubramanian 1970; Dewey and Sullivan 1977; Soltanieh and Sadraei 1991). In these models, the axial dispersion coefficient is determined as a fraction (time dependent) of Taylor's axial dispersion coefficient calculated using Equation (3.24).

Soltanieh and Sadraei (1991) proposed a simple first order growth type exponential relationship to estimate the axial dispersion coefficient for short pipe lengths. The time dependent axial dispersion coefficient was expressed as

$$K(t) = K_{\infty} \cdot \left(1 - e^{-t/T}\right) \tag{3.29}$$

where K_{∞} is the steady state value of the axial dispersion coefficient, t is the residence time of the fluid in the pipe, and T is the time required to achieve steady state. Soltanieh and Sadraei (1991) performed mathematical manipulations on laminar flow dispersion equation and showed that the value of T should be estimated using Equation (3.28). Such an analysis was out of the scope of this investigation; however, simple trial-and-error estimations were carried out and dispersion fractions of 0.35 and 0.31 were determined for the 0.124" and 0.313" cases respectively. The steady state axial dispersion coefficients were estimated using these fractions and the axial dispersion coefficient values calculated from the short pipe experimental data (Figure 3.17). The proposed model (Equation 3.24) was able to predict the calculated steady state axial dispersion values with an accuracy of up to 5.1% *AAD* for the 0.124" pipe data and 8.2% *AAD* for the 0.313" pipe data. It should be noted that the above results were obtained by applying a constant value of the dispersion fraction to all experimental data for a particular pipe diameter. This however

would just be an approximation as the dispersion fractions should vary with the experimental pipe length. It would therefore be reasonable to suggest that better estimates for the dispersion fractions will reduce the bias and improve the accuracy of the current model.

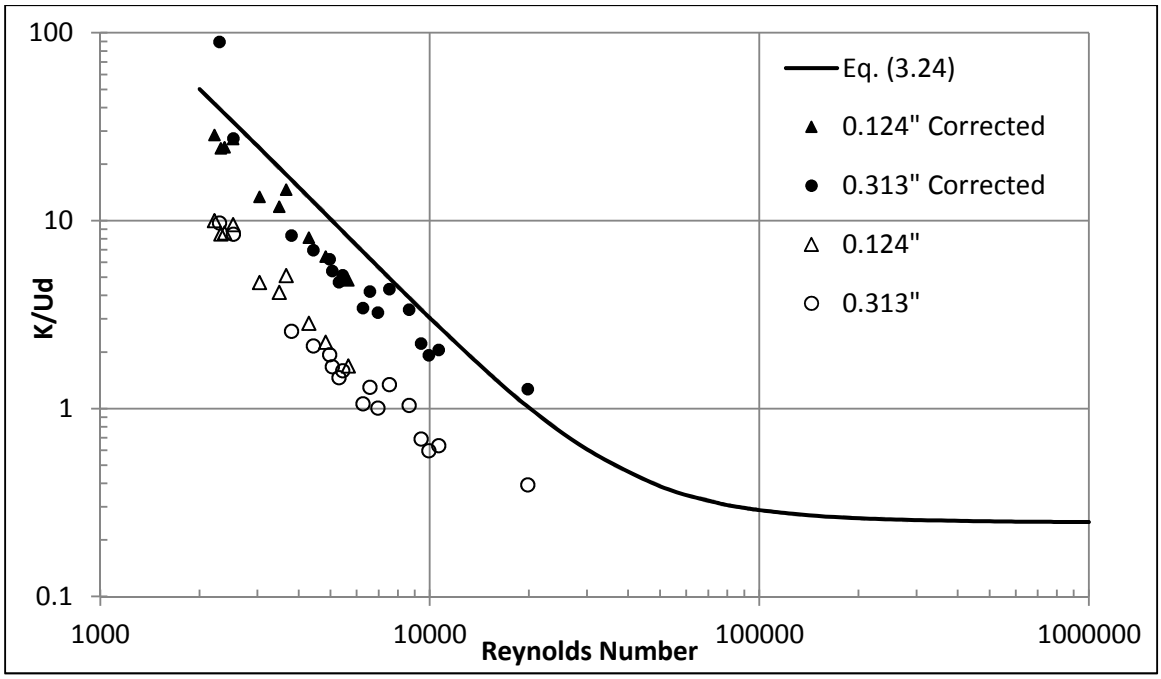

Figure 3.17: Model (Equation 3.24) performance on corrected short pipe experimental data (Fowler and Brown 1943).

Dewey and Sullivan (1977) in a separate investigation performed mathematical analysis to determine order of magnitude estimates (Equation 3.30) for the steady state time (T). Equation (3.30) resulted in values of T of the order of 5 sec for the conditions in the 0.124" experimental data and around 30 sec for the conditions in the 0.313" pipe data. Using these values of T in Equation (3.29) gives dispersion fractions in the order of 0.3 for the 0.124" pipe data and around 0.1 for the case of 0.313" pipe conditions respectively. These numbers are reasonably similar to the dispersion fractions estimated through trial-and-error procedures.

$$T = \mathcal{O}\left(\frac{1}{D}\left(\frac{15d}{\mathrm{Re}_\tau}\right)^2\right) \tag{3.30}$$

where, $\mathcal{O}$ denotes the order-of-magnitude operator, Re_τ is the Reynolds number based on the friction velocity instead of the average flow velocity.

Summary

This study was aimed at providing an insight into the effects of viscous forces on axial dispersion, while suggesting possible methodologies for incorporating the same in a mathematical form. The experimental results and their comparisons with the theory of wall bounded shear flows reveal a significant contribution of viscous effects to axial mixing during batched fluid transportations. A straightforward model has been proposed for predicting the axial dispersion coefficient (extent of contamination) for flow through straight pipes of circular cross-section without considering the effects of pipe fittings and other transport devices. The model builds on the basic theory of dispersion (Taylor 1922; Taylor 1953; Taylor 1954) by combining the convective-diffusion transport equation and boundary layer theory.

One possible technique for integrating the viscous and the turbulent effects into a single equation is to selectively add the contributions from the two effects. The resultant increase in the axial dispersion coefficient was more evident in transitional, low Reynolds number turbulent flow and it decreased rapidly at higher Reynolds numbers. This is very much in concurrence with the experimental observations. A value of 30 non-dimensional wall units has been proposed for approximating the thickness of the viscous region. It should be noted that the proposed model is a variation of Taylor's equations (Equation 2.9 and Equation 2.12) and the assumptions in Taylor's analysis (Taylor 1953; Taylor 1954) also apply to the current model. Therefore, the model would not be applicable for short pipe lengths where the convective and diffusive transports have not reached equilibrium.

As expected, the model performs much better than Taylor's turbulent dispersion analysis for low Reynolds number turbulent flows and its performance is also comparable with that of the

Austin and Palfrey empirical model (Equations 2.1-2.3). The predictions exhibit little or no bias in the contamination predictions over the range of Reynolds number and pipe dimensions investigated, signifying the robustness of the model. This is a substantial improvement for a conceptual model that does not use any of the experimental evidence on axial dispersion to formulate the equations. It should also be noted that the model is not completely theoretical in nature on account of the indirect empiricisms introduced by use the of the power-law velocity profile and friction factor correlations.

CHAPTER IV

ROLE OF TURBULENCE MECHANICS IN AXIAL DISPERSION

Axial dispersion is highly sensitive to variations in the Reynolds number and velocity profile. The extent or intensity of turbulence also has a significant influence on the process. A relatively slow moving, viscosity dominated near-wall region of the flow (the viscous sublayer) has been demonstrated to have a significant influence on axial dispersion (**Chapter III, Combined Taylor model of viscous and turbulent contributions**). Also, recent advancements in the field of turbulent flow have shown the viscous sublayer to be highly unsteady and constantly experiencing disturbances that result in ejections of the slow moving fluid from the viscous region into the faster moving turbulent core. Prior researches (Tichacek, Barkelew et al. 1957; Flint and Eisenklam 1969; Chatwin 1973; Krantz and Wasan 1974; Rachid, Araujo et al. 2002; Ekambara and Joshi 2003) have largely focused on improving the material transport property predictions and using improved velocity profile predictions. Not much effort has been devoted to quantifying the effects of the near-wall turbulence producing mechanisms on axial dispersion. In this work, it is hypothesized that the radial diffusion mentioned by Taylor (1954) in his visualization of the phenomenon, is a consequence of the ejection of materials from the viscous sublayer into the turbulent core. This chapter offers a phenomenological account of the influence of the near-wall turbulence producing bursts on longitudinal mixing. The purpose of this work is

to provide a framework that incorporates the turbulence producing events into the axial dispersion equation and thereby analyze the viability of the assumptions made in Taylor's (Taylor 1953; 1954) visualization of the phenomena.

Coherent structures in turbulent flow

Studies (Fage and Townsend 1932; Kline, Reynolds et al. 1967; Corino and Brodkey 1969; Kim, Kline et al. 1971; Morrison, Bullock et al. 1971; Narahari Rao, Narasimha et al. 1971; Wallace, Brodkey et al. 1972; Eckelman.H, Wallace et al. 1974; Wallace, Brodkey et al. 1977; Blackwelder and Haritonidis 1983; Tiederman 1988; Robinson 1991; Antonia and Krogstad 1993; Metzger, McKeon et al. 2010) on the production and dissipation of near-wall or boundary-layer turbulence have shown that the near-wall region contributes significantly to the total turbulent stress in a flow system. Studies report flow visualizations that identify the presence of turbulent structures arising from spanwise vortices in the viscous sublayer, with a hairpin or worm shaped head at the top end of these structures. These structures are not completely random; they have characteristic periodic and spatial patterns associated to their presence. The term turbulent bursts was first used by Kim et al. (1971) to describe a process in which slow moving fluid from near the wall suddenly lift upwards into the high speed flow that exists farther towards the pipe center, and break up releasing low momentum fluid into the outer region of the turbulent boundary layer. The phenomenon of turbulent bursts along with turbulent sweeps is collectively termed as a turbulent bursting event. Turbulent sweeps refer to a large scale motion of the high speed fluid in the outer region, moving towards the wall (Corino and Brodkey 1969). Turbulent bursting events contribute to almost all of the turbulent production in the near-wall region (Kim, Kline et al. 1971; Metzger, McKeon et al. 2010), and are therefore extremely important in understanding the physics of turbulence.

Many different theories (Kline, Reynolds et al. 1967; Kim, Kline et al. 1971; Robinson 1991) have been proposed for the generation of hairpin and worm vortices that lead to the turbulent bursting events. One commonly discussed mechanism for generation of hairpin vortices involves a sudden streamwise perturbation disturbing the spanwise vortices commonly visualized in the viscous near-wall region. Figure 4.1 depicts a typical sequence for a bursting event. The incoming streamwise disturbances bend the unperturbed spanwise vortices into arcs that resemble a hairpin. This influences the vortices to rotate in the streamwise direction and push the slow moving fluid in the viscous region away from the wall. The fluid elements that are pushed upwards, initially travel slowly away from the wall and soon reach a region with a higher mean stream velocity, stretching even further and leading to a sudden loss of stability, resulting in violent bursts. It should be noted that the above description of generation of a turbulent burst is highly idealized, and is one of the commonly cited theories in literature. Alternative theories for turbulent bursts can be found in literature (Robinson 1991) and are not considered for further discussion as they fall outside the scope of this study.

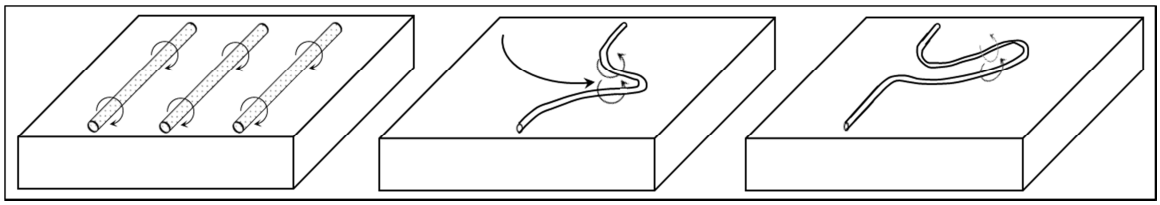

Figure 4.1: Cycle of events resulting in turbulent bursts. Adapted from Davidson (2004).

Turbulent bursts are considered as a major contributor to momentum (kinetic energy) transfer from the near-wall region into the turbulent core. Similar conclusions can also be made on the influence of bursting events on transport of mass from the viscous region to the turbulent core. Turbulent bursting events result in ejection of slow moving fluid from the viscous region in a direction away from the wall. They therefore can be considered as a major contributor to the transport of mass (and energy), in addition to that of momentum from the viscous region into the

turbulent core. Models incorporating turbulent bursting events have been employed with a certain degree of success in depicting the transport of sedimentary particles in river beds (Cleaver and Yates 1973; Cao 1997) and for convective heat transfer calculations (Hetsroni, Yarin et al. 1996; Chen 2007) in turbulent flow. The success of these models bolsters the notion that the theory of transport caused by turbulent bursts should also be applicable to axial dispersion, and probably is one of the significant mechanisms that control the extent of longitudinal dispersion.

Estimation of the exact contribution of the bursting mechanism to mass transport would require information pertaining to the spatial and periodic distribution of turbulent bursts in a flow field. Numerous investigators (Fage and Townsend 1932; Kline, Reynolds et al. 1967; Kim, Kline et al. 1971; Narahari Rao, Narasimha et al. 1971; Wallace, Brodkey et al. 1972; Wallace, Brodkey et al. 1977; Smith and Metzler 1983) have performed flow visualization experiments to study the structure of the viscous region in turbulent flow conditions. Coherent structures and slow moving streaks are observed at distances as close as 3 non-dimensional wall units (y^+) from the wall (Wallace, Brodkey et al. 1972), as well as some reporting streaks visualized to distances of $y^+ \sim 100$ from the wall (Kline, Reynolds et al. 1967; Corino and Brodkey 1969; Morrison, Bullock et al. 1971; Wallace, Brodkey et al. 1972). Most streaks and coherent structures, though, are observed up to a distance of around 10-40 wall units from the wall (Corino and Brodkey 1969; Morrison, Bullock et al. 1971), which has been reported as a statistical average in some studies. From the various quantities reported in the literature, a typical coherent structure (hairpin shaped vortex) that ends in a turbulent burst can be approximated as rectangular jets with a cross-section spanning 40 × 25 wall units (or cylindrical jets with diameters of about 25 wall units), inclined at around $40 \sim 50^o$ to the wall surface, the angle of inclination of the legs of the hairpin (Kline, Reynolds et al. 1967; Kim, Kline et al. 1971; Narahari Rao, Narasimha et al. 1971; Wallace, Brodkey et al. 1972). This information on the size of the coherent structures is useful in quantifying the amount of material being transported per burst in a turbulent flow environment.

Kline et al. (1967), Morrison et al. (1971), and Fage and Townsend (1932) have all reported the presence of characteristic spatial patterns to the bursting streaks. Kline et al. (1967) reported the average value of spanwise streak spacing to be approximately 100~130 wall units, with Morrison et al. (1971) also reporting a similar number (~ 135). There exists some deviation in literature on the streamwise wavelength (spacing) of the bursting streaks. Morrison et al. (1971) from their measurements estimated the streamwise spacing of the streaks to be 630 wall units, while Kline et al. (1967) suggests that the structures could grow to as long as 1000 wall units in the streamwise direction before disintegrating and begin the formation of the next streak. Other researchers have reported numbers varying in the range x^+ = 250~600, with Pope (2000) reporting a value of $80\delta_V$-120 δ_V (400~600 wall units), which are similar to numbers reported by Morrison et al. (1971) for the streamwise spacing between the streaks. For consistency, the streak wavelengths as reported by Morrison et al. (1971) for flow through pipes will be used in this study.

A large number of studies (Runstadler, Kline et al. 1963; Laufer and Badri Narayan 1971; Strickland and Simpson 1975; Blackwelder and Kaplan 1976; Bandyopadhyay 1982; Luchik and Tiederman 1987; Alfredsson and Johansson 1988; Shah and Antonia 1989) have been conducted to quantify the time scales related to bursting, as compared to the spatial distributions of the bursts. Turbulent bursts are random events and there exist no defined relation to quantify the time between two consecutive bursts (Tiederman 1988). Multiple burst detection methods are available in literature; these include the U-level method, Quadrant method, Variable Integral Time Average (VITA) method, and the modified U-level method. Each method uses a unique technique to detect bursting events and therefore the data obtained from each of these analyses are varied in nature. These variation in determining the average turbulent burst period ($\overline{T}$) have resulted in significant scatter in the information available in the literature (Bandyopadhyay 1982; Robinson 1991). Even though extensive investigations have been carried out; there exists a

considerable debate on scaling aspects for turbulent bursting event time scales. Several different parameters have been identified for scaling the average time between the turbulent bursts in a boundary layer. The scaling can be carried out in terms of inner variables, outer variables, or a mixture of the two or based on Taylor microscales. Different authors report different findings based on the observations from their respective experiments. The inner and the mixed variables have been frequently reported to be successful in scaling the burst frequency for high Reynolds number turbulent flows. Recent studies on rough wall boundary layers though indicate otherwise (Antonia and Krogstad 1993). Certain investigations (Metzger, McKeon et al. 2010) also report that the Reynolds number and wall normal trends observed in the outer and inner variable scaling techniques can be eliminated by using Taylor microscales for scaling the burst period. This lack of agreement has been commonly attributed to the scatter in the turbulent bursting period data obtained from different burst detection techniques (Blackwelder and Haritonidis 1983). A detailed discussion of the different scaling techniques in literature would be outside the scope of this study. The turbulent burst period obtained based on inner (viscous wall) variables will be employed in the current study and a commonly quoted value in the range 60-90 would be used as the non-dimensional bursting period (Narahari Rao, Narasimha et al. 1971; Cleaver and Yates 1973; Kim and Spalart 1987; Luchik and Tiederman 1987; Hetsroni and Mosyak 1996).

Role of turbulent bursts in axial dispersion

Experimental visualizations reveal a distinct persistence in the pattern of how low-speed streaks appear in the near-wall region of shear flows. Knowledge of the structure of low-speed streaks and turbulent bursts as obtained from experimental evidence can be used to estimate the total amount of lateral or radial mixing that might occur in a system. An idealized picture of the experimental visualizations is considered in the current analysis. The pipe cross-section is considered to be composed of two distinct areas visualized as concentric pipes. The inner cylinder in the cross-section representing the turbulent core, and the area in the annulus

considered to represent the viscous wall region. It is assumed that the surface of the viscous wall region is covered with upward rising jets that eject fluid from the viscous region in the turbulent core. Each jet represents a coherent structure in the near-wall region that develops into a bursting event farther away from the pipe wall (Figure 4.2). The size and distribution of these jets of fluids can be approximated from the visualizations of the coherent structures and the slow moving streaks that have been summarized in the previous section.

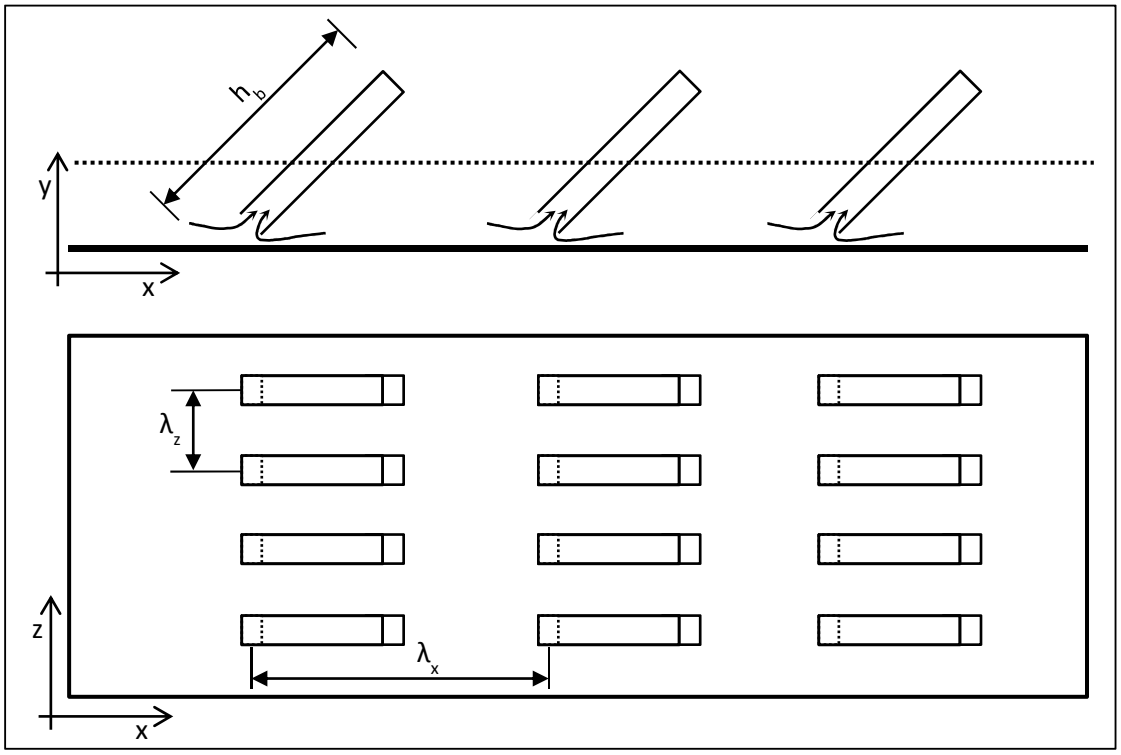

Figure 4.2: Elevation and plan view of the modeled visualization of the distribution of the coherent structures and slow moving streaks.

Turbulent bursts affect the extent of axial dispersion by directly influencing the magnitude of radial mixing. According to Taylor's visualization of axial dispersion (Taylor 1953; Taylor 1954), the amount of radial diffusion of materials between the layers of fluid moving at different velocities in the flow field regulates axial dispersion. Taylor's theory of axial dispersion, being sensitive to radial mixing, has been experimentally and theoretically supported

by investigations that study the effect of secondary flow on axial dispersion (Koutsky and Adler 1964; Aunicky 1968; Cassell and Perona 1969; Zhao and Bau 2007). The onset of secondary flow results in circular motions in the fluid, resulting in rapid mixing across the cross-section. Studies have shown that secondary flow in pipes results in increased radial mixing and therefore a reduction in axial dispersion as compared to cases without secondary flow (Koutsky and Adler 1964; Aunicky 1968; Cassell and Perona 1969; Zhao and Bau 2007).

As described earlier, slow moving vortex tubes that culminate in turbulent bursts pull liquid from the viscous region and eject them into the turbulent core. The total size (or intensity) and frequency of these bursts would therefore directly influence the amount of material being pushed in the radial direction, thereby dictating the total intensity of radial mixing. Turbulent bursting events can consequently be believed to have a significant influence on the extent of axial dispersion and quantifying these effects would be crucial in accurate estimation of the axial dispersion coefficient.

The intensity of radial mixing caused by turbulent bursts can be expressed as the volume of liquid being ejected from the bursts, per unit area of the bursting surface. The total volume of liquid being ejected from a single burst can be calculated as

$$V_{Ejected}/Burst = \left(l_b^+ \nu/u_\tau\right)\left(w_b^+ \nu/u_\tau\right)\left(h_b^+ \nu/u_\tau\right) \tag{4.1}$$

This volume of liquid ejected per burst multiplied by the spatial frequency of the bursts would give the total volume of liquid ejected into the turbulent core per unit area of the bursting surface. The spatial distribution of the bursts can be determined based on the experimentally observed burst spacing/wavelengths. Typically, one turbulent ejection is observed in an area defined by the longitudinal and transverse wavelengths. The spatial frequency can therefore be estimated as

$$Burst/Area = 1/A_b = 1/\left(\lambda_x^+ \nu/u_\tau\right)\left(\lambda_z^+ \nu/u_\tau\right) \tag{4.2}$$

The total volume of fluid ejected per unit area per unit time can therefore be given using

$$\dot{V}/A_b = \frac{\left(l_b^+\nu/u_\tau\right)\left(w_b^+\nu/u_\tau\right)\left(h_b^+\nu/u_\tau\right)}{\left(\lambda_x^+\nu/u_\tau\right)\left(\lambda_z^+\nu/u_\tau\right)\overline{T}} = \left(\frac{l_b^+ \cdot w_b^+ \cdot h_b^+}{\lambda_x^+ \cdot \lambda_z^+}\right)\frac{\nu}{u_\tau \overline{T}} \tag{4.3}$$

where, $\overline{T}$ is the average time between two burst (inverse of the periodic bursting frequency). This can be further simplified using the expression for the bursting period in terms of the inner variables, the friction velocity, and viscosity to give

$$\dot{V}/A_b = \left(\frac{l_b^+ \cdot w_b^+ \cdot h_b^+}{\lambda_x^+ \cdot \lambda_z^+}\right)\frac{\nu}{u_\tau}\frac{u_\tau^2}{T_b^+\nu} = \left(\frac{l_b^+ \cdot w_b^+ \cdot h_b^+}{\lambda_x^+ \cdot \lambda_z^+ \cdot T_b^+}\right)u_\tau \tag{4.4}$$

The total radial eddy diffusivity can therefore be estimated by assuming the same constant rate of volume ejection from one layer in the turbulent core to the next.

$$\varepsilon_r = \left(\frac{l_b^+ \cdot w_b^+ \cdot h_b^+}{\lambda_x^+ \cdot \lambda_z^+ \cdot T_b^+}\right)u_\tau \cdot \left(2\pi R\right) = 2\pi u_\tau R \cdot k'' \tag{4.5}$$

$$k'' = \left(\frac{l_b^+ \cdot w_b^+ \cdot h_b^+}{\lambda_x^+ \cdot \lambda_z^+ \cdot T_b^+}\right) \tag{4.6}$$

where, k'' is a constant, used to consolidate the burst terms into a single parameter.

Estimation of turbulent axial dispersion coefficient

The expression for radial mixing due to the turbulent bursting structures can be translated into axial dispersion coefficient by substituting Equation (4.5) for the eddy diffusivity term for D in the convective-diffusion equation (Equation 2.7).

$$\frac{\partial C}{\partial t} + \left(u - \bar{U}\right)\frac{\partial C}{\partial x} = D\left[\frac{\partial^2 C}{\partial x^2} + \frac{1}{r}\frac{\partial}{\partial r}\left(r\frac{\partial C}{\partial r}\right)\right] \tag{2.7}$$

Use of Equation (4.5) as the only source of diffusion coefficient is justified as the contribution of molecular diffusivity to radial mixing in the turbulent core would be negligible compared to the mixing due to turbulent bursts. It should be noted that Taylor (1954) used Reynolds analogy to approximate the eddy diffusivity in turbulent flow systems. This investigation solves the convective-diffusion equation using the same velocity profile used in Taylor's analysis (1954), so as to focus on the improvements to the analysis purely from the turbulent burst perspective. The convective-diffusion equation for the transport of concentration in the axial direction (x) using the eddy diffusivity determined from turbulent structures can therefore be written as

$$\frac{\partial C}{\partial t} + u\frac{\partial C}{\partial x} = \frac{1}{r}\frac{\partial}{\partial r}\left(\varepsilon_r r \frac{\partial C}{\partial r}\right) \tag{4.7}$$

$$\therefore \frac{\partial C}{\partial t} + u\frac{\partial C}{\partial x} = \frac{1}{r}\frac{\partial}{\partial r}\left(2\pi u_\tau R k'' r \frac{\partial C}{\partial r}\right) \tag{4.8}$$

Replacing the radius terms with its scaled form gives

$$Rz\left(\frac{\partial C}{\partial t} + u\frac{\partial C}{\partial x}\right) = 2\pi u_\tau k''\frac{\partial}{\partial z}\left(z\frac{\partial C}{\partial z}\right) \tag{4.9}$$

where, $z = r / R$. Transforming the above equation to an axis that moves with the mean speed of flow ($\bar{U}$) results in

$$Rz\left(\left.\frac{\partial C}{\partial t}\right|_1 + \left(u - \bar{U}\right)\frac{\partial C}{\partial x_1}\right) = 2\pi u_\tau k''\frac{\partial}{\partial z}\left(z\frac{\partial C}{\partial z}\right) \tag{4.10}$$

$$\left.\frac{\partial C}{\partial t}\right|_1 = \frac{\partial C}{\partial t} + \bar{U}\frac{\partial C}{\partial x} \tag{4.11}$$

where, x_1 is the moving axis calculated as: $x_1 = x - \bar{U}\,t$. Now, substituting the scaled velocity profile in the above equation for the case of $\partial C/\partial t|_1 \rightarrow 0$, results in,

$$-Rz\left\{u_\tau f\left(z\right)-u_0+\bar{U}\right\}\frac{\partial C}{\partial x_1}=2\pi u_\tau k''\frac{\partial}{\partial z}\left(z\frac{\partial C}{\partial z}\right) \tag{4.12}$$

with, the velocity profile being expressed using Equation (2.10) and u_0 being the pipe centerline velocity. Expressing the mean flow velocity in terms of the centerline velocity and the friction velocity (refer to Taylor (Taylor 1954) for details) the above equation can be rewritten as

$$\therefore \frac{\partial}{\partial z}\left(z\frac{\partial C}{\partial z}\right)=-\frac{Rz}{2\pi k''}\left\{f\left(z\right)-2\int_0^1\left\{zf\left(z\right)\right\}dz\right\}\frac{\partial C}{\partial x_1} \tag{4.13}$$

$$\bar{U}=u_0-2u_\tau\cdot\int_0^1\left\{zf\left(z\right)\right\}dz=u_0-4.25u_\tau \tag{4.14}$$

$$f\left(z\right)=\frac{u_0-u_\tau}{u_\tau} \tag{2.10}$$

The solution for the concentration profile (C_z) across the cross section of the pipe can be obtained by solving Equation (4.13), assuming $\partial C/\partial x_1$ to be constant across the cross-section of the pipe. The numerical calculations involved in the solution to above equation are listed in Table 4.1. Each column in Table 4.1 lists the value of a particular expression as a function of the scaled radius (z). The function terminologies are chosen so as to be consistent with Taylor's solution (Taylor 1954).

$$\phi\left(z\right)=\int_0^z z\left(f\left(z\right)-2\int_0^1\left\{zf\left(z\right)\right\}dz\right)dz \tag{4.15}$$

$$\psi\left(z\right)=\phi\left(z\right)/z \tag{4.16}$$

$$\therefore \frac{\partial C}{\partial z}=-\frac{1}{z}\left(\frac{Ru_\tau}{k}\frac{\partial C}{\partial x_1}\right)\phi\left(z\right)=-\left(\frac{R}{2\pi k}\frac{\partial C}{\partial x_1}\right)\psi\left(z\right) \tag{4.17}$$

Table 4.1: Calculations to solve the convective-diffusion equation.

z	$f(z)$	$f'(z)$	$zf(z)$	$\int zf(z)$	$f(z)-2\int zf(z)$	$\phi(z)$	$\int\phi(z)$	$-\int\phi(z)$	$1/z$	$-\psi(z)$	$-\int\psi(z)$	$\chi(z)$	$\int\chi(z)$
0.00	0.00	0.00	0.00	0.00	-4.70	0.00	0.00	0.00	-	-	0.00	0.00	0.00
0.10	0.059	1.18	0.01	0.00	-4.64	-0.46	-0.05	0.05	10.00	0.46	0.05	0.02	0.00
0.20	0.236	2.36	0.05	0.01	-4.46	-0.89	-0.14	0.14	5.00	0.68	0.11	0.10	0.01
0.30	0.53	3.43	0.16	0.02	-4.17	-1.25	-0.26	0.26	3.33	0.87	0.20	0.25	0.04
0.35	0.75	4.8	0.26	0.03	-3.95	-1.38	-0.33	0.33	2.86	0.94	0.25	0.34	0.05
0.40	1.01	5.4	0.40	0.05	-3.69	-1.47	-0.40	0.40	2.50	1.01	0.30	0.44	0.08
0.45	1.29	6.1	0.58	0.08	-3.41	-1.53	-0.48	0.48	2.22	1.07	0.35	0.54	0.10
0.50	1.62	7.1	0.81	0.12	-3.08	-1.54	-0.56	0.56	2.00	1.11	0.41	0.63	0.13
0.55	2	8	1.10	0.18	-2.70	-1.48	-0.63	0.63	1.82	1.15	0.46	0.69	0.17
0.60	2.42	8.9	1.45	0.25	-2.28	-1.37	-0.70	0.70	1.67	1.17	0.52	0.71	0.20
0.65	2.89	9.8	1.88	0.35	-1.81	-1.17	-0.76	0.76	1.54	1.17	0.58	0.68	0.24
0.70	3.4	11.6	2.38	0.46	-1.30	-0.91	-0.80	0.80	1.43	1.15	0.64	0.58	0.27
0.75	4.05	14	3.04	0.62	-0.65	-0.48	-0.83	0.83	1.33	1.10	0.69	0.34	0.28
0.80	4.8	17.4	3.84	0.81	0.10	0.08	-0.82	0.82	1.25	1.03	0.75	-0.06	0.28
0.85	5.79	23	4.92	1.05	1.09	0.93	-0.78	0.78	1.18	0.91	0.79	-0.74	0.24
0.90	7.1	26.71	6.39	1.37	2.40	2.16	-0.67	0.67	1.11	0.74	0.83	-1.79	0.16
0.92	7.66	31.75	7.05	1.51	2.96	2.73	-0.61	0.61	1.09	0.67	0.84	-2.30	0.11
0.94	8.37	42.5	7.87	1.67	3.67	3.45	-0.54	0.54	1.06	0.58	0.85	-2.95	0.05
0.96	9.36	58	8.99	1.85	4.66	4.48	-0.46	0.46	1.04	0.47	0.86	-3.86	-0.03
0.97	10.11	88	9.81	1.95	5.41	5.25	-0.40	0.40	1.03	0.42	0.87	-4.55	-0.07
0.98	11.12	137	10.90	2.06	6.42	6.30	-0.34	0.34	1.02	0.35	0.87	-5.48	-0.13
0.99	12.85	250	12.72	2.19	8.15	8.07	-0.26	0.26	1.01	0.26	0.87	-7.05	-0.20
1	16.12	327	16.12	2.35	11.42	11.42	-0.14	0.14	1.00	0.14	0.87	-9.99	-0.2975

$$\therefore C_z = -\left(\frac{R}{2\pi k''}\frac{\partial C}{\partial x_1}\right)\int_0^z \psi(z) \tag{4.18}$$

Simple numerical techniques are used in the calculations of these parameters. The derivatives are estimated using the forward or central difference approximations, while the integration is carried out using the rectangular rule of integration.

The total transport of the material across the pipe cross section can therefore be calculated as

$$Q = \left(\pi R^2\right)\int_0^1 2\left(u - \bar{U}\right)zC_z dz \tag{4.19}$$

$$\therefore Q = 2\pi R^2\left(\frac{R}{2\pi k''}\frac{\partial C}{\partial x_1}\right)\int_0^1 \chi(z)\,dz \tag{4.20}$$

where, $\chi(z) = -u_\tau z\{f(z) - 4.25\}\int_0^z \psi(z)\,dz$

The overall axial dispersion coefficient can be calculated by dividing the total transport of the material across the cross section (Q) by the concentration gradient and the cross-sectional area.

$$Q = -\left(\pi R^2\right)K_T\frac{\partial C}{\partial x_1} \tag{4.21}$$

$$\therefore K_T = \left[-\frac{1}{\pi k''}\int_0^1 \chi(z)\,dz\right]Ru_\tau \tag{4.22}$$

The structure of the above axial dispersion equation is very similar to the one proposed by Taylor (1954) for turbulent flow, with the difference that the constant number in Taylor's equation (Equation 2.12) is replaced with the bracketed term in Equation (4.22). The value of this term

would be obtained from the characteristics of the turbulent bursting structures. Substituting Equation (4.6) in the above expression gives,

$$K_T = \left[-\frac{1}{\pi} \left(\frac{\lambda_x^+ \cdot \lambda_z^+ \cdot T_b^+}{l_b^+ \cdot w_b^+ \cdot h_b^+} \right) \int_0^1 \chi(z)\, dz \right] Ru_\tau \tag{4.23}$$

The value for $\int \chi(z) dz$ is estimated using numerical approximations (Table 4.1) to be -0.2975. Substituting this number, and dividing with the value of π reduces Equation (4.23) to

$$K_T = 0.0947 \left(\frac{\lambda_x^+ \cdot \lambda_z^+ \cdot T_b^+}{l_b^+ \cdot w_b^+ \cdot h_b^+} \right) Ru_\tau \tag{4.24}$$

This equation can be further simplified by inserting values for the various characteristic dimensions of the low-speed streaks to obtain the final form of the axial dispersion equation similar to the one proposed by Taylor (1954). Using the values of the turbulent burst characteristic dimensions listed in Table 4.2, the axial dispersion coefficient equation reads

$$K_T = 14.238 Ru_\tau \tag{4.25}$$

Table 4.2: Characteristic scales used in axial dispersion coefficient estimation (Equation 4.25).

Burst Characteristic	Value (dimensionless)	Scaling Equation
Longitudinal Spacing (λ_x^+)	630	$\lambda_x^+ = \lambda_x u_\tau / \nu$
Lateral Spacing (λ_z^+)	135	$\lambda_z^+ = \lambda_z u_\tau / \nu$
Period (T_b^+)	75	$T_b^+ = \overline{T} u_\tau^2 / \nu$
Angle (degrees)	45	
Length (l_b^+)	40	$l_b^+ = l_b u_\tau / \nu$
Width (w_b^+)	25	$w_b^+ = w_b u_\tau / \nu$
Height (h_b^+)	30 / Sin(45^o)	$h_b^+ = h_b u_\tau / \nu$

Comparison with Taylor's dispersion equation

The current equation for axial dispersion coefficient (Equation 4.23), which has been developed considering the influence of turbulent bursting events suggests the axial dispersion coefficient to be directly proportional to pipe diameter, the average velocity in the pipe and the friction factor. This is exactly the same as proposed by Taylor (1954) in his analysis, assuming Reynolds analogy for equivalence between mass and momentum transport. The similarity to Taylor's analysis seems reasonable considering that turbulent bursts have been suggested to be a major contributor to transport of momentum from the near-wall regions to the turbulent core. If such a scenario does exist, it can be concluded that the same mechanism results in the transport of momentum, mass, and even energy from the wall to the turbulent core, thereby supporting Taylor's (1954) assumption of the Reynolds analogy in his initial development of axial dispersion coefficient in turbulent flow of liquids through straight pipes.

The proposed model differs from Taylor's equation for axial dispersion (Equation 2.12) in just the constant multiplying term. It should however be noted that the constant of proportionality is of the same order of magnitude as in Taylor's (1954) equation, though higher by around 40%. The reason for the increased magnitude of prediction is the influence of the viscous region, which was excluded by Taylor in his analysis. Similar deviations from Taylor's model (Equation 2.12) have also been reported by Chatwin (Chatwin 1971; Chatwin 1973), Tichacek et al. (1957), Flint and Eisenklam (1970), and Chikwendu and Ojiakor (1985) through their respective investigations. Tichacek et al. (1957) reported deviations in the order of 50% in the axial dispersion coefficient prediction when solving the convective-diffusion equation, resulting from as little as 3% variations in the velocity profile. Employing the correct velocity profile however does not improve the accuracy of the predictions at lower Reynolds numbers, where deviations as high as 1000% (from Taylor's equation (Equation 2.12)) have been observed. Such deviations can only be explained by the absence of the viscous molecular diffusion

parameter, which would play a significant role in the viscosity dominated near-wall regions of the flow.

The proposed equation (Equation 4.23) only partially considers the effects of viscous dispersion (diffusion), and would therefore not improve the predictions for low Reynolds number turbulent flows similar to Taylor's analysis (Equation 2.12). Improved predictions in the low Reynolds number turbulent flow regions will require the model to consider separate diffusion/mixing characteristics in the viscosity dominated region of the flow. These parameters have not fully considered in the proposed equation. One way to incorporate the effects of viscous mixing on axial dispersion would be by modeling the overall axial dispersion as an area weighted average of the turbulent dispersion and viscous dispersion coefficients as described in Chapter III (**Combined Taylor model of viscous and turbulent contributions**).

The magnitude of axial dispersion coefficient estimated by the current model uses empirical values for several parameters, specifically the turbulent bursting characteristic scales. In addition to the empirical nature of these parameters, literature sources (Fage and Townsend 1932; Kline, Reynolds et al. 1967; Kim, Kline et al. 1971; Narahari Rao, Narasimha et al. 1971; Wallace, Brodkey et al. 1972; Wallace, Brodkey et al. 1977; Smith and Metzler 1983) listing the values of these parameters do not agree on a single value but rather a range of values that might be possible for each characteristic scale. It would therefore not be correct to highlight the similarity of magnitude of proposed calculations to Taylor's (1954) equations; it would however be reasonable to suggest that the model vindicates Taylor's assumptions, while providing a mechanistic standpoint to the phenomenon resulting in axial dispersion. From a physical perspective, the mechanism indicates that increasing the Reynolds number of flow will result in quicker, closely spaced bursts than at a lower Reynolds number, thus resulting in uniform mixing of the material in the viscous and turbulent core regions and therefore lower axial dispersion.

Rigorous recalculations in the viscous sublayer region

Taylor's technique (Taylor 1954) of deriving an expression for axial dispersion coefficient as a function of the diffusion characteristics and velocity profile can be reformulated to obtain better accuracy even in the low Reynolds number turbulent regime. Chapter III introduced a straight-forward technique to estimate an effective axial dispersion coefficient as a combination of Taylor's laminar (Equation 2.9) and turbulent (Equation 2.12) axial dispersion equations (Taylor 1953; Taylor 1954). The model presented in Chapter III was based on elementary mathematical manipulations using the concepts of transport phenomena, as opposed to rigorous solutions of the fundamental convective-diffusion equation (Equation 2.7). Various articles (Tichacek, Barkelew et al. 1957; Atesman, Baldwin et al. 1971; Chatwin 1971; Chatwin 1973; Maron 1978; Ekambara and Joshi 2003) are available in the literature that have reported such estimations. The use of accurate velocity profiles along with a multi-layer type formulation has been suggested to significantly improve predictions for axial dispersion coefficient (Chatwin 1971; Chatwin 1973; Udoetok and Nguyen 2009). Most of the multi-layer models have been solved using different velocities at the various layers, but the same diffusion characteristics (turbulent diffusivity) and therefore do not provide accurate estimations. The success of the combined Taylor model from Chapter III suggests that the use of molecular diffusivity in the viscous region and turbulent diffusivity in the central region would improve the model predictions. This section presents an attempt to verify if an equation of similar structure to Equation (3.24) can be derived directly from the convective-diffusion equation as opposed to a direct modification as presented in Chapter III.

Velocity profile

The velocity profile employed in the calculations would play a significant role when performing rigorous estimations to include the viscous effects. Taylor (1954) employed the

universal velocity profile for all estimations in the turbulent regime and assumed that this velocity profile would remain the same for all Reynolds numbers in turbulent flow. This however would not be correct as the velocity profile is known to change drastically with varying Reynolds numbers, and this is especially true for the near-wall region of the flow. In addition to the velocity profiles, it is also common knowledge (Pope 2000) that the thickness of the various regions of the flow-field (viscous sublayer, buffer layer, etc.) change with the Reynolds number (Figure 4.3). Since the basic idea of this work is to employ a multi-layer type of framework, the thicknesses of the various layers in the flow field are of extreme importance. It is therefore imperative that better formulations of the velocity profiles are employed in axial dispersion estimations.

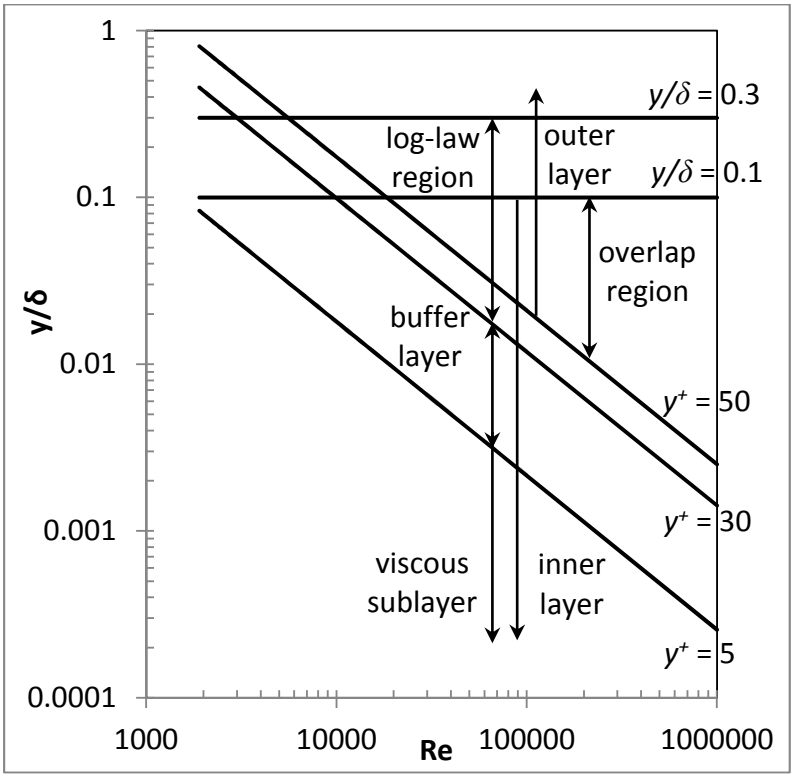

Figure 4.3: Thickness of various regions of a flow-field in turbulent channel flow as a function of the Reynolds number. Adapted from Pope (2000).

A commonly employed version of the universal turbulent velocity equations (McCabe, Smith et al. 2005) are used to estimate the velocity profile over the cross-section for the current set of axial dispersion calculations. The equations based on three layers observed in a turbulent flow cross-section are given as

$$u^+ = y^+ \tag{4.26}$$

$$u^+ = 5.00 \cdot \ln\left(y^+\right) - 3.05 \tag{4.27}$$

$$u^+ = 2.5 \cdot \ln\left(y^+\right) + 5.5 \tag{4.28}$$

where, u^+ is the dimensionless velocity quotient defined as a ratio of the local velocity (u) to the friction velocity (u_τ). Equation (4.26) is applicable in the viscous sublayer ($y^+ \leq 5$), Equation (4.27) in the buffer layer ($y^+ \leq 30$), and Equation (4.28) for the turbulent core ($y^+ > 30$) extending up to the center of the pipe.

The variations in the velocity profile (Equation 2.10) for different Reynolds numbers is given in Figure 4.4. The universal velocity profile employed by Taylor is also added to the figure in order to compare the extent of deviation from the currently used equations. The velocity profiles do not deviate by much for the different Reynolds numbers in the central turbulent core ($1 - z > 0.2$). The deviations in the velocity profile are however very noticeable in the near-wall regions of the flow. The deviations are particularly noticeable for the low Reynolds number (Re = 4119) case, where the steep velocity profile region extends up to around a dimensionless distance of 0.1 from the wall as opposed to the velocity profile employed by Taylor.

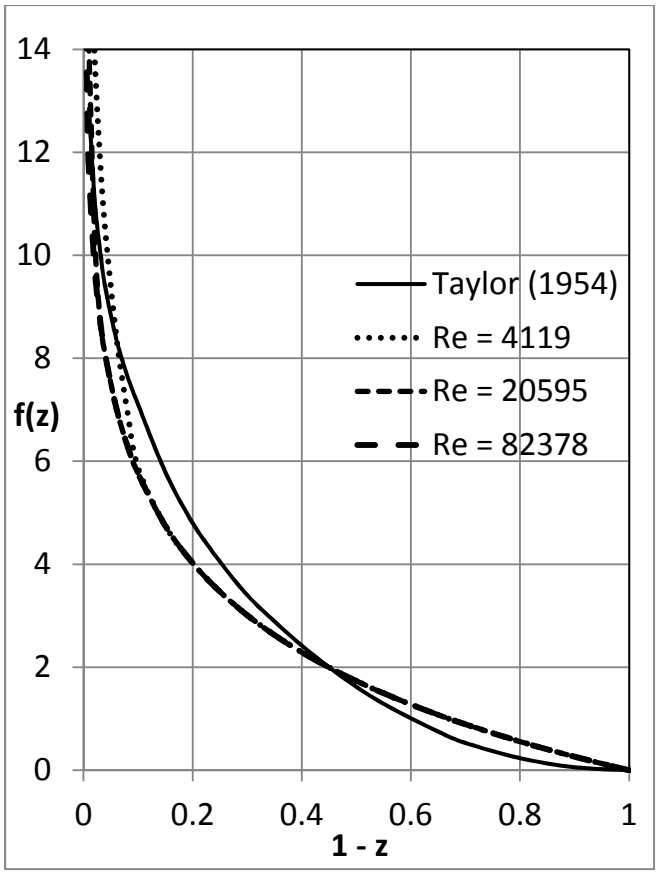

Figure 4.4: Comparison of dimensionless velocity profiles (Equation 2.10) for flow through a 12" pipe at various Reynolds numbers against the universal velocity profile in Taylor's analysis.

The turbulent core velocity profile (Equation 4.28) results in a discontinuity in the velocity profile at the center of the pipe. This is because the observed mean velocity in this region (defect layer, $y/\delta > 0.2$) deviates from the log-law and needs to be corrected according to the velocity-defect equation. Applying this correction would not make much of a difference to the final axial dispersion estimations simply because the velocity profile in the central core is a less significant factor as compared to the velocity profile in the inner wall regions.

Recalculations of the axial dispersion coefficient

The convective-diffusion equation will be re-evaluated with the velocity profile described by Equations (4.26-4.28) and an expression of axial dispersion coefficient will be determined

using numerical approximations. It has been assumed that the flow field can be divided into two distinct regions, a) the near-wall viscous flow region dominated by molecular diffusion, and b) the central turbulent flow region dominated by eddy diffusion due to velocity shear. The axial dispersion coefficient for purely turbulent flow has been derived in the previous section (**Estimation of turbulent axial dispersion coefficient**). This section will focus on solving the convective-diffusion equation (Equation 4.7) in just the viscous region of the flow. The convective-diffusion equation can be rewritten for the viscous region by replacing the eddy diffusivity term in Equation (4.7) with the molecular diffusivity. The convective-diffusion equation therefore takes the form

$$\frac{\partial C}{\partial t} + u\frac{\partial C}{\partial x} = \frac{1}{r}\frac{\partial}{\partial r}\left(Dr\frac{\partial C}{\partial r}\right) \tag{4.29}$$

where, D is the molecular diffusion coefficient. Transforming the above equation to an axis moving with the mean speed of flow given by $x_1 = x - \bar{U}\,t$ and converting the radius to its dimensionless form ($z = r / R$) gives

$$\left(u - \bar{U}\right)\frac{\partial C}{\partial x_1} = \frac{D}{zR^2}\frac{\partial}{\partial z}\left(z\frac{\partial C}{\partial z}\right) \tag{4.30}$$

Substituting for the local velocity in in terms of dimensionless velocity function (Equation 2.10) and using Equation (4.14) to represent the average velocity, we have

$$-u_\tau\left(f\left(z\right) - 2\int_0^1 \left\{zf\left(z\right)\right\} dz\right)\frac{\partial C}{\partial x_1} = \frac{D}{zR^2}\frac{\partial}{\partial z}\left(z\frac{\partial C}{\partial z}\right) \tag{4.31}$$

$$\bar{U} = U_0 - 2u_\tau \cdot \int_0^1 \left\{zf\left(z\right)\right\} dz \tag{4.14}$$

$$f(z) = \frac{u_0 - u_\tau}{u_\tau} \tag{2.10}$$

Equation (4.31) can be rearranged to the form

$$\frac{\partial}{\partial z}\left(z\frac{\partial C}{\partial z} \right) = -z\left(f(z) - 2\int_0^1 \{ zf(z) \}\, dz \right) \cdot \left[\frac{R^2 u_\tau}{D} \cdot \frac{\partial C}{\partial x_1} \right] \tag{4.32}$$

The same terminology as listed in Equations (4.15-4.16) can be used to integrate the above equation and the concentration gradient in the radial direction can be estimated as

$$\therefore \frac{\partial C}{\partial z} = -\frac{1}{z}\left(\frac{R^2 u_\tau}{D} \cdot \frac{\partial C}{\partial x_1} \right)\phi(z) = -\left(\frac{R^2 u_\tau}{D} \cdot \frac{\partial C}{\partial x_1} \right)\psi(z) \tag{4.33}$$

$$\phi(z) = \int_0^z z\left(f(z) - 2\int_0^1 \{ zf(z) \}\, dz \right) dz \tag{4.15}$$

$$\psi(z) = \phi(z)/z \tag{4.16}$$

Equation (4.33) can be considered as an estimate for the rate of mass transfer across the layers. The concentration in the viscous region can therefore be estimated by integrating this equation from the dimensionless radial distance (z_V) at the cusp of the viscous region to the pipe wall ($z = 1$).

$$\therefore C_z = -\left(\frac{R^2 u_\tau}{D} \cdot \frac{\partial C}{\partial x_1} \right)\int_{z_V}^{z} \psi(z) \tag{4.34}$$

The radial concentration profile can be used to estimate the axial dispersion coefficient using the procedure listed in Equations (4.19-4.22). The axial dispersion coefficient in the viscous region thus comes out to be

$$K_V = -\frac{2u_\tau^2 R^2}{D}\int_{z_V}^{1}\chi(z)\,dz \tag{4.35}$$

where, $\chi(z) = -u_\tau z\left[f(z) - 2\int_0^1\{zf(z)\}\,dz\right]\int_{z_V}^{z}\psi(z)\,dz$

Note that the limits on the integration of $\chi(z)$ range from the viscous region ($z = z_V$) to the pipe wall ($z = 1$). The above equation can be written as

$$K_V = c\frac{R^2 u_\tau^2}{D} \tag{4.36}$$

$$K_L = \frac{R^2\bar{U}^2}{48D} \tag{2.9}$$

where, c would be a number depending on the velocity profile (and therefore the Reynolds number of the system). The above equation is very similar to the laminar dispersion equation proposed by Taylor (Equation 2.9). The multiplying term in the above equation would however be different from that in Equation (2.9) because, a) the above equation is in terms of the friction velocity (u_τ) as opposed to Equation (2.9), which is in terms of the average flow velocity, and b) the above equation is only applicable to the near-wall regions of the flow and not the entire flow cross-section as is the case with Equation (2.9). The effective axial dispersion coefficient for the system can therefore be estimated as the sum of the viscous (Equation 4.35) and turbulent (Equation 4.23) axial dispersion coefficients and can be written as

$$K_E = -Ru_\tau\cdot\left[\frac{2u_\tau R}{D}\int_{z_V}^{1}\chi(z)\,dz + \frac{1}{\pi}\left(\frac{\lambda_x^+\cdot\lambda_z^+\cdot T_b^+}{l_b^+\cdot w_b^+\cdot h_b^+}\right)\int_0^1\chi(z)\,dz\right] \tag{4.37}$$

The terms on the left of the addition sign in the above equation represents the viscous term, while the terms on the right represent the turbulent dispersion terms. The above equation expressed in the form of dimensionless axial dispersion coefficient is

$$\frac{K_E}{\bar{U}d} = -\frac{1}{2}\sqrt{\frac{f}{2}} \cdot \left[\frac{\bar{U}d}{D}\sqrt{\frac{f}{2}} \int_{z_V}^{1} \chi(z)\,dz + \frac{1}{\pi}\left(\frac{\lambda_x^+ \cdot \lambda_z^+ \cdot T_b^+}{l_b^+ \cdot w_b^+ \cdot h_b^+} \right) \int_0^1 \chi(z)\,dz \right] \tag{4.38}$$

since $u_\tau = \bar{U}\,(f/2)^{0.5}$, where f is the friction factor.

The value of z_V in the above equations would be the dimensionless radial distance beyond which the flow is highly streamline in nature and where viscous effects are dominant. It is more common to denote the thickness of the various regions in a flow field in terms of the dimensionless distance away from the wall. The dimensionless radial distance as a function of the dimensionless distance from the wall can be expressed as

$$y^+ = \frac{(1-z)Ru_\tau}{\nu} \tag{4.39}$$

where, y^+ is the dimensionless distance from the pipe wall. The parameter z_V should therefore ideally be the dimensionless radial distance of the viscous sublayer ($y^+ \approx 5$) from the pipe center. The value for z_V however might be slightly higher than that estimated using $y^+ = 5$, as the flow slightly above the viscous sublayer is also considerably close to streamline conditions.

Evaluation of the model performance

Table 4.3 lists the various calculations involved with the estimations for the effective axial dispersion coefficient. In order to obtain a reasonable accuracy, estimations were performed at z increments of 0.005 in the range $0 \le z \le 0.8$, increments of 0.002 were employed in the range $0.8 < z < 0.999$, and increments of 0.001 beyond $z = 0.999$. This resulted in a total of 266 z-locations where the calculations had to be performed. All calculations in Table 4.3 were

Table 4.3: Calculations to solve the convective-diffusion equation in the viscous sublayer.

z	y^+	u	$f(z)$	$zf(z)$	$\int zf(z)$	$-\phi(z)$	$1/z$	$-\psi(z)$	$-\int\psi(z)$	$\chi(z)$	$\int\chi(z)$
0.938	5.0	0.0241	11.4767	10.7651	1.7560	0.5449	1.0661	0.5809	0	0	0
0.94	4.8	0.0233	11.6379	10.9396	1.7778	0.5328	1.0638	0.5668	0.0011	-0.0069	-1.37×10^{-5}
0.942	4.7	0.0225	11.7991	11.1147	1.8001	0.5203	1.0616	0.5524	0.0022	-0.0139	-4.15×10^{-5}
0.944	4.5	0.0218	11.9603	11.2905	1.8226	0.5076	1.0593	0.5377	0.0033	-0.0211	-8.38×10^{-5}
0.946	4.4	0.0210	12.1215	11.4669	1.8456	0.4945	1.0571	0.5227	0.0044	-0.0285	-1.41×10^{-4}
0.948	4.2	0.0202	12.2826	11.6439	1.8689	0.4811	1.0549	0.5075	0.0054	-0.0361	-0.0002
0.95	4.0	0.0194	12.4438	11.8216	1.8925	0.4673	1.0526	0.4919	0.0064	-0.0437	-0.0003
0.952	3.9	0.0187	12.6050	12.0000	1.9165	0.4532	1.0504	0.4761	0.0073	-0.0515	-0.0004
0.954	3.7	0.0179	12.7662	12.1790	1.9409	0.4388	1.0482	0.4600	0.0082	-0.0594	-0.0005
0.956	3.5	0.0171	12.9274	12.3586	1.9656	0.4240	1.0460	0.4436	0.0091	-0.0673	-0.0007
0.958	3.4	0.0163	13.0886	12.5389	1.9907	0.4089	1.0438	0.4269	0.0100	-0.0753	-0.0008
0.96	3.2	0.0155	13.2498	12.7198	2.0161	0.3935	1.0417	0.4099	0.0108	-0.0833	-0.0010
0.962	3.1	0.0148	13.4110	12.9014	2.0419	0.3777	1.0395	0.3926	0.0116	-0.0914	-0.0012
0.964	2.9	0.0140	13.5722	13.0836	2.0681	0.3616	1.0373	0.3751	0.0123	-0.0994	-0.0014
0.966	2.7	0.0132	13.7334	13.2664	2.0946	0.3451	1.0352	0.3572	0.0130	-0.1074	-0.0016
0.968	2.6	0.0124	13.8946	13.4499	2.1215	0.3283	1.0331	0.3391	0.0137	-0.1154	-0.0018
0.97	2.4	0.0117	14.0557	13.6341	2.1488	0.3111	1.0309	0.3207	0.0144	-0.1233	-0.0020
0.972	2.3	0.0109	14.2169	13.8189	2.1764	0.2936	1.0288	0.3020	0.0150	-0.1311	-0.0023
0.974	2.1	0.0101	14.3781	14.0043	2.2044	0.2757	1.0267	0.2831	0.0155	-0.1388	-0.0026
0.976	1.9	0.0093	14.5393	14.1904	2.2328	0.2575	1.0246	0.2638	0.0161	-0.1463	-0.0029
0.978	1.8	0.0085	14.7005	14.3771	2.2616	0.2389	1.0225	0.2443	0.0165	-0.1537	-0.0032
0.98	1.6	0.0078	14.8617	14.5645	2.2907	0.2200	1.0204	0.2245	0.0170	-0.1608	-0.0035
0.982	1.5	0.0070	15.0229	14.7525	2.3202	0.2007	1.0183	0.2044	0.0174	-0.1678	-0.0038
0.984	1.3	0.0062	15.1841	14.9411	2.3501	0.1811	1.0163	0.1840	0.0178	-0.1745	-0.0042
0.986	1.1	0.0054	15.3453	15.1304	2.3803	0.1611	1.0142	0.1634	0.0181	-0.1810	-0.0046
0.988	1.0	0.0047	15.5065	15.3204	2.4110	0.1407	1.0121	0.1424	0.0184	-0.1871	-0.0049
0.99	0.8	0.0039	15.6676	15.5110	2.4420	0.1200	1.0101	0.1212	0.0186	-0.1929	-0.0053
0.991	0.7	0.0035	15.7482	15.6065	2.4576	0.1096	1.0091	0.1105	0.0187	-0.1958	-0.0055
0.992	0.6	0.0031	15.8288	15.7022	2.4733	0.0990	1.0081	0.0998	0.0188	-0.1985	-0.0057
0.993	0.6	0.0027	15.9094	15.7981	2.4891	0.0884	1.0070	0.0890	0.0189	-0.2012	-0.0059
0.994	0.5	0.0023	15.9900	15.8941	2.5050	0.0777	1.0060	0.0781	0.0190	-0.2037	-0.0061
0.995	0.4	0.0019	16.0706	15.9903	2.5210	0.0669	1.0050	0.0672	0.0191	-0.2062	-0.0063
0.996	0.3	0.0015	16.1512	16.0866	2.5371	0.0559	1.0040	0.0562	0.0191	-0.2085	-0.0065
0.997	0.2	0.0012	16.2318	16.1831	2.5533	0.0450	1.0030	0.0451	0.0192	-0.2108	-0.0067
0.998	0.2	0.0008	16.3124	16.2798	2.5695	0.0339	1.0020	0.0339	0.0192	-0.2129	-0.0070
0.999	0.1	0.0004	16.3930	16.3766	2.5859	0.0227	1.0010	0.0227	0.0192	-0.2149	-0.0072
1	0.0	0	16.4736	16.4736	2.6024	0.0114	1.0000	0.0114	0.0192	-0.2168	-0.0074

performed for a fluid flowing in a 2" pipe at a Reynolds number of around 2,000. The velocity profile and therefore the dimensionless velocity function, *f(z)* was estimated using Equations (4.26-4.28) based on the value of y^+ from Equation (4.39). The values for the various functions such as ϕ and ψ were estimated using Equation (4.15) and Equation (4.16) respectively. The values of the integral of the functions ψ and χ for $0 \le z \le 1$ were estimated to be -0.785 and -0.44 respectively (Appendix D). This information is however not included in Table 4.3 because only the integrals of the functions ψ and χ from the range $z_V \le z \le 1$ ($0 \le y^+ \le 5$) is required for calculations in the viscous region. Based on these calculations, Table 4.3 suggests the value of the integrals of the functions ψ and χ for $z_V \le z \le 1$ to be -0.01924 and -7.385×10^{-3} respectively. Substituting the values of χ in Equation (4.38) gives

$$\frac{K_E}{\bar{U}d} = \frac{1}{2}\sqrt{\frac{f}{2}} \cdot \left[\left(7.385\times10^{-3}\right)\frac{\bar{U}d}{D}\sqrt{\frac{f}{2}} + \left(0.4398\right)\left(\frac{\lambda_x^+ \cdot \lambda_z^+ \cdot T_b^+}{l_b^+ \cdot w_b^+ \cdot h_b^+} \right) \right] \tag{4.40}$$

Using a value for the friction factor determined using the Swamee-Jain equation and substituting for the values of the turbulent burst characteristics from Table 4.2 into the above equation results in a value of 19.071 for the dimensionless effective dispersion coefficient.

Similar estimations have been performed for other Reynolds numbers in the range $2{,}000 \le Re \le 1{,}000{,}000$. Dimensionless dispersion coefficients are reported in Table 4.4. The pattern of the dimensionless dispersion coefficient follows the trend observed in the experimental data, with a rapid decrease in the dispersion coefficient at lower Reynolds numbers ($Re \le 20{,}000$) and a gradual decrease beyond this point. Table 4.4 also illustrates how the different axial dispersion equations available in literature perform in comparison with the current theory and the simplified model presented in Chapter III (Equation 3.24).

Table 4.4: Comparison of the dimensionless dispersion coefficients determined using Equation (4.38) against Equation (3.24) and other models available in the literature.

Re	Eq. (4.38)	Eq. (3.24)	Taylor, Eq. (2.12)	Austin and Palfrey, Eq. (2.1-2.3)	Fowler and Brown, Eq. (A.2)
2000	19.07	50.21	0.39	24.21	47.05
3000	11.63	24.98	0.37	11.63	21.33
4000	8.38	15.10	0.36	6.93	13.21
5000	6.31	10.18	0.35	4.65	9.48
6000	4.81	7.38	0.34	3.35	7.41
7500	3.50	4.99	0.33	2.24	5.63
9000	2.91	3.64	0.33	1.61	4.58
10000	2.55	3.04	0.32	1.33	4.10
15000	1.46	1.56	0.31	0.64	2.80
20000	1.01	1.01	0.30	0.44	2.22
30000	0.66	0.61	0.29	0.41	1.68
50000	0.43	0.39	0.28	0.37	1.27
75000	0.33	0.31	0.27	0.34	1.05
90000	0.30	0.30	0.27	0.33	0.98
100000	0.29	0.29	0.26	0.32	0.94
150000	0.26	0.27	0.26	0.30	0.83
250000	0.23	0.26	0.26	0.27	0.72
500000	0.22	0.25	0.25	0.23	0.62
750000	0.21	0.25	0.25	0.21	0.59
1000000	0.21	0.25	0.25	0.20	0.56

Figure 4.5 compares the dimensionless effective axial dispersion coefficient estimated using Equation (4.38) against experimental data from the literature. The model (Equation 4.38) performance is excellent at moderate to higher Reynolds numbers ($Re \geq 10{,}000$). There seems to be a discontinuity (abrupt change of slope) in the model prediction at Reynolds number of around 10,000. The slope of the line seems to decrease slightly, which seems opposite to the observed trend. The model therefore under-predicts axial dispersion at very low turbulent Reynolds number ($Re \leq 4{,}000$). One possible explanation for this could be the inaccuracies of the velocity

equations (Equation 4.26-4.28) used to represent the velocity profile in the model calculations. These equations are known to lose their precision at low Reynolds numbers, $Re < 10{,}000$ (McCabe, Smith et al. 2005) and therefore could add to the inaccuracy in the estimation of the axial dispersion coefficient.

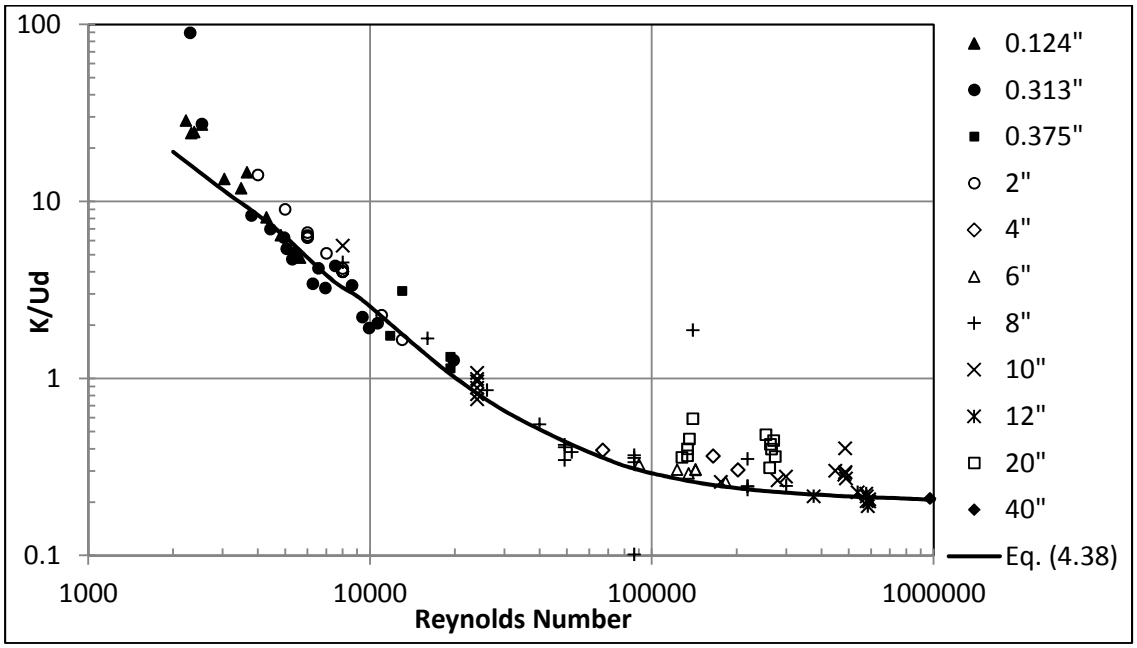

Figure 4.5: Dimensionless axial dispersion coefficient (Equation 4.38) against Reynolds number.

The deviations could also be due to the extent of resolution available at the low Reynolds numbers. Higher resolution (smaller z increments), especially in the viscous region ($y^+ \leq 30$) might help improve the prediction accuracy at these Reynolds numbers. Another reason worth consideration is the enhanced effects of the viscous sublayer at these Reynolds numbers. As stated earlier in this section, a slightly higher value of the viscous region thickness ($y^+ \leq 6$) at these higher Reynolds number would also help reduce the deviations. This however would not be technically correct as a value of $y^+ = 5$ is universally accepted as the demarcation for the viscous sublayer. Opting for an accurate velocity profile equation at lower Reynolds numbers should therefore be the preferred choice instead.

Summary

This study tries to provide a mechanistic viewpoint to Taylor's analysis (Taylor 1954) of axial dispersion and derives an expression for axial dispersion coefficient as a function of the characteristic dimensions of the near-wall structures and turbulent bursts. It is assumed that the mechanism of development of the slow moving streaks in the near-wall region, which ultimately culminate into violent turbulent bursting events, is instrumental to the process of axial dispersion and can be used to predict the magnitude of the dispersion coefficient. The consequent relation obtained for the dispersion coefficient tallies with Taylor's theory (Equation 2.12) that was developed assuming the Reynolds analogy (Taylor 1954). The study thus justifies Taylor's (1954) assumption. The analysis presented provides a physical backing to Taylor's theory (Taylor 1954) while providing new conceptual visualizations of the processes governing axial mixing of fluids in a straight pipe. It has also been revealed that the accuracy of the axial dispersion coefficient prediction in the lower Reynolds number turbulent regime can be improved by performing rigorous calculations in the viscous sublayer employing the molecular diffusion coefficient along with a turbulent dispersion coefficient determined from the theory of turbulent bursts.

The model proposed in this chapter (Equation 4.38) like the counterpart from Chapter III (Equation 3.24) though based on theoretical concepts, is also dependent upon indirect empiricisms. The various turbulent burst scales, turbulent flow-field region thicknesses, velocity profiles, etc. all contribute to the empiricisms of the current equation. The model can therefore be termed semi-empirical at best. However, the concepts proposed in this chapter meet the basic objective of this work, which is to provide an understanding of the physics resulting in axial dispersion in liquids flowing through a straight pipe. It should be noted that with precise information of the fluid densities and viscosities, the concept can also be applied to estimate axial dispersion coefficient for the flow of gases through a straight pipe. Furthermore, the proposed

concept could also be used in identifying techniques to help reduce axial dispersion in straight pipes.

CHAPTER V

AXIAL DISPERSION IN FLOW THROUGH PIPE BENDS

Most axial dispersion studies available in the literature as well as those presented in the previous chapters of this work were mostly formulated for axial mixing through straight pipes. The idealized studies need to be modified to include the effects of non-idealities such as the presence of bends and other fittings. The petroleum pipeline network in the United States is approximately 200,000 miles long spanning all 50 states and carries more than 14 billion barrels (over 600 billion gallons) of product every year (Trench 2001; Rabinow 2004). These lines might have long sections of essentially straight piping, but are not always straight. Practical applications always have bends and fittings associated with pipelines for various reasons – to counter thermal expansions and contractions due to climate changes, to bypass immovable bodies (lakes, rivers, etc.), land constraints, etc. Flow through bends is therefore a very important aspect from a practical point of view when dealing with petroleum transportation.

Only a handful of studies (Smith and Sulze 1948; Taylor 1954; Davidson, Farquharson et al. 1955; Carter and Bir 1962; Bischoff 1964; Koutsky and Adler 1964; Gomezplata and Park 1966; Aunicky 1968; Cassell and Perona 1969; Park and Gomezplata 1971; Castelain, Mokrani et al. 1997) on the influences of bent pipes on axial dispersion are available in the literature. Most

of the work reported in the literature concentrate on axial mixing for flow through helical systems. Even among these, fewer investigations (Smith and Sulze 1948; Carter and Bir 1962; Aunicky 1968; Cassell and Perona 1969; Park and Gomezplata 1971) have reported experimental data for axial dispersion in the presence of conventional bends and pipe fittings. The influences of bends and fittings on axial dispersion are therefore a relatively unknown quantity. This chapter gives an account of the various techniques and mathematical formulations proposed to incorporate the effects of bends on axial dispersion at the interface formed between two liquids. The information collected from literature studies is utilized to propose a more accurate empirical formulation to estimate axial dispersion coefficient in pipes with conventional bends.

Studies on axial mixing in bent pipes

Studies (Taylor 1954; Carter and Bir 1962; Koutsky and Adler 1964; Aunicky 1968; Cassell and Perona 1969; Park and Gomezplata 1971; Castelain, Mokrani et al. 1997) on axial dispersion in bends report varied and contradicting findings. Experiments (Smith and Sulze 1948; Carter and Bir 1962; Aunicky 1968; Park and Gomezplata 1971) carried out on systems with straight pipes and conventional bends have generally shown an increase in the extent of axial dispersion, while experiments (Koutsky and Adler 1964; Cassell and Perona 1969; Castelain, Mokrani et al. 1997) on unconventional systems mimicking helical coils result in a reduction in the axial dispersion coefficient. These contrasting observations can be explained by the fact that multiple mechanisms are contributing to axial dispersion during flow through bends and curved pipes. The viscous effects and bend geometry result in a skewed, non-uniform velocity profile, which according to Taylor's hypothesis enhances axial dispersion. At the same time, chaotic mixing across the cross-section due to turbulent eddies and secondary flows result in a reduction in axial mixing (Koutsky and Adler 1964; Cassell and Perona 1969; Zhao and Bau 2007). The net effect observed is therefore sensitive to the configuration and orientation of the system, which influences the magnitude of the contributions from each of the two mechanisms listed above.

Taylor's formulation of axial dispersion (Taylor 1953) does not include the effects of secondary flows as these effects are not observed for ideal flow through straight pipes. Secondary flow refers to the circular motion of fluid in a plane perpendicular to the observed direction in a flowing system. Secondary flow patterns usually occur in flow through curved pipes, resulting due to increased centripetal forces on the flow field. The onset of secondary flow results in circular motions of the fluid molecules (Figure 5.1), leading to rapid mixing across the cross-section of the pipe and therefore a reduction in the radial concentration gradient (Koutsky and Adler 1964). In accordance with Taylor's theories (Taylor 1953; 1954), radial mixing is one of the primary governing factors in longitudinal dispersion. Enhanced radial mixing due to secondary flows will reduce the concentration gradients across the cross-section of the pipe and therefore lead to lower than expected axial dispersion.

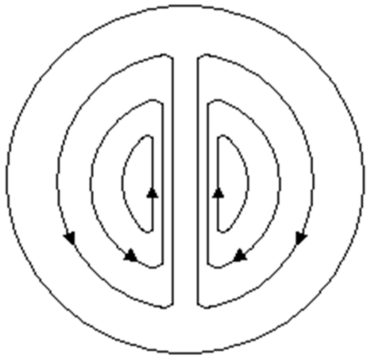

Figure 5.1: Secondary flow lines along the cross-section of a circular pipe. Adapted from Koutsky and Adler (1964).

The effects of secondary flow on axial dispersion coefficient have also been validated using experimental analysis (Koutsky and Adler 1964; Cassell and Perona 1969; Castelain, Mokrani et al. 1997; Zhao and Bau 2007; Vashisth and Nigam 2008). The experiments reveal a significant reduction in the axial dispersion coefficient for systems that experience sustained secondary flow effects. For cases with isolated conventional bends, secondary flow, though generated, is not a continuous influence and therefore is less significant. Zhao and Bau (2007)

report the isolated effects of secondary flow without secondary flow producing mechanisms such as flow through curved pipes, bends, etc. They induced secondary flow in a straight pipe by electro-kinetic and electro-osmotic means and controlled the intensity of secondary flow with the intensity of the electric field. They demonstrated a substantial reduction in the axial dispersion coefficient in systems with continuous, high intensity secondary flow currents.

As stated earlier, high intensity, continuous secondary flow currents are only possible for systems inducing near continuous centripetal forces on the flow field. Such effects are not encountered in systems with isolated conventional bends, where the effect of one bend is not discernible farther downstream and secondary flow is only persistent for a short duration of time. Takeuchi and Murai (2010) carried out CFD simulations for flow of gases through isolated bends and observed that the reduction in the axial dispersion coefficient due to secondary flow currents would be insignificant in comparison with the increase in axial dispersion because of the skewed velocity profiles and other non-idealities resulting because of the pipe curvature. Petroleum pipelines would most commonly have conventional bends as opposed to helical configurations and thus would not experience significant secondary flow effects. Secondary flow effects are therefore ignored in axial mixing estimations proposed in this work.

Studies on flow through pipes with conventional bends are scarce in the literature. The present study analyzes the experimental data that has been published in open literature (Smith and Sulze 1948; Carter and Bir 1962; Cassell and Perona 1969; Aunicky 1970) and proposes a model equation that builds on the theories and observations presented by Bischoff (1964), Gomezplata and Park (1966), Park and Gomezplata (1971), and Cassell and Perona (1969).

Most of the investigations on axial mixing in bent pipes are variations of a combined mixed model proposed by Bischoff (1964). Bischoff (1964) utilized the additive nature of the various phenomena contributing to axial dispersion and proposed to model systems with bends as

a combination of ideal plug flow to model the straight section followed by a perfect mixer to model the bends. The system would therefore act like a tank-in-series model, with the first tank being replaced by a straight pipe region. Bischoff (1964) then estimated the first and second moments of the concentration distribution for each of the two regions (plug flow and well mixed). The systems-in-series type of formulation allows the moments of the concentration to be additive, resulting in

$$\frac{K_{E,B}}{\bar{U}d} = \frac{K_{SP}}{\bar{U}d}\left(\frac{L_{SP}}{L}\right) + \frac{1}{2n}\frac{L_{SP}}{d}\left(\frac{L_{B,Eq}}{L}\right)^2 \tag{5.1}$$

where, $L_{B,Eq}$ is the length of a straight pipe that would result in the same amount of mixing as the bend (equivalent length), n is the number of repeating sections in the system consisting of a single straight pipe and a bend, and L being the effective length of the system (L_{SP} + $L_{B,Eq}$). Bischoff (1964) applied this equation to the experimental data reported by Carter and Bir (1962) and estimated the value for the equivalent bend length to be around 26 pipe diameters, which is similar to the number used for equivalent length for pressure drop calculations. During the course of his analysis, Bischoff (1964) noted the inability of the above model to incorporate the variations in axial dispersion in bends with changing Reynolds numbers and suggested the need for further experimental work to obtain improved estimations.

Cassell and Perona (1969) performed experiments on systems with closely spaced 90^o bends for different sets of configurations and published a list of equivalent length values applicable to Bischoff's model (Equation 5.1). They noted the equivalent bend length to be a non-linear function of the Reynolds number and more importantly the configuration of the system. The dependence on the system configuration can be attributed to the closely positioned bends, which would lead to the effects of the upstream bend on the flow field being transmitted to the downstream bend.

Park and Gomezplata (1971) extended this analysis by suggesting that the amount of mixing in a pipe bend would be in direct proportion to the axial dispersion in the straight section (Equation 5.2). They suggested the proportionality factor in Equation (5.2) to be a function of the Reynolds number, similar to the coefficients employed in pressure drop estimations (drag coefficient, discharge coefficient, etc.).

$$\frac{K_{E,B}}{\bar{U}d} = \frac{K_{SP}}{\bar{U}d}\left(\frac{L_{SP}}{L}\right) + F(Re)\frac{K_{SP}}{\bar{U}d}\cdot\left(\frac{L_{B,Eq}}{L}\right) \tag{5.2}$$

where, *F(Re)* is the proportionality factor. Park and Gomezplata (1971) performed experiments for varying Reynolds number and obtained system specific values for the proportionality constant. They observed *F(Re)* to be nearly constant (slight downward trend) for increasing Reynolds number in the experimental range and suggested a constant value of 3 for the range $4000 \leq Re \leq 10000$. Based on this number for *F(Re)*, they found the equivalent bend length to be similar to that used in pressure drop estimations (around 30 pipe diameters).

Aunicky (1968) in a separate investigation carried out a set of experiments for flow through different types of bends at Reynolds numbers in the range 15,000 to 90,000. The results from these experiments were translated to a set of empirical equations to correct the axial dispersion coefficient as a function of the bend angle, radius of curvature, and Reynolds number. The equations suggested are applicable for flow through bends with bend angle up to 90^{o}. Aunicky (1968) suggested that the flow through a single bend would almost always results in enhanced axial dispersion, with the extent of increase depending upon the system parameters.

All of the above models were formulated and tested on one particular type of system based on the experiments carried out by the investigators. They therefore only perform well for the system considered in the analysis and are not sufficiently consistent when tested on other

axial dispersion data available in the literature. This clearly evident need for a generalized formulation for axial dispersion estimations for flow through bends is addressed in this work.

Model development

The developments and evidences reported by Bischoff (1964), Cassell and Perona (1969), and Park and Gomezplata (1971) are utilized to propose a comprehensive mathematical formulation to estimate axial mixing in systems with bends. The model is built on the assumption that the effects of the bends and the straight pipes are additive and proposes an equation similar to Equations (5.1-5.2) for the effective axial dispersion coefficient for system with bends. The investigations available in the open literature (Bischoff 1964; Gomezplata and Park 1966; Cassell and Perona 1969; Park and Gomezplata 1971) suggest an obvious similarity between axial mixing and pressure drop estimates for flow through pipe bends. Furthermore, as revealed in the previous chapters of this work, both axial mixing and pressure drop are effects of shear distribution across the flow field and therefore similar techniques and parameters can be used for calculating the magnitude both these quantities.

Taylor's analysis (1954) for axial dispersion through straight pipes suggests that the dimensionless axial dispersion coefficient would be directly proportional to the square root of the friction factor in turbulent flow. If the axial mixing in bends is considered to be entirely caused by turbulent chaotic mixing, Taylor's equation for axial dispersion can be rewritten for the bend region as

$$\frac{K_B}{\bar{U}d} \propto \sqrt{f_B} \tag{5.3}$$

$$e_{f,B} = \left(4 f_{SP} \frac{L_{B,Eq}}{d}\right)\frac{\bar{U}^2}{2} = K_{f,B}\frac{\bar{U}^2}{2} \tag{5.4}$$

where, f_B would represent the friction factor based on the losses in pipe bends, f_{SP} is the friction factor through a straight pipe and $K_{f,B}$ is the loss coefficient for the bend/fitting. The total friction loses in a pipe fitting ($e_{f,B}$) can be expressed as a function of the loss coefficients (Equation 5.4). In crude terms, the apparent friction factor in a pipe is directly proportional to the loss coefficient for that particular fitting. Equation (5.3) can therefore be rewritten as

$$\frac{K_B}{\bar{U}d} \propto \sqrt{K_{f,B}} \tag{5.5}$$

Standardized values and equations for estimating the loss coefficients for pressure drop calculations in different types of pipe fittings are available in abundance in the literature (Perry and Green 1997). The 3-K method (Equation 5.6) suggested by Darby (2001) is employed for loss coefficient estimations in this work.

$$K_{f,B} = \frac{K_1}{Re} + K_i\left(1 + \frac{K_d}{d^{0.3}}\right) \tag{5.6}$$

where, K_1, K_i and K_d are empirical constants for various bends and fittings that have been estimated and summarized by Darby (2001).

Equation (5.5) conforms with the deduction that the axial dispersion coefficient for flow through a bend is directly proportional to the axial dispersion coefficient for flow through a straight pipe (Park and Gomezplata 1971). Furthermore, the variations in the loss coefficient with the Reynolds number (Equation 5.6) would translate to Equation (5.5) thus enabling a Reynolds number dependent formulation for the axial dispersion coefficient for flow through bends (Bischoff 1964; Aunicky 1968; Cassell and Perona 1969).

Equation (5.5) represents the value of the axial dispersion coefficient for flow through the bent sections of the system. The axial dispersion coefficient obtained from Equation (5.5) can therefore only be applied to the part of the system affected by the presence of bends. An effective

axial dispersion coefficient estimated by adding Equation (5.5) to the axial dispersion coefficient for flow through the straight sections of the system would therefore overestimate the amount of dispersion in the system.

The non-idealities and turbulence introduced by a bend are not confined to just the actual volume occupied by the bend, but extend up to a certain distance downstream of the bend depending on the radius of curvature and the central bend angle (Figure 5.2). Since part of the straight section downstream of the bend is affected by the presence of the bend, this volume can be considered to be part of the region where the bend dispersion equations would be applicable. The effective length of the straight section where the straight pipe dispersion equation can be applied would therefore be reduced by an equivalent amount.

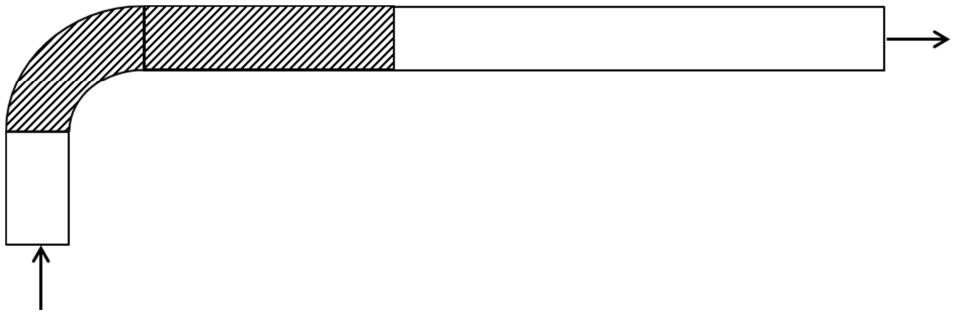

Figure 5.2: Schematic of the effective influence of a bend in the downstream section (shaded).

The more the number of bends in the system, the longer would be the time spent by the interface travelling through the regions under the influence of the bends, and therefore the higher the contribution of bends to the extent of mixing. The effective axial dispersion coefficient for the system can therefore be estimated based on the fraction of time the interface would spend in the bend section as opposed to the straight section. The effective axial dispersion coefficient for a system with bends can therefore be estimated by

$$\frac{K_{E,B}}{\bar{U}d} = \left(1 - \frac{t_B}{t_T}\right)\frac{K_{SP}}{\bar{U}d} + \left(\frac{t_B}{t_T}\right)\frac{K_B}{\bar{U}d} \tag{5.7}$$

where, t_B indicates the time spent by the interface in the bend regions and t_T indicates the total time spent by the interface in the system (straight and bend regions). Equation (5.7) can also be written by replacing the time ratios (t_B/t_T) with the easily quantifiable length ratios (L_B/L_T). The parameter L_B would represent the total length of the downstream straight section that is under the influence of the bend. Assuming the actual volume occupied by the bend to be insignificant in comparison to length of the straight section, the length ratio would be (L_B/L_{SP}), where L_{SP} is the length of the straight pipe section in the system. Substituting for the dimensionless dispersion coefficients in terms of the friction factors, Equation (5.7) can be rewritten as

$$\frac{K_{E,B}}{\bar{U}d} = \left(1 - \frac{L_B}{L_{SP}}\right)\left(\alpha\sqrt{f_{SP}}\right) + \left(\frac{L_B}{L_{SP}}\right)\left(\beta\sqrt{K_{f,B}}\right) \tag{5.8}$$

where, α is the proportionality constant for flow through a straight pipe, given as 3.57 in Taylor's analysis (1954) and β is the proportionality constant for flow through a bend. For a 90^o elbow, the influence of the bend can last up to as far as 30 pipe diameters downstream of the bend, which is also the equivalent length used for pressure drop estimations. The value of β is empirically estimated to be around 1.2 when using the equivalent length ($L_{B,Eq}$) for the length of the straight pipe being affected by the bend (L_B). For the case of a liquid interface, the values for the straight pipe dimensionless dispersion coefficient ($K_{SP}/\bar{U}\,d$) can be estimated using Equation (3.24) or directly taken from Figure 3.14A.

Equation (5.8) is defined for a system that only consists of a single bend. For systems comprising multiple bends, the effective loss coefficient ($\Sigma K_{f,B}$) and the effective equivalent length ($\Sigma L_{B,Eq}$) should be used instead of $K_{f,B}$ and L_B respectively (Equation 5.9).

$$\frac{K_{E,B}}{\bar{U}d} = \left(1 - \frac{\sum L_{B,Eq}}{\sum L_{SP}}\right)\left(\alpha\sqrt{f_{SP}}\right) + \left(\frac{\sum L_{B,Eq}}{\sum L_{SP}}\right)\left(\beta\sqrt{\sum K_{f,B}}\right) \tag{5.9}$$

ΣL_{SP} in the above equation refers to the summation of the lengths of all straight sections in the system under investigation.

Comparison of model estimates against experimental data

Axial dispersion experimental data for systems with 90^o elbows and 180^o return bends have been reported by Carter and Bir (1962), Smith and Schulze (1948) and Park and Gomezplata (1971). The data provided by Park and Gomezplata (1971) were based on experiments on short pipes, which need to be corrected to accurately represent the axial dispersion that would exist in long pipes. These corrections (fraction of steady state straight pipe dispersion) were estimated based on the data provided by Park and Gomezplata (1971) for their experiments using the initial straight pipe section of their experimental setup. The corrections were then translated to the measurements reported for axial dispersion coefficient in the downstream bend section of the setup. A detailed description of the correction calculations are provided in Appendix-E.

Two other experimental investigations (Aunicky 1968; Cassell and Perona 1969) on setups with conventional 90^o elbows available in the literature have not been considered in this work. Cassell and Perona (1969) performed experiments on setups with high bend region to straight section ratios. In such cases, the influence of one bend would transmit to the following bend resulting in complicated effects such as secondary flows. The experimental data reported by Aunicky (1968) has been ignored due to the insufficient description of the experimental setup and the absence of adequate details on measured quantities such as the straight pipe axial dispersion coefficient.

Carter and Bir (1962) experimental data

Figure 5.3A depicts the performance of the model (Equation 5.9) in comparison to the experimental data reported by Carter and Bir (1962). Equation (5.9) is able to accurately estimate the effective axial dispersion coefficient at higher Reynolds numbers (> 20,000). The

performance of the model though seems to deteriorate at lower Reynolds numbers (≤ 20,000), with the predictions being consistently higher than the observed axial dispersion coefficient. This discrepancy is caused by the use of the straight pipe dispersion coefficient from Figure 3.14A, which corresponds to liquid interfaces estimated for Schmidt number of the order of 1000. Higher Schmidt numbers indicate lower molecular diffusivities and therefore higher mixing at lower Reynolds numbers. The axial dispersion data reported by Carter and Bir (1962) were obtained for experiments using high pressure ethylene in supercritical conditions. The molecular diffusivities would be much higher under such conditions, thus resulting to lower Schmidt numbers (order of magnitude differences). Furthermore, as explained in the previous chapters, higher molecular diffusivity (radial direction) would lead to lower axial dispersion. Figure 5.3B depicts the estimates for the effective axial dispersion coefficient using Equation (5.9) at different Schmidt numbers. The solid line in Figure 5.3 indicates the axial dispersion coefficient in a straight pipe and the dotted and dashed lines represent the axial dispersion coefficient in the presence of bends.

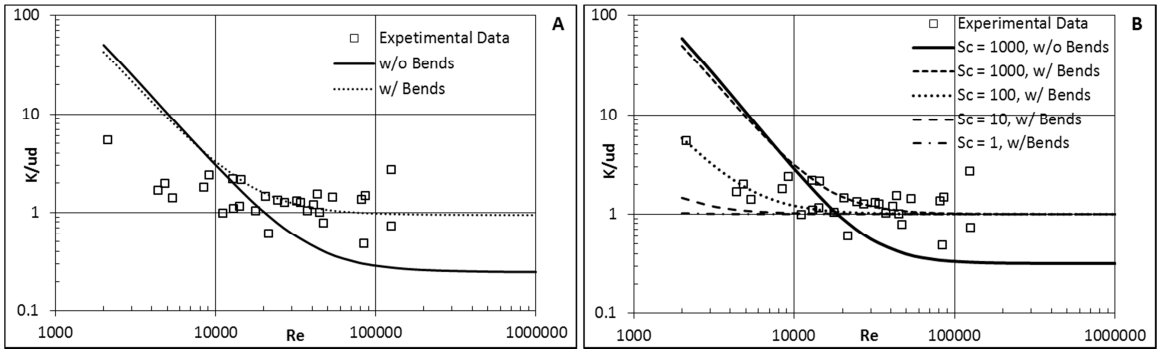

Figure 5.3: A) Comparison of model predictions (Equation 5.9) against Carter and Bir (1962) experimental data, B) Effect of the Schmidt number on axial dispersion predictions.

The presence of bends in the system appears to enhance the axial dispersion coefficient by a constant magnitude at higher Reynolds number. Bischoff (1964) reached a similar conclusion based on his analysis assuming the bend regions to act similar to perfect mixers. The

increase in the axial dispersion coefficient estimated using Bischoff's model (1964) is higher than that estimated using Equation (5.9). Such an observation is expected considering the perfect mixer (CSTR) assumption in Bischoff's analysis (1964).

Park and Gomezplata (1971) experimental data

Park and Gomezplata (1971) performed experiments on a short length experimental unit, which resulted in axial dispersion coefficients lower than the actual equilibrium values observed in long pipes. The experimental data were therefore amended to indicate their equivalent steady state values for dispersion in long pipes (Appendix-E). The amended steady state values were used for comparison with the effective axial dispersion coefficient predictions using Equation (5.9). A comparison of the predictions using Equation (5.9) against the reported experimental data is presented in Figure 5.4.

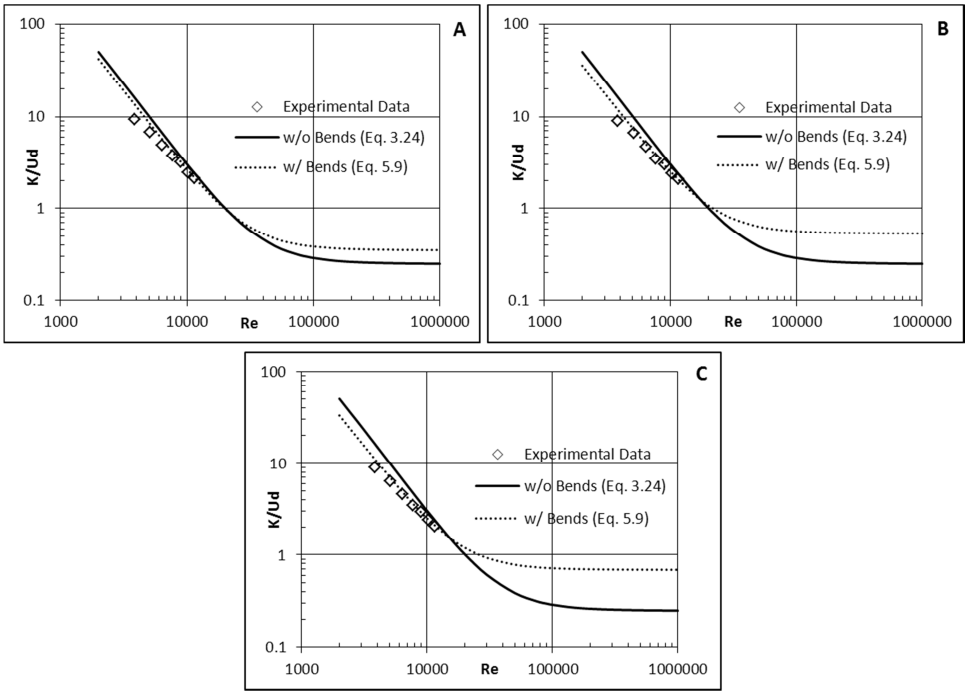

Figure 5.4: Comparison of model predictions (Equation 5.9) against experimental data reported by Park and Gomezplata (1971), with A) one bend, B) two bends, C) three bends.

The model prediction agrees with the experimentally observed reduction in the dimensionless axial dispersion coefficient in the investigated Reynolds number range. Equation (5.9) also correctly demonstrates the change in slope of the dispersion coefficient curves observed in the experimental data. These encouraging results are however only a crude approximation considering the simplistic procedures employed for amending the available data to represent axial dispersion coefficient in long pipes. Additionally, the experimental data used for comparison were taken from log-log plots from the original article and therefore can be said to exhibit a higher degree of uncertainty on top of the uncertainties introduced from experimental errors.

Smith and Schulze (1948) experimental data

Smith and Schulze (1948) reported experimental data for mixed interface lengths collected on a 5000 ft., 2" diameter pilot-scale pipe loop. The experiments were performed by introducing two fluids into the loop setup. The interface formed between the two fluids was continuously pumped around the loop. The total pipe length traveled by the interface is estimated based on the number of times the interface circles around the loop. The setup consisted of roughly twelve 90^o elbows and four 180^o return bends. If an interface is pumped though the loop ten times, the interface would have the collective influence of 120 elbows and 40 return bends. The axial dispersion coefficient would therefore not be independent of the pipe length as would be the case for a fixed experimental setup (Carter and Bir (1962) and Park and Gomezplata (1971)). All comparisons for the model performance are therefore in terms of the predicted interface length instead of the axial dispersion coefficients, which were used in the previous two comparisons.

The calculations for the interface lengths were estimated using Equation (3.25) by substituting the value of the axial dispersion coefficient estimated using Equation (5.9). Table 5.1 compares the predictions for the calculated interface length against the data for gasoline-

kerosene, gasoline-gasoline, and gasoline-fuel oil interfaces reported by Smith and Schulze at three Reynolds numbers. The model over predicted the interface length at a Reynolds number of 14,160, while it performed reasonably for the Reynolds numbers of 25,420 and 121,000. The reason for the discrepancy at 14,160 is that the prediction for the straight pipe dispersion coefficient itself is higher than the reported experimental data. Possible reasons for the disagreement with the straight pipe equation are the differences in the transport properties of the fluids used in the experiments to the ones used in the model estimations or errors in the reported data at this particular Reynolds number. The model also appears to, slightly but consistently under predict the contamination length at the Reynolds numbers of 26,420 and 121,000. This tendency of the model can be attributed to the other minor pipe fittings such as valves that have not been considered in the estimations. It should however be noted that the model predictions for the contamination length never differs from the experimental data by more than 10%.

Table 5.1: Comparison of model predictions against Smith and Schulze (1948) experimental data.

Reynolds Number	Pipe Travel Length (ft.)	Percent deviations in interface length	
		Eq. (3.24) and Eq. (3.25)	Eq. (5.9) and Eq. (3.25)
14,160	50,000	24.44	32.81
14,160	100,000	16.71	28.17
14,160	150,000	10.85	24.30
26,420	50,000	-14.83	-0.52
26,420	100,000	-20.16	-1.42
26,420	150,000	-23.66	-2.01
26,420	200,000	-25.00	-0.76
121,000	100,000	-39.64	-7.66
121,000	200,000	-44.59	-5.56
121,000	300,000	-47.37	-3.85

Summary

An empirical model has been proposed to estimate axial dispersion in systems involving long straight pipe regions with intermittent bends and pipe fittings. The foremost intention of this work has been to test the applicability of conventional techniques used for pressure drop estimations for flow through bends to axial dispersion estimations. A mathematical formulation that employs the loss coefficient ($\Sigma K_{f,B}$) and equivalent length ($\Sigma L_{B,Eq}$) concepts has been proposed (Equation 5.9) and tested on experimental data reported in three separate investigations (Carter and Bir 1962; Bischoff 1964; Park and Gomezplata 1971). A comparison of the model predictions to the reported data demonstrates the applicability of the concepts and empirical parameters used in pressure drop estimations to axial dispersion calculations. Though encouraging results are obtained, it is important to note that the model has only been tested on three sets of experimental data. Further validations by comparing with other experimental data are necessary before any conclusions regarding the practical applicability of the model can be reached. The availability of insufficient open literature experimental axial dispersion data for flow through systems with isolated bends is a major contributing factor for insufficient validation of the proposed model. The ability to estimate axial dispersion for systems with bends is critical from a practical stand point. A model can only be classified trustworthy if it has been validated using experimental measurements. There is therefore a significant need to perform further experimental work to obtain data on dispersion in non-ideal systems.

CHAPTER VI

CONCLUDING REMARKS AND FUTURE WORK

The topic of axial dispersion in turbulent flow processes has been a widely investigated area in fluid mechanics. Taylor was one of the first to provide a logical explanation of the processes governing axial dispersion. Most studies thereafter have focused on expanding on Taylor's theories, albeit with limited success. Theoretical investigation of axial dispersion seemed to have reached saturation, resulting in more recent investigative efforts directed towards empirical modeling of the process. The literature review presented in Chapter II of this work reveals that most investigations kept revolving around Taylor's analysis and are unable to break away from this circular pattern. The few investigations that have been able to branch away were either extremely complicated or did not provide a mathematical formulation. This work is an attempt to connect the dots and branches provided by previous investigators to Taylor's theories on axial dispersion. A simplified mathematical formulation describing axial dispersion has been developed by integrating the fundamental convective-diffusion equation employed by Taylor, together with the concepts of boundary layer theory and near-wall turbulence mechanisms in flow through pipes. The concepts introduced in this work provide a direction for uncovering what might be considered as the missing link in Taylor's analysis. This Chapter summarizes the various outcomes of this investigation and provides a brief overview of the direction of future

work in topics associated with axial dispersion and other related phenomena.

Major findings and contributions

This work focuses on theoretical aspects of axial dispersion. A mathematical formulation to accurately represent the extent of axial mixing is the most visible contribution of this work. Furthermore, the investigation also introduces concepts that had not been considered earlier in modeling axial dispersion processes. The various contributions of this investigation are enumerated below.

a) This investigation provides definitive mathematical evidence linking the extent of axial dispersion (dispersion coefficient and contamination length) to viscous sublayer thickness and related boundary layer parameters. Prior researchers had only hypothesized this as a crucial factor to axial dispersion.

b) Taylor's formulations for axial dispersion coefficient provide an accurate representation of the process under idealized flow conditions, namely ideal viscous laminar and turbulent flows with negligible viscous stresses. They however lose their accuracy when applied to real systems, where turbulent flows are not in their ideal state.

c) A weighted addition of Taylor's idealized formulations for the laminar and turbulent flow systems can be used to describe axial dispersion in real turbulent flows. The weighting coefficient being a means to account for the viscous effects present in turbulent flow, which were not considered by Taylor. An expression for the weighted coefficient has been developed based on boundary layer theory and the pipe geometry.

d) Taylor's assumption of the Reynolds analogy in formulating the expression for turbulent axial dispersion coefficient has been validated to be accurate. This however is only applicable to highly idealized systems flowing at high Reynolds numbers ($Re > 100{,}000$).

e) Near-wall turbulent mechanics play an important role in axial dispersion. Turbulent bursting events resulting in ejections from the near wall regions into the central turbulent core can be considered to be one of the stages contributing to axial dispersion. The characteristic scales of these turbulent bursting events have been employed to develop a phenomenological mathematical formulation of the axial dispersion process.

f) Pressure drop and axial dispersion are both a consequence of the shear stress exerted by the flowing fluid. The theories and equation applicable to pressure drop calculation in pipes are therefore also applicable, albeit with some modifications to axial dispersion estimations.

g) High accuracy mathematical formulations of axial dispersion coefficient for flow through pipes with bends have been developed using friction parameters used for estimating pressure drop through pipe bends. The mathematical formulations thus developed resemble very closely the semi-empirical relations proposed by prior researchers for such systems.

Pipeline heuristics and economic impact

Transmix volume estimation in multiproduct pipeline transport is the motivation behind this work. It therefore also serves as one of the major applications of the various theories and models that have been developed by means of various investigations conducted as part of this work. Identifying the causes of transmix formation and providing logical explanation to the

various empirical heuristics employed in the industry for transmix growth has been one of the objectives of this work. This section discusses in detail the theories behind the heuristics, and provides an overview of the applications and the economic impact of the dispersion models proposed in this work.

Transmix estimation heuristics based on five major system parameters are described below. Of these, four parameters have been conventionally known to be of significance to transmix contamination. The fifth parameter discussed has been a less common feature in comparison to the other four.

Pipe diameter and length: Contamination volume is known to increase with increasing pipe lengths and diameters. The square root dependence on pipe length has been well explained by previous investigators, with the square root power being a result of a diffusion type of process. Some investigators suggested that the square root dependence on pipe diameter could be related to the near-wall viscous region, but did not provide any conclusive evidences. The theoretical models and the mathematical validation presented in this work suggest that contamination volume follows a square root behavior with respect to the pipe diameter. This dependence is directly associated to the near-wall viscous sublayer thickness. Increasing pipe diameter (all other parameters constant) results in larger viscous sublayer thicknesses, which in turn results in enhanced axial dispersion.

Velocity: A distinct discontinuity has been observed in the axial dispersion coefficient curve with increasing Reynolds numbers for a pipeline of constant diameter. This has led to suggestions of two separate mechanisms governing the process. This study suggests that the viscous and turbulent flow effects are the two mechanisms described by prior researchers, and that the observed discontinuity in dispersion predictions can be attributed to the sublayer thickness. The viscous sublayer has been suggested to be an important parameter by some

investigators but without any conclusive evidence. The accuracy and robustness of the models developed in this work provide the necessary evidence to bolster this argument. Velocity also indirectly affects axial dispersion by influencing the near-wall turbulence mechanisms. The frequency and strength of turbulent bursts are shown to be important in axial dispersion studies (Chapter IV). Furthermore, these parameters are dependent on the mean stream velocity of the system. Velocity is therefore correctly considered as one of the more significant parameters in the empirical studies.

Kinematic viscosity and density differences: Fluid properties influence contamination growth by affecting the near-wall turbulent bursting events. Increasing the kinematic viscosity of the fluid at a constant Reynolds number will result in reduced radial mixing and therefore higher axial dispersion in a pipe of similar dimension. On the contrary, increasing the kinematic viscosity with the velocity and diameter held constant will result in reduced dispersion. Based on the analysis presented in Chapter IV, the density difference between the two liquids forming the interface would influence the extent of axial dispersion. However, the transmix formed between the fluids greatly reduces the influence of this parameter. These effects would therefore only be significant in short pipe systems, where the contaminated region would not be large enough to buffer the variation in densities. Density differences would also be significant for cases of multiphase flow. These systems are however outside the scope of this work.

Pipe roughness: The pipe roughness is a significant parameter and should be considered in all axial dispersion studies. Pipe roughness affects axial dispersion in two ways, a) by introducing turbulence and increasing the friction factor, and b) by reducing or eliminating the effect of the viscous sublayer. Eliminating the influence of the viscous sublayer would help reduce axial contamination, as viscous effects play a major role at Reynolds numbers under 100,000. The pipe roughness can therefore be considered an effective means to contain axial

dispersion. It should also be noted that increasing the pipe roughness can result in higher pressure drop and therefore adversely affect the economics of the transport.

A direct application of the models developed in this investigation is the optimization of batch scheduling operations. The sequence and size of the batches to be transported through a pipeline are estimated based on the demand of the products at the distributor end. The batch scheduling algorithms are programmed so as to move the batches at minimum possible operating costs incurred during transportation. Most scheduling algorithms employed currently ignore the dynamic nature of contamination growth and assign a constant value to account for the interfacial losses in products. This is mainly because current transmix estimation models are unreliable over the entire flow rate (Reynolds number) of operation.

Multiproduct pipelines are known to operate at Reynolds numbers ranging from 10,000 up to 500,000. Prior axial dispersion models are only known to provide an acceptable accuracy of ±10% at Reynolds numbers greater than 100,000. Their prediction accuracy however deteriorates as the Reynolds number decreases; with errors ±30% or more being very common. The operations of the Plantation and Calnev pipelines are used as a case study to analyze the effectiveness of the proposed model. Depending on the liquids being transported and the pipe diameter, the operating Reynolds numbers range from 25,000 to 350,000 for the Plantation pipeline and around 50,000 to 300,000 for the Calnev pipeline. Table 6.1 provides a comparison of the difference in barrels of transmix and the cost of the products lost as predicted by the Taylor model (Equation 2.12), the Austin and Palfrey model (Equations 2.1-2.3) and the model proposed in the current study (Equation 3.24).

Table 6.1: Comparison of transmix volume estimated using the proposed model (Equation 3.24) against the predictions using the Austin and Palfrey (1964) model and the Taylor (1954) model.

Reynolds Number	Pipeline Diameter (in.)	Barrels of transmix			*%D* from Eq. (3.24)	
		Proposed model (Eq. 3.24)	Austin & Palfrey (Eq. 2.1-2.3)	Taylor (Eq. 2.12)	Austin & Palfrey	Taylor
Plantation pipeline						
25000	30	21910	45774	11580	108.9	-47.2
150000	30	11048	11886	10542	7.6	-4.6
350000	6	190	196	189	3.2	-0.5
Calnev pipeline						
50000	14	1547	1408	1175	-8.9	-24.1
200000	8	282	300	276	6.4	-2.1
300000	8	275	288	273	4.7	-0.7

Three Reynolds numbers comprising of a low, a moderate and a high value are considered for comparison in each of the two case studies. All three models provide comparable results at extremely high Reynolds numbers. The Taylor model (Equation 2.12)_consistently under-predicts the contamination volumes in comparison to the other two models at all Reynolds number. The differences in the barrels of lost product estimated using the three equations is clearly visible at the low Reynolds number cases and these become more prominent for higher diameter pipelines. The model predictions at higher Reynolds numbers differ by ±10%. It should be noted that even a 10% deviation from the actual transmix volume can have a major effect on the final optimized solution for scheduling, leading to losses in hundreds of thousands or even millions of dollars.

Incorporating the proposed axial dispersion model in pipeline scheduling calculations would significantly improve the predictions at lower Reynolds numbers. The model also fine-tunes the predictions at higher Reynolds numbers thus providing a robustness that has been missing in the other models. Apart from the accuracy, the theoretical background employed for the development of the model facilitates understanding of the complete process resulting in interfacial contamination, thus making the model a very exciting prospect for industrial application.

The proposed model also finds a direct application in designing of new multiproduct pipelines. The model equation can be employed to estimate the pipe dimensions that best reduce interfacial mixing and thus improve the economics of transportation. In crude terms, the proposed model suggests that building of small diameter pipelines that operate at high Reynolds numbers would minimize axial contamination. Operating smaller diameter pipelines at higher Reynolds numbers would however result in an increase in the pumping costs. It is therefore necessary to choose an optimum pipe diameter that would provide a reduction in the extent of axial contamination at reasonable energy consumption rates. The various outcomes of this work will also prove useful in studies involving convective heat transfer for heat exchanger design, RTD studies for design of chemical reactors, and mixing in water supply lines and other convective processes.

Conclusions

Taylor provided mathematical formulations to mimic the asymptotic conditions of axial dispersion. The simplicity, robustness, and the theoretical background involved make Taylor's formulation of axial dispersion the closest approximation to the actual process. The amount of insight involved in coming up with the visualization and the subsequent concepts is incredible, considering the resources and knowledgebase available in those times. Taylor's concepts on axial

dispersion are therefore rightly considered as the initial stage for all subsequent studies on axial dispersion.

Taylor's models are however only applicable to the asymptotic extreme conditions, while many actual systems operate in the non-asymptotic low to moderate Reynolds number region. The fundamental convective-diffusion equations employed in formulating Taylor's formulations can be combined with the concepts of boundary layer theory to model the non-asymptotic Reynolds number region of the process. The model equations proposed in this work are developed based on phenomenological concepts and they provide theoretical and mathematical justifications to the importance of accounting the viscous region in turbulent transport studies. The proposed model is robust and has the effectiveness to replace current axial dispersion models available in the open literature.

Reynolds analogy of similarity between mass, momentum, and heat transfer, while true, provides an incomplete description of the processes involved and therefore is only applicable to specific idealized systems. The concept of the turbulent bursting event is suggested to be the answer to complete the picture of studies involving convective processes. It is revealed that Reynolds analogy when employed together with the principles of turbulent bursts is applicable to model heat, mass, and momentum transfer across the entire flow field even for low to moderate Reynolds number systems.

The concepts and model equations proposed in this work are developed from conventional theories. The results obtained are therefore very similar to the concepts that have been introduced in other aspects of transport studies. The model equations and plots developed in this study bear a remarkable resemblance to the Darcy, Forchheimer and Ergun equation for pressure drop through packed beds, the Lockhart-Martinelli plots, shear stress distribution plots, friction factor charts, and empirical relations for convective heat transfer. Such similarity

suggests that all convective processes might be governed by a common set of occurrences or events and can therefore be described using universal theories and equations. The applicability of Reynolds analogy integrated with the principles of turbulent bursts to axial dispersion studies is a promising clue. This information could form the base for future investigations involving convective processes.

Direction of future studies

A number of questions remain unanswered despite of the new concepts and solution techniques introduced in this work. Most of these questions remain unanswered on account of the lack of experimental data for experiments based on various untraditional parameters associated with axial dispersion such as pipe roughness, density and viscosity differences, entrance lengths, etc. Also, most data available in the open literature are based on gasoline-kerosene, water-water (with solute), and gasoline-gasoline systems and additional data on other types of fluid combinations will help bolster the validity of the proposed model.

The current investigation focuses on furthering the understanding of axial dispersion in long straight pipes and therefore not much effort is directed towards studies involving axial mixing in short pipes, eccentric pipes or pipes with bends. Most prior studies on these topics, like dispersion in straight pipes are empirical and not enough theoretical evidences exist to describe these systems. Furthermore, only a limited number of investigations in open literature report experimental data for such systems, thereby restricting the overall understanding of how nature works in such conditions. Experimental data on axial dispersion in pipe bends is especially lacking and future works should focus on generating such data. Investigations should focus on obtaining experimental data for axial dispersion in short pipes of varying lengths, systems with varying number of bends located at different distances from each other, and dispersion in bends of varying curvature and bend angles to name a few. Developing the theoretical or

phenomenological understanding of axial dispersion in such systems should also be investigated. The proposed axial dispersion model and the various findings reported in this work may be put into immediate use by the petroleum industry by designing new multiproduct pipelines on experimental basis. These experimental systems should be continuously monitored and should be used for generation of experimental data. This will help improve the understanding of the process and eventually in the development of axial dispersion models with higher efficiency and accuracy.

The current investigation provides a theoretical perspective to the significance of near-wall turbulence mechanics in axial dispersion studies. The ideas introduced are however merely conceptual in nature, though with a strong logical and theoretical backing. Visual confirmation of the involvement of turbulent bursting events on axial dispersion would help strengthen the concepts proposed in this study. Furthermore as described in Chapter IV, the understanding of turbulent bursting events and the characteristic scales involved in these events is still an area of science that is not completely understood and further developments in this area would definitely assist in accelerating the developments in the field of axial dispersion.

The concepts proposed in this work direct towards the existence of a universal phenomenon governing all convective processes. Future investigations should focus on making inroads to developing this universal theory, if such a theory exists. The concepts proposed in this work could also be used to explain the characteristic features of the Nikuradse friction factor charts and its differences from the Moody charts. The turbulent bursting events seem to be a major influence on most of the characteristic behavior associated with turbulent flow processes. The current research in association with prior information has illustrated a technique that could be successfully used to capture these effects into a mathematical form, though in a skeletal form. Further investigations are however necessary to provide supplementary meat and skin.

REFERENCES

Alfredsson, P. H. and A. V. Johansson (1988). The art of detection of turbulence structures. 1988 Zoran Zarić Memorial Conference, Dubrovnik, Yugoslavia, Hemisphere Publishing Corporation.

Antonia, R. A. and P. Å. Krogstad (1993). "Scaling of the bursting period in turbulent rough wall boundary layers." Experiments in Fluids **15**(1): 82-84.

AOPL (2011). "Report on shifts in petroleum transportation." Association of Oil Pipe Lines, Washington, D.C.

Aris, R. (1956). "On the dispersion of a solute in a fluid flowing through a tube." Proceedings of the Royal Society of London, Series A, Mathematical and Physical Sciences **235**(1200): 67-77.

Atesman, K. M., L. V. Baldwin and R. D. Haberstroh (1971). "The dispersion of matter in turbulent pipe flows." Journal of Basic Engineering, ASME Transactions **93**(4): 461-474.

Aunicky, Z. (1968). "The longitudinal mixing of liquids in bends." The Canadian Journal of Chemical Engineering **46**: 27-31.

Aunicky, Z. (1970). "The Longitudinal Mixing of Liquids Flowing Successively in Pipelines." The Canadian Journal of Chemical Engineering **48**: 12-16.

Austin, J. E. and J. R. Palfrey (1964). "Mixing of miscible but dissimilar liquids in serial flow in pipelines." Proceeding of Institution of Mechanical Engineers **17**(15): 377-395.

Bandyopadhyay, P. R. (1982). "Period between bursting in turbulent boundary-layers." Physics of Fluids **25**(10): 1751-1754.

Bennett Jr., P. R. and J. L. Taylor III (2000). "Minimizing transmix with FuelCheck - completely interactive pipeline interface detection." Innovative Sensor Solutions Ltd., Houston, TX.

Birge, E. A. (1947). "Contamination control in products pipelines." Oil and Gas Journal **46**: 176.

Bischoff, K. B. (1964). "An example of the use of combined models - Mixing in a tubular reactor with return bends." AIChE Journal **10**(4): 584.

Bischoff, K. B. and O. Levenspiel (1962). "Fluid dispersion-generalization and comparison of mathematical models-I." Chemical Engineering Science **17**: 245-255.

Bischoff, K. B. and O. Levenspiel (1962). "Fluid dispersion-generalization and comparison of mathematical models-II." Chemical Engineering Science **17**: 257-264.

Blackwelder, R. F. and J. H. Haritonidis (1983). "Scaling of the bursting frequency in turbulent boundary-layers." Journal of Fluid Mechanics **132**(JUL): 87-103.

Blackwelder, R. F. and R. E. Kaplan (1976). "Wall structure of turbulent boundary-layer." Journal of Fluid Mechanics **76**(JUL14): 89-112.

Buschmann, M. H. and M. Gad-El-Hak (2003). "Debate concerning the mean-velocity profile of a turbulent boundary layer." AIAA Journal **41**(4): 565-572.

Cao, Z. X. (1997). "Turbulent bursting-based sediment entrainment function." Journal of Hydraulic Engineering-Asce **123**(3): 233-236.

Carter, D. and W. G. Bir (1962). "Axial mixing in a tubular high pressure reactor." Chemical Engineering Progress **58**(3): 40-43.

Cassell, R. E. and J. J. Perona (1969). "Axial dispersion in turbulent flow through standard 90 degree elbows." AIChE Journal **15**(1): 81-85.

Castelain, C., A. Mokrani, P. Legentilhomme and H. Peerhossaini (1997). "Residence time distribution in twisted pipe flows: Helically coiled system and chaotic system." Experiments in Fluids **22**(5): 359-368.

Chatwin, P. C. (1971). "On the interpretation of some longitudinal dispersion experiments." Journal of Fluid Mechanics **48**: 689-702.

Chatwin, P. C. (1973). "Calculation illustrating effects of the viscous sub-layer on longitudinal dispersion." Quarterly Journal of Mechanics and Applied Mathematics **26**(4): 427-439.

Chen, X. D. (2007). "A mechanistic insight of convective heat transfer in turbulent flow in smooth round pipe with a turbulent 'scoops' concept." Chemical Engineering Research & Design **85**(A4): 465-472.

Chikwendu, S. C. and G. U. Ojiakor (1985). "Slow-zone model for longitudinal dispersion in two-dimensional shear flows." Journal of Fluid Mechanics **152**: 15-38.

Cleaver, J. W. and B. Yates (1973). "Mechanism of destachment of colloidal particles from a flat substrate in a turbulent-flow." Journal of Colloid and Interface Science **44**(3): 464-474.

Corino, E. R. and R. S. Brodkey (1969). "A visual investivation of the wall region in turbulent flow." Journal of Fluid Mechanics **37**: 1-30.

Danckwerts, P. V. (1953). "Continuous flow systems - Distribution of residence times." Chemical Engineering Science **2**(1): 1-13.

Darby, R. (2001). Chemical Engineering Fluid Mechanics. New York, Marcel Dekker, Inc.

Davidson, J. F., D. C. Farquharson, J. Q. Picken and D. C. Taylor (1955). "Gas mixing in long pipelines." Chemical Engineering Science **4**(5): 201-205.

Davidson, P. A. (2004). Turbulence: An introduction for scientists and engineers. New York, Oxford University Press Inc.

Dewey, R. and P. J. Sullivan (1977). "Asymptotic stage of longitudinal turbulent dispersion within a tube." Journal of Fluid Mechanics **80**(APR25): 293-303.

Eckelman.H, J. M. Wallace and R. S. Brodkey (1974). "Pattern-recognition of structured turbulence." Bulletin of the American Physical Society **19**(10): 1151-1151.

Ekambara, K. and J. B. Joshi (2003). "Axial mixing in pipe fows: turbulent and transition regions." Chemical Engineering Science **58**: 2715-2724.

Ergun, S. (1952). "Fluid flow through packed columns." Chemical Engineering Progress **48**(2): 89-94.

Fage, A. and H. C. H. Townsend (1932). "An examination of turbulent flow with an ultramicroscope." Proceedings of the Royal Society of London, Series A, Mathematical and Physical Sciences **135**: 656-677.

Flint, L. F. and P. Eisenklam (1969). "Longitudinal gas dispersion in transitional and turbulent flow through a straight tube." Canadian Journal of Chemical Engineering **47**(2): 101-106.

Flint, L. F. and P. Eisenklam (1970). "Dispersion of matter in transitional flow through straight tubes." Proceedings of the Royal Society of London, Series A, Mathematical and Physical Sciences **315**: 519-533.

Fowler, F. C. and G. G. Brown (1943). "Contamination by successive flow in pipe lines." Transactions of the American Institute of Chemical Engineers **39**: 491-516.

Gill, W. N. (1966). "Analysis of axial disperison with time variable flow." Chemical Engineering Science **22**: 1013-1017.

Gill, W. N. and R. Sankarasubramanian (1970). "Exact analysis of unsteady convective diffusion." Proceedings of the Royal Society of London, Series A, Mathematical and Physical Sciences **316**: 341-350.

Gomezplata, A. and C. M. Park (1966). "Effective dispersion in a tubular flow reactor with return bends." AIChE Journal **12**(6): 1225-1227.

Hetsroni, G. and A. Mosyak (1996). "Bursting process in turbulent boundary layers at low Reynolds numbers." Chemical Engineering Communications **150**: 85-104.

Hetsroni, G., L. P. Yarin and D. Kaftori (1996). "A mechanistic model for heat transfer from a wall to a fluid." International Journal of Heat and Mass Transfer **39**(7): 1475-1478.

Hull, D. E. and J. W. Kent (1952). "Radioactive tracers to mark interfaces and measure intermixing in pipelines." Industrial and Engineering chemistry **44**(11): 2745-2750.

Johnson, M. and R. D. Kamm (1986). "Numerical-studies of steady flow dispersion at low dean number in a gently curving tube." Journal of Fluid Mechanics **172**: 329-345.

Kim, H. T., S. J. Kline and W. C. Reynolds (1971). "The production of turbulence near a smooth wall in a turbulent boundary layer." Journal of Fluid Mechanics **50**(1): 133-160.

Kim, J. and P. R. Spalart (1987). "Scaling of the bursting frequency in turbulent boundary-layers at low Reynolds numbers." Physics of Fluids **30**(11): 3326-3328.

Kline, S. J., W. C. Reynolds, F. A. Schraub and Runstadl.Pw (1967). "Structure of turbulent boundary layers." Journal of Fluid Mechanics **30**: 741-773.

Klinkenberg, A. and F. Sjenitzer (1956). "Holding-time distributions of the Gaussian type." Chemical Engineering Science **5**: 258-270.

Koutsky, J. A. and R. J. Adler (1964). "Minimization of axial dispersion by use of secondary flow in helical tubes." The Canadian Journal of Chemical Engineering **42**(6): 239-246.

Krantz, W. B. and D. T. Wasan (1974). "Axial dispersion in the turbulent flow of power-law fluids in straight tubes." Industrial and Engineering Chemistry Fundamentals **13**(1): 56-62.

Laufer, J. and M. A. Badri Narayan (1971). "Mean period of turbulent production mechanism in a boundary layer." Physics of Fluids **14**(1): 182-183.

Lee, J. C. (1960). "Tracer measurements on a large diameter pipe." Chemical Engineering Science **12**: 191-197.

Levenspiel, O. (1958). "Longitudinal mixing of fluids flowing in circular pipes." Industrial and Engineering chemistry **50**(3): 343-346.

Levenspiel, O. and W. K. Smith (1957). "Notes on the diffusion-type model for the longitudinal mixing of fluids in flow." Chemical Engineering Science **6**(4-5): 227-233.

Luchik, T. S. and W. G. Tiederman (1987). "Timescale and structure of ejections and bursts in turbulent channel flows." Journal of Fluid Mechanics **174**: 529-552.

Maron, V. I. (1978). "Longitudinal diffusion in a flow through a tube." International Journal of Multiphase Flow **4**: 339-355.

McCabe, W. L., J. C. Smith and P. Harriott (2005). Unit operations in chemical engineering, McGraw-Hill Higher Education.

Metzger, M., B. McKeon and E. Arce-Larreta (2010). "Scaling the characteristic time of the bursting process in the turbulent boundary layer." Physica D: Nonlinear Phenomena **239**(14): 1296-1304.

Morrison, W. R. B., K. J. Bullock and R. E. Kronauer (1971). "Experimental evidence of waves in the sublayer." Journal of Fluid Mechanics **47**: 639-656.

Narahari Rao, K., R. Narasimha and M. A. Badri Narayan (1971). "Bursting phenomena in a turbulent boundary layer." Journal of Fluid Mechanics **48**(JUL28): 339-352.

Park, C. M. and A. Gomezplata (1971). "Axial dispersion in a tubular flow vessel with bends." The Canadian Journal of Chemical Engineering **49**: 202-206.

Perry, R. H. and D. W. Green (1997). Perry's Chemical Engineers' Handbook, McGraw-Hill.

Pope, S. B. (2000). Turbulent Flows, University Press, Cambridge.

Rabinow, R. A. (2004). "The liquid pipeline industry in the United States: Where it's been, Where it's going." A. o. O. P. Lines.

Rachid, F. B. F., J. H. C. d. Araujo and R. M. Baptista (2002). "Predicting mixing volumes in serial transport in pipelines." Journal of Fluids Engineering **124**: 528-534.

Robinson, S. K. (1991). "Coherent motions in the turbulent boundary-layer." Annual Review of Fluid Mechanics **23**: 601-639.

Runstadler, P. W., S. J. Kline and W. C. Reynolds (1963). "An experimental investigation of the flow structure of turbulent boundary layer." Thermosciences Division Department of Mechanical Engineering, Stanford University, Stanford, CA.

Schlichting, H. and K. Gersten (2000). Boundary layer theory. New York, Springer-Verlag Berlin Heidelberg.

Shah, D. A. and R. A. Antonia (1989). "Scaling of the bursting period in turbulent boundary-layer and duct flows." Physics of Fluids a-Fluid Dynamics **1**(2): 318-325.

Shaker, N. O. and R. Mansour (1999). "Pilot line verifies calculations for interface length, mixing." Oil & Gas Journal **97**(21): 66-69.

Sittel, C. N., Threadgi.Wd and K. B. Schnelle (1968). "LONGITUDINAL DISPERSION FOR TURBULENT FLOW IN PIPES." Industrial & Engineering Chemistry Fundamentals **7**(1): 39-43.

Sjenitzer, F. (1958). "How much do products mix in a pipeline?" Pipeline Engineer **30**: 31-34.

Smith, C. R. and S. P. Metzler (1983). "The characteristics of low-speed streaks in the near-wall region of a turbulent boundary-layer." Journal of Fluid Mechanics **129**(APR): 27-54.

Smith, R. (1987). "Diffusion in shear flows made easy - the Taylor limit." Journal of Fluid Mechanics **175**: 201-214.

Smith, S. S. and R. K. Sulze (1948). "Interfacial mixing characteristics of products in products pipeline - Part 1." The Petroleum Engineer **19**(13): 94-104.

Smith, S. S. and R. K. Sulze (1948). "Interfacial mixing characteristics of products in products pipeline - Part 2." The Petroleum Engineer **20**: 330-337.

Soltanieh, M. and S. Sadraei (1991). "A simplified model for prediction of time-dependent axial dispersion coefficient." Chemical Engineering Science **46**(1): 301-305.

Strickland, J. H. and R. L. Simpson (1975). "Bursting frequencies obtained from wall shear stress fluctuations in a turbulent boundary layer." Physics of Fluids **18**(3): 306-308.

Swamee, P. K. and A. K. Jain (1976). "Explicit equations for pipe-flow problems." Journal of Hydraulics Division **102**(5): 657-664.

Takeuchi, T. and Y. Murai (2010). "Flowmetering of natural gas pipelines by tracer gas pulse injection." Measurement Science & Technology **21**(1): 1-10.

Taylor, G. I. (1922). "Diffusion by continuous movements." Proceedings of the London Mathematical Society **20**: 196-212.

Taylor, G. I. (1953). "Dispersion of soluble matter in solvent flowing slowly through a tube." Proceedings of the Royal Society of London, Series A, Mathematical and Physical Sciences **219**(1137): 186-203.

Taylor, G. I. (1954). "The dispersion of matter in turbulent flow through a pipe." Proceedings of the Royal Society of London, Series A, Mathematical and Physical Sciences **223**(1155): 446-468.

Tichacek, L. J., C. H. Barkelew and T. Baron (1957). "Axial Mixing in Pipes." AIChE Journal **3**(4): 439-442.

Tiederman, W. G. (1988). Eulerian detection of turbulent bursts. 1988 Zoran Zarić Memorial Conference, Dubrovnik, Yugoslavia, Hemisphere Publishing Corporation.

Trench, C. J. (2001). "How pipelines make the oil market work - Their networks, operation and regulation." New York, NY, Allegro Energy Group.

Udoetok, E. S. and A. N. Nguyen (2009). "A disc pig model for estimating the mixing volumes between product batches in multi-product pipelines." Journal of Pipeline Engineering **8**: 195-201.

Vashisth, S. and K. D. P. Nigam (2008). "Liquid-phase residence time distribution for two-phase flow in coiled flow inverter." Industrial and Engineering Chemistry Research **47**: 3630-3638.

Wallace, J. M., R. S. Brodkey and Eckelman.H (1972). "Wall region in turbulent shear-flow." Journal of Fluid Mechanics **54**(1): 39-48.

Wallace, J. M., R. S. Brodkey and H. Eckelmann (1977). "Pattern-recognized structures in bounded turbulent shear flows." Journal of Fluid Mechanics **83**(DEC): 673-693.

Weyer, M. (1962). "The intermixing of successive flows in pipelines." Brennst-Wärmekr **14**(6): 267.

Zhao, H. and H. H. Bau (2007). "Effect of Secondary Flows on Taylor-Aris Dispersion." Analytical chemistry **79**: 7792-7798.

APPENDIX A

EMPIRICAL CORRELATIONS FOR AXIAL DISPERSION ESTIMATION

Fowler and Brown (1943)

$$S = 10^{C} d^{0.4} L^{0.6} \tag{A.1}$$

$$\frac{K_E}{\bar{u}d} = (0.023) \cdot 10^{2C} \left(\frac{L}{d} \right)^{0.2} \tag{A.2}$$

where, C is an empirically determined as a function of the Reynolds number and the cut-of composition defining the interface.

Birge (1947)

$$S = aL^{b} \tag{A.3}$$

$$\frac{K_E}{\bar{u}d} = (0.023) \cdot a^2 L^{2b-1} \tag{A.4}$$

where, a and b are empirically determined constants dependent on the two fluids forming the interface. The value of 2b-1 in the dimensionless dispersion coefficient equation comes out to be 0.058 for a Kerosene-Gasoline interface and -0.036 for a Gasoline-Gasoline interface in an 8" pipeline.

Smith and Schulze (1948)

$$S = \left(\frac{1.075}{\mathrm{Re}^{0.87}} + 0.55 \right) \cdot L^{0.62} \tag{A.5}$$

$$\frac{K_E}{\bar{u}d} = 0.023 \cdot \left(\frac{1.075}{\mathrm{Re}^{0.87}} + 0.55 \right)^2 \cdot L^{0.24} \cdot d^{-1} \tag{A.6}$$

Sjenitzer (1958)

$$S = \left(7300\right) \cdot f^{1.8} \cdot L^{0.57} \cdot d^{0.43} \tag{A.7}$$

$$\frac{K_E}{\bar{u}d} = \left(1.32 \times 10^7\right) \cdot \left(\frac{L}{d} \right)^{0.141} \cdot f^{3.6} \tag{A.8}$$

Austin and Palfrey (1964)

$$\mathrm{Re}_C = 10,000 e^{1.52\sqrt{d}} \tag{A.9}$$

$$S = 18,420 \sqrt{d \cdot L}\, \mathrm{Re}^{-0.9}\, e^{1.21\sqrt{d}} \qquad \text{for } Re < Re_C \tag{A.10}$$

$$\frac{K_E}{\bar{u}d} = \left(7.84 \times 10^6\right) \cdot e^{2.42\sqrt{d}} \cdot \mathrm{Re}^{-1.8} \tag{A.11}$$

$$S = 11.75 \sqrt{d \cdot L}\, \mathrm{Re}^{-0.1} \qquad \text{for } Re \geq Re_C \tag{A.12}$$

$$\frac{K_E}{\bar{u}d} = \left(3.188\right) \cdot \mathrm{Re}^{-0.2} \tag{A.13}$$

Sittel et al. (1968)

$$S = (0.04) \cdot \mathrm{Re}^{0.382} \cdot \sqrt{\frac{L}{\bar{u}}} \tag{A.14}$$

$$\frac{K_E}{\bar{u}d} = \left(3.87 \times 10^{-5}\right) \cdot \frac{\mathrm{Re}^{0.764}}{\bar{u}d} \tag{A.15}$$

Aunicky (1970)

$$S = (0.455) \cdot \left[1 - (0.0234) \cdot \log\left(\frac{C_{\min}}{C_{\max}}\right) \cdot 100\right] \cdot \mathrm{Re}^{0.887} \cdot L^{\left(\frac{0.805}{\mathrm{Re}^{0.2987}}\right)} \left(\frac{L}{\bar{u}}\right)^{0.5} \tag{A.16}$$

$$\frac{K_E}{\bar{u}d} = (0.0031) \cdot L^{\left(\frac{1.61}{\mathrm{Re}^{0..2987}}\right)} \cdot \frac{\mathrm{Re}^{0.8172}}{\bar{u}d} \tag{A.17}$$

where, C_{min} and C_{max} are the minimum and maximum concentrations of the fluids considered in percent of weight.

Udoetok and Nguyen (2009)

$$S = \left[1 - \left\{1 - \left(\frac{0.585 \times 2n^2}{(2n+1)(n+1)}\right)^n\right\}^2\right] \cdot L \tag{A.18}$$

$$\frac{K_E}{\bar{u}d} = (0.023) \cdot \left(\frac{L}{d}\right) \cdot \left[1 - \left\{1 - \left(\frac{0.585 \times 2n^2}{(2n+1)(n+1)}\right)^n\right\}^2\right]^2 \tag{A.19}$$

where, n is the power law exponent in Prandtl's velocity profile model and is estimated as the inverse of the square root of the friction factor.

APPENDIX B

DERIVATION OF THE CONTAMINATION LENGTH EQUATION

Derivation for contamination length from transient diffusion equation (Equation 2.6)

Taylor proposed the use of a fictional axial dispersion coefficient (K) to model interfacial mixing in flow through pipes. Taylor started with the convective-diffusion equation to derive a simplified expression for the dispersion coefficient that takes into account both the convective and diffusive effects prevalent in such processes. Taylor suggested that the axial dispersion coefficient thus obtained could be employed to model the convective-diffusion system as a simple transient diffusion problem. The transient diffusion equation in its conventional one dimensional (1-D) form can be written as

$$\frac{\partial C}{\partial t} = K \frac{\partial^2 C}{\partial x^2} \tag{2.6}$$

with, the boundary conditions for the case of one fluid following another in flow through a pipe being

$$C = C_0 \quad at \;\; x = 0, \;\; all \quad t \tag{B.1}$$

$$C = 0 \quad as \;\; x \to \infty, \;\; all \quad t \tag{B.2}$$

where, x indicates the direction of mass transfer and t is the time elapsed. The solution to Equation (2.6) gives the concentration profile in the x-direction. The concentration profile could be rearranged to obtain the total distance that the diffusing species has penetrated the medium, which would be equivalent to the contamination length for interfacial mixing in a straight pipe.

Equation (2.6) in the non-dimensional form is given by

$$\frac{\partial G(x,t)}{\partial t} = K \frac{\partial^2 G(x,t)}{\partial x^2} \tag{B.3}$$

where, $G(x, t) = C/C_o$, C_o being the concentration of the diffusing species at the boundary (Figure B.1).

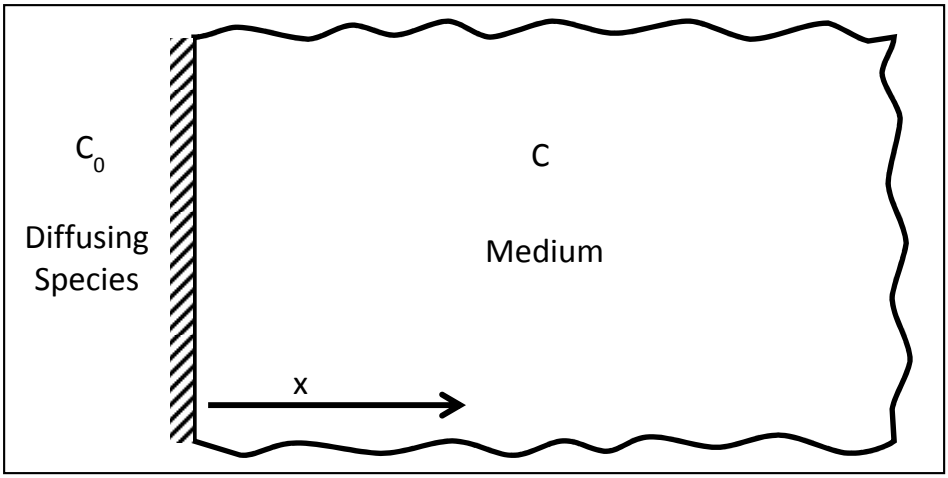

Figure B.1: Schematic for transient 1-D diffusion in an infinite medium.

The above partial differential equation (PDE) can be converted into an ordinary differential equation (ODE) by combining the two independent variables x and t into a single similarity variable η as follows

$$\frac{C}{C_0} = g(\eta) \tag{B.4}$$

Assuming a trial form for the similarity variable

$$\eta = A\frac{x}{t^n} \tag{B.5}$$

where, A is a constant to make η dimensionless. Equation (2.6) can be converted from its PDE form to an ODE

$$\frac{\partial C}{\partial t} = C_0 \frac{dg}{d\eta}\frac{\partial \eta}{\partial t} \tag{B.6}$$

using the relation for η from Equation (B.5) gives

$$\frac{\partial C}{\partial t} = C_0 \frac{dg}{d\eta}\left(-\frac{nax}{t^{n+1}}\right) \tag{B.7}$$

The term in the parenthesis can be expressed in terms of η (Equation B.5) to give

$$\therefore \frac{\partial C}{\partial t} = \left(\frac{-nC_0\eta}{t}\right)\frac{dg}{d\eta} = \left(\frac{-nC_0\eta}{t}\right)g' \tag{B.8}$$

Similarly, Equation (B.4) can be differentiated twice with respect to *x* to give

$$\therefore \frac{\partial^2 C}{\partial x^2} = \frac{C_0 A^2}{t^{2n}}\frac{d^2 g}{d\eta^2} = \frac{C_0 A^2}{t^{2n}}g'' \tag{B.9}$$

Substituting Equations (B.8-B.9) in Equation (2.6) results in

$$\left(\frac{-nC_0\eta}{t}\right)g' = K\left(\frac{C_0 A^2}{t^{2n}}\right)g'' \tag{B.10}$$

Rearranging into the standard form,

$$g'' + \left(\frac{n \cdot \eta}{K \cdot A^2} t^{2n-1} \right) g' = 0 \tag{B.11}$$

The above equation is not in the standard form yet. Eliminating variable t from the above equation using n = 1/2 will give

$$g'' + \left(\frac{1}{2} \frac{\eta}{K \cdot A^2} \right) g' = 0 \tag{B.12}$$

For n = 1/2, Equation (B.5) becomes

$$\eta = A \frac{x}{\sqrt{t}} \tag{B.13}$$

With the above form of η, (Equation B.4) can only be dimensionless if

$$A = \frac{1}{2\sqrt{K}} \tag{B.14}$$

The constant two in the above expression is chosen for convenience. Equation (B.13) can therefore be rewritten as

$$\eta = \frac{x}{2\sqrt{K \cdot t}} \tag{B.15}$$

Substituting Equation (B.15) in Equation (B.12) gives the final ODE representation of Equation (2.6),

$$g'' + 2\eta g' = 0 \tag{B.16}$$

The boundary conditions (Equations B.1-B.2) would therefore transform to

$$g(\eta) = 1 \ at \ \eta = 0 \tag{B.17}$$

$$g(\eta) \to 0 \quad as \ \eta \to \infty \tag{B.18}$$

Equation (B.16) along with the boundary conditions Equations (B.17-B.18) is a non-linear second order ODE that can be solved with standard solution techniques to give

$$g(\eta) = erfc(\eta) = 1 - erf(\eta) \tag{B.19}$$

where, *erf(η)* and *erfc(η)* are the error function and complementary error function of the similarity variable η.

The concentration profile can therefore be obtained by substituting Equation (B.19) in Equation (B.4). The concentration at a point *x*, at a time t can therefore be estimated as

$$C = C_0 \left[1 - erf\left(\frac{x}{2\sqrt{Kt}} \right) \right] \tag{B.20}$$

Assuming the concentration at the center of the interface to be 0.5, and *S/2* is the length of the interface into one particular direction in the fluid for $0.01 < C < 0.99$, Equation (B.20) can be rearranged to give

$$0.01 = 0.5 \left[1 - erf\left(\frac{S/2}{2\sqrt{Kt}} \right) \right] \tag{B.21}$$

$$\therefore erf\left(\frac{S}{4\sqrt{Kt}} \right) = 0.98 \tag{B.22}$$

From the error function tables, *erf*(1.645) = 0.98

$$\therefore \frac{S}{4\sqrt{Kt}} = 1.645 \tag{B.23}$$

$$\therefore S = 6.57\sqrt{Kt} = 6.57\sqrt{\frac{K \cdot L}{\bar{U}}} \tag{B.24}$$

where, t is the total residence time of the fluids in the pipe, which can also be expressed in terms of the pipe length L and the average flow velocity $\bar{U}$ as in Equation (B.24).

APPENDIX C

MODEL (EQUATION 3.24) VALIDATION

Page left blank intentionally. Turn to next page for the table with comparison of model predictions against each individual experimental data.

Re	Pipe Length (ft.)	Contamination Length (ft.)		*%D*	*%AD*
		Predicted (Eq. 3.24)	Experimental		
		Diameter = 0.124''			
2220	105.60	20.07	21.72	-7.60	7.60
2320	105.60	19.34	20.02	-3.40	3.40
2380	50.25	13.06	13.90	-6.07	6.07
2530	22.00	8.20	9.67	-15.16	15.16
3040	105.60	15.38	14.86	3.49	3.49
3490	50.25	9.43	9.65	-2.27	2.27
3660	50.25	9.06	10.71	-15.45	15.45
4290	8.12	3.18	3.21	-0.96	0.96
4830	8.12	2.87	2.86	0.50	0.50
5650	22.00	4.14	4.07	1.81	1.81
				%AAD	5.67
		Diameter = 0.313''			
2300	4.98	6.22	7.38	-15.68	15.68
2531	4.98	5.74	6.90	-16.82	16.82
3800	10.33	5.85	5.48	6.74	6.74
4430	4.98	3.56	3.48	2.40	2.40
4960	20.61	6.58	6.70	-1.72	1.72
5060	20.61	6.47	6.23	3.92	3.92
5300	20.61	6.23	5.82	6.97	6.97
5440	10.33	4.31	4.30	0.28	0.28
6270	15.60	4.70	4.32	8.87	8.87
6570	10.33	3.68	3.89	-5.37	5.37
6950	20.61	4.96	4.83	2.73	2.73
7530	4.97	2.28	2.74	-16.74	16.74
8640	10.33	2.94	3.48	-15.46	15.46
9400	15.60	3.38	3.48	-2.86	2.86
9935	20.61	3.72	3.72	0.00	0.00
10635	20.61	3.53	3.84	-8.11	8.11
19800	20.61	2.29	3.02	-24.12	24.12
				%AAD	8.16

Re	Pipe Length (ft.)	Contamination Length (ft.)		*%D*	*%AD*
		Predicted (Eq. 3.24)	Experimental		
		Diameter = 2"			
4000	2500	519.61	503.46	3.21	3.21
5000	2500	426.84	403.05	5.90	5.90
6000	2500	363.47	346.48	4.90	4.90
6000	100000	2298.77	2121.32	8.37	8.37
6000	300000	3981.59	3676.96	8.28	8.28
6000	500000	5140.21	4808.33	6.90	6.90
6000	700000	6081.98	5656.85	7.52	7.52
7000	2500	317.45	302.64	4.89	4.89
8000	2500	282.54	268.70	5.15	5.15
8000	100000	1786.92	1697.06	5.30	5.30
8000	200000	2527.09	2404.16	5.11	5.11
8000	400000	3573.85	3394.11	5.30	5.30
8000	600000	4377.05	4242.64	3.17	3.17
8000	800000	5054.18	4808.33	5.11	5.11
8000	1000000	5650.75	5374.01	5.15	5.15
11000	2500	215.14	202.23	6.38	6.38
13000	2500	187.37	172.53	8.60	8.60
14160	2500	174.90	137.20	27.48	27.48
14160	50000	782.19	630.00	24.16	24.16
14160	100000	1106.19	950.00	16.44	16.44
14160	150000	1354.80	1225.00	10.60	10.60
15000	2500	167.11	144.25	15.84	15.84
26400	2500	112.22	125.87	-10.84	10.84
26420	50000	501.65	590.00	-14.97	14.97
26420	100000	709.45	890.00	-20.29	20.29
26420	150000	868.89	1140.00	-23.78	23.78
26420	200000	1003.31	1340.00	-25.13	25.13
121000	2500	70.61	74.00	-4.58	4.58
121000	100000	446.57	740.00	-39.65	39.65
121000	200000	631.55	1140.00	-44.60	44.60
121000	300000	773.48	1470.00	-47.38	47.38
250000	2500	68.05	70.00	-2.78	2.78
				%AAD	13.37

Re	Pipe Length (ft.)	Contamination Length (ft.)		*%D*	*%AD*
		Predicted (Eq. 3.24)	Experimental		
		Diameter = 4''			
67000	447000	1456.32	1590.00	-8.41	8.41
165000	447000	1333.71	1530.00	-12.83	12.83
202000	447000	1324.84	1400.00	-5.37	5.37
				%AAD	8.87
		Diameter = 6''			
90000	3100	140.99	148.00	-4.74	4.74
123000	3100	136.38	143.00	-4.63	4.63
135000	11600	261.97	270.00	-2.97	2.97
143000	299060	1325.11	1401.00	-5.42	5.42
143000	517440	1743.02	1850.00	-5.78	5.78
183000	3100	133.21	132.00	0.92	0.92
				%AAD	4.08
		Diameter = 8''			
8000	246000	5635.91	5662.00	-0.46	0.46
16000	246000	3176.09	3452.00	-7.99	7.99
26000	246000	2263.03	2466.00	-8.23	8.23
40000	246000	1805.41	1973.00	-8.49	8.49
49000	292000	1818.28	1853.00	-1.87	1.87
49000	607000	2621.58	2460.00	6.57	6.57
49000	903000	3197.52	3310.00	-3.40	3.40
52000	246000	1636.25	1650.00	-0.83	0.83
86700	606514	2281.56	2422.00	-5.80	5.80
86700	895488	2772.31	3080.00	-9.99	9.99
86700	1168147	3166.37	3460.00	-8.49	8.49
218800	291298	1464.47	1406.00	4.16	4.16
218800	606514	2113.16	2070.00	2.09	2.09
218800	895488	2567.69	2520.00	1.89	1.89
218800	1168147	2932.66	3435.00	-14.62	14.62
300000	129500	967.53	960.00	0.78	0.78
				%AAD	5.4

Re	Pipe Length (ft.)	Contamination Length (ft.)		*%D*	*%AD*
		Predicted (Eq. 3.24)	Experimental		
		Diameter = 10''			
8000	3000	699.70	780.00	-10.29	10.29
24000	72850	1459.16	1414.00	3.19	3.19
24000	227520	2578.68	2693.00	-4.25	4.25
24000	572760	4091.42	4523.00	-9.54	9.54
24000	660000	4391.98	4400.00	-0.18	0.18
24000	688512	4485.84	5159.00	-13.05	13.05
24000	968700	5320.87	5790.00	-8.10	8.10
176000	1885000	4175.61	4200.00	-0.58	0.58
280000	1650898	3834.19	3970.00	-3.42	3.42
299000	1883746	4088.29	4350.00	-6.02	6.02
448000	1885000	4056.23	4520.00	-10.26	10.26
485000	289915	1588.89	2050.00	-22.49	22.49
486000	591730	2269.90	2510.00	-9.57	9.57
482000	859003	2735.22	2970.00	-7.90	7.90
485000	1134250	3142.77	3460.00	-9.17	9.17
489000	1393867	3483.52	3695.00	-5.72	5.72
				%AAD	7.73
		Diameter = 12''			
375000	2270000	4854.66	4600.00	5.54	5.54
538000	2270000	4823.88	4720.00	2.20	2.20
590000	322186	1815.08	1700.00	6.77	6.77
576500	611109	2500.54	2430.00	2.90	2.90
584000	1018301	3227.30	2890.00	11.67	11.67
591000	1402896	3787.45	3500.00	8.21	8.21
579000	1726085	4202.24	3890.00	8.03	8.03
579000	2033803	4561.46	4350.00	4.86	4.86
				%AAD	6.27

Re	Pipe Length (ft.)	Contamination Length (ft.)		*%D*	*%AD*
		Predicted (Eq. 3.24)	Experimental		
		Diameter = 20''			
140000	420000	2795.16	4230.00	-33.92	33.92
136000	420000	2803.27	3710.00	-24.44	24.44
134000	716000	3665.71	4340.00	-15.54	15.54
134000	716000	3665.71	4540.00	-19.26	19.26
128000	1230000	4828.23	5630.00	-14.24	14.24
274000	420000	2676.01	3310.00	-19.15	19.15
271000	420000	2677.23	3670.00	-27.05	27.05
264000	716000	3499.44	4680.00	-25.23	25.23
266000	716000	3498.31	4530.00	-22.77	22.77
254000	1230000	4594.44	6530.00	-29.64	29.64
262000	1230000	4588.15	5260.00	-12.77	12.77
				%AAD	22.18
		Diameter = 40''			
970000	355	104.22	103.60	0.60	0.60
				%AAD	0.60

APPENDIX D

NUMERICAL SOLUTION OF THE CONVECTIVE-DIFFUSION EQUATION

Page left blank intentionally. Turn to next page for the numerical calculations to solve the convective-diffusion equation for the entire pipe cross-section.

z	y^+	u	$f(z)$	$zf(z)$	$\int zf(z)$	$-\phi(z)$	$1/z$	$-\psi(z)$	$-\int\psi(z)$	$\chi(z)$	$\int\chi(z)$
0	80.6	0.0795	0	0	0	0	-	-	0	0	0
0.005	80.2	0.0794	0.0125	6.27×10^{-5}	3.13×10^{-7}	1.30×10^{-4}	200	0.0260	1.30×10^{-4}	3.37×10^{-6}	1.68×10^{-8}
0.01	79.8	0.0793	0.0251	2.51×10^{-4}	1.57×10^{-6}	3.89×10^{-4}	100	0.0389	3.24×10^{-4}	1.68×10^{-5}	1.01×10^{-7}
0.015	79.4	0.0793	0.0378	5.67×10^{-4}	4.40×10^{-6}	0.0008	66.6667	0.0518	5.83×10^{-4}	4.52×10^{-5}	3.27×10^{-7}
0.02	79.0	0.0792	0.0505	0.0010	9.45×10^{-6}	0.0013	50	0.0646	0.0009	9.34×10^{-5}	7.94×10^{-7}
0.025	78.6	0.0791	0.0633	0.0016	1.74×10^{-5}	0.0019	40	0.0774	0.0013	1.66×10^{-4}	1.62×10^{-6}
0.03	78.2	0.0791	0.0761	0.0023	2.88×10^{-5}	0.0027	33.3333	0.0901	0.0017	2.68×10^{-4}	2.97×10^{-6}
0.035	77.8	0.0790	0.0891	0.0031	4.44×10^{-5}	0.0036	28.5714	0.1028	0.0023	4.04×10^{-4}	4.99×10^{-6}
0.04	77.4	0.0790	0.1021	0.0041	6.48×10^{-5}	0.0046	25.0000	0.1155	0.0028	0.0006	7.88×10^{-6}
0.045	77.0	0.0789	0.1151	0.0052	9.07×10^{-5}	0.0058	22.2222	0.1281	0.0035	0.0008	1.19×10^{-5}
0.05	76.6	0.0788	0.1282	0.0064	1.23×10^{-4}	0.0070	20	0.1407	0.0042	0.0011	1.72×10^{-5}
0.055	76.2	0.0788	0.1414	0.0078	1.62×10^{-4}	0.0084	18.1818	0.1532	0.0049	0.0014	2.40×10^{-5}
0.06	75.8	0.0787	0.1547	0.0093	2.08×10^{-4}	0.0099	16.6667	0.1657	0.0058	0.0017	3.28×10^{-5}
0.065	75.4	0.0786	0.1680	0.0109	2.63×10^{-4}	0.0116	15.3846	0.1781	0.0067	0.0022	4.37×10^{-5}
0.07	75.0	0.0786	0.1814	0.0127	3.26×10^{-4}	0.0133	14.2857	0.1905	0.0076	0.0027	5.71×10^{-5}
0.075	74.6	0.0785	0.1949	0.0146	3.99×10^{-4}	0.0152	13.3333	0.2029	0.0086	0.0032	7.33×10^{-5}
0.08	74.1	0.0784	0.2085	0.0167	4.83×10^{-4}	0.0172	12.5000	0.2152	0.0097	0.0039	9.27×10^{-5}
0.085	73.7	0.0784	0.2221	0.0189	0.0006	0.0193	11.7647	0.2274	0.0108	0.0046	1.16×10^{-4}
0.09	73.3	0.0783	0.2358	0.0212	0.0007	0.0216	11.1111	0.2396	0.0120	0.0054	1.43×10^{-4}
0.095	72.9	0.0782	0.2496	0.0237	0.0008	0.0239	10.5263	0.2518	0.0133	0.0063	1.74×10^{-4}
0.1	72.5	0.0782	0.2634	0.0263	0.0009	0.0264	10	0.2639	0.0146	0.0072	2.10×10^{-4}
0.105	72.1	0.0781	0.2773	0.0291	0.0011	0.0290	9.5238	0.2760	0.0160	0.0083	2.51×10^{-4}
0.11	71.7	0.0780	0.2913	0.0320	0.0012	0.0317	9.0909	0.2880	0.0174	0.0094	2.99×10^{-4}
0.115	71.3	0.0780	0.3054	0.0351	0.0014	0.0345	8.6957	0.3000	0.0189	0.0107	3.52×10^{-4}
0.12	70.9	0.0779	0.3196	0.0384	0.0016	0.0374	8.3333	0.3119	0.0205	0.0120	4.12×10^{-4}
0.125	70.5	0.0778	0.3338	0.0417	0.0018	0.0405	8.0000	0.3238	0.0221	0.0135	4.79×10^{-4}
0.13	70.1	0.0778	0.3482	0.0453	0.0020	0.0436	7.6923	0.3356	0.0238	0.0150	0.0006
0.135	69.7	0.0777	0.3626	0.0489	0.0023	0.0469	7.4074	0.3474	0.0255	0.0167	0.0006
0.14	69.3	0.0776	0.3771	0.0528	0.0026	0.0503	7.1429	0.3591	0.0273	0.0185	0.0007
0.145	68.9	0.0776	0.3916	0.0568	0.0028	0.0538	6.8966	0.3708	0.0292	0.0204	0.0008
0.15	68.5	0.0775	0.4063	0.0609	0.0031	0.0574	6.6667	0.3824	0.0311	0.0224	0.0009
0.155	68.1	0.0774	0.4210	0.0653	0.0035	0.0611	6.4516	0.3940	0.0331	0.0245	0.0011
0.16	67.7	0.0774	0.4359	0.0697	0.0038	0.0649	6.2500	0.4056	0.0351	0.0268	0.0012
0.165	67.3	0.0773	0.4508	0.0744	0.0042	0.0688	6.0606	0.4170	0.0372	0.0292	0.0013
0.17	66.9	0.0772	0.4658	0.0792	0.0046	0.0728	5.8824	0.4285	0.0393	0.0317	0.0015
0.175	66.5	0.0771	0.4809	0.0842	0.0050	0.0770	5.7143	0.4398	0.0415	0.0343	0.0017
0.18	66.1	0.0771	0.4961	0.0893	0.0054	0.0812	5.5556	0.4512	0.0438	0.0371	0.0019

z	y^+	u	$f(z)$	$zf(z)$	$\int zf(z)$	$-\phi(z)$	$1/z$	$-\psi(z)$	$-\int\psi(z)$	$\chi(z)$	$\int\chi(z)$
0.185	65.7	0.0770	0.5114	0.0946	0.0059	0.0856	5.4054	0.4624	0.0461	0.0400	0.0021
0.19	65.3	0.0769	0.5268	0.1001	0.0064	0.0900	5.2632	0.4737	0.0485	0.0431	0.0023
0.195	64.9	0.0768	0.5423	0.1057	0.0070	0.0945	5.1282	0.4848	0.0509	0.0463	0.0025
0.2	64.5	0.0768	0.5579	0.1116	0.0075	0.0992	5	0.4959	0.0534	0.0496	0.0028
0.205	64.1	0.0767	0.5735	0.1176	0.0081	0.1039	4.8780	0.5070	0.0559	0.0531	0.0030
0.21	63.7	0.0766	0.5893	0.1238	0.0087	0.1088	4.7619	0.5180	0.0585	0.0567	0.0033
0.215	63.3	0.0765	0.6052	0.1301	0.0094	0.1137	4.6512	0.5290	0.0611	0.0605	0.0036
0.22	62.9	0.0765	0.6212	0.1367	0.0100	0.1188	4.5455	0.5399	0.0638	0.0644	0.0039
0.225	62.5	0.0764	0.6372	0.1434	0.0108	0.1239	4.4444	0.5507	0.0666	0.0684	0.0043
0.23	62.1	0.0763	0.6534	0.1503	0.0115	0.1291	4.3478	0.5615	0.0694	0.0726	0.0046
0.235	61.7	0.0762	0.6697	0.1574	0.0123	0.1345	4.2553	0.5722	0.0723	0.0770	0.0050
0.24	61.3	0.0761	0.6861	0.1647	0.0131	0.1399	4.1667	0.5829	0.0752	0.0815	0.0054
0.245	60.8	0.0761	0.7026	0.1721	0.0140	0.1454	4.0816	0.5935	0.0781	0.0862	0.0059
0.25	60.4	0.0760	0.7192	0.1798	0.0149	0.1510	4	0.6041	0.0812	0.0910	0.0063
0.255	60.0	0.0759	0.7359	0.1877	0.0158	0.1567	3.9216	0.6146	0.0842	0.0960	0.0068
0.26	59.6	0.0758	0.7528	0.1957	0.0168	0.1625	3.8462	0.6250	0.0874	0.1011	0.0073
0.265	59.2	0.0757	0.7697	0.2040	0.0178	0.1684	3.7736	0.6354	0.0905	0.1064	0.0078
0.27	58.8	0.0757	0.7868	0.2124	0.0189	0.1743	3.7037	0.6457	0.0938	0.1118	0.0084
0.275	58.4	0.0756	0.8040	0.2211	0.0200	0.1804	3.6364	0.6560	0.0970	0.1174	0.0090
0.28	58.0	0.0755	0.8213	0.2300	0.0211	0.1865	3.5714	0.6662	0.1004	0.1232	0.0096
0.285	57.6	0.0754	0.8387	0.2390	0.0223	0.1928	3.5088	0.6763	0.1037	0.1291	0.0102
0.29	57.2	0.0753	0.8562	0.2483	0.0236	0.1991	3.4483	0.6864	0.1072	0.1352	0.0109
0.295	56.8	0.0752	0.8739	0.2578	0.0249	0.2054	3.3898	0.6964	0.1107	0.1414	0.0116
0.3	56.4	0.0752	0.8917	0.2675	0.0262	0.2119	3.3333	0.7064	0.1142	0.1478	0.0124
0.305	56.0	0.0751	0.9096	0.2774	0.0276	0.2185	3.2787	0.7163	0.1178	0.1543	0.0131
0.31	55.6	0.0750	0.9277	0.2876	0.0290	0.2251	3.2258	0.7261	0.1214	0.1610	0.0139
0.315	55.2	0.0749	0.9458	0.2979	0.0305	0.2318	3.1746	0.7359	0.1251	0.1678	0.0148
0.32	54.8	0.0748	0.9642	0.3085	0.0321	0.2386	3.1250	0.7456	0.1288	0.1748	0.0156
0.325	54.4	0.0747	0.9826	0.3193	0.0337	0.2454	3.0769	0.7552	0.1326	0.1819	0.0166
0.33	54.0	0.0746	1.0012	0.3304	0.0353	0.2524	3.0303	0.7648	0.1364	0.1892	0.0175
0.335	53.6	0.0745	1.0199	0.3417	0.0370	0.2594	2.9851	0.7743	0.1403	0.1967	0.0185
0.34	53.2	0.0744	1.0388	0.3532	0.0388	0.2665	2.9412	0.7837	0.1442	0.2043	0.0195
0.345	52.8	0.0744	1.0578	0.3649	0.0406	0.2736	2.8986	0.7931	0.1482	0.2120	0.0206
0.35	52.4	0.0743	1.0770	0.3769	0.0425	0.2809	2.8571	0.8024	0.1522	0.2199	0.0217
0.355	52.0	0.0742	1.0963	0.3892	0.0444	0.2881	2.8169	0.8117	0.1562	0.2279	0.0228
0.36	51.6	0.0741	1.1157	0.4017	0.0464	0.2955	2.7778	0.8208	0.1603	0.2360	0.0240
0.365	51.2	0.0740	1.1353	0.4144	0.0485	0.3029	2.7397	0.8299	0.1645	0.2443	0.0252

z	y^+	u	$f(z)$	$zf(z)$	$\int zf(z)$	$-\phi(z)$	$1/z$	$-\psi(z)$	$-\int\psi(z)$	$\chi(z)$	$\int\chi(z)$
0.37	50.8	0.0739	1.1551	0.4274	0.0507	0.3104	2.7027	0.8390	0.1687	0.2528	0.0265
0.375	50.4	0.0738	1.1750	0.4406	0.0529	0.3180	2.6667	0.8479	0.1729	0.2613	0.0278
0.38	50.0	0.0737	1.1951	0.4541	0.0551	0.3256	2.6316	0.8568	0.1772	0.2700	0.0291
0.385	49.6	0.0736	1.2153	0.4679	0.0575	0.3333	2.5974	0.8657	0.1815	0.2788	0.0305
0.39	49.2	0.0735	1.2357	0.4819	0.0599	0.3410	2.5641	0.8744	0.1859	0.2878	0.0320
0.395	48.8	0.0734	1.2563	0.4962	0.0624	0.3488	2.5316	0.8831	0.1903	0.2968	0.0334
0.4	48.4	0.0733	1.2771	0.5108	0.0649	0.3567	2.5000	0.8917	0.1948	0.3060	0.0350
0.405	48.0	0.0732	1.2980	0.5257	0.0675	0.3646	2.4691	0.9002	0.1993	0.3153	0.0366
0.41	47.6	0.0731	1.3191	0.5408	0.0702	0.3725	2.4390	0.9087	0.2038	0.3247	0.0382
0.415	47.1	0.0730	1.3404	0.5562	0.0730	0.3806	2.4096	0.9170	0.2084	0.3342	0.0399
0.42	46.7	0.0729	1.3618	0.5720	0.0759	0.3886	2.3810	0.9253	0.2130	0.3439	0.0416
0.425	46.3	0.0728	1.3835	0.5880	0.0788	0.3968	2.3529	0.9335	0.2177	0.3536	0.0433
0.43	45.9	0.0727	1.4053	0.6043	0.0819	0.4049	2.3256	0.9417	0.2224	0.3634	0.0452
0.435	45.5	0.0726	1.4273	0.6209	0.0850	0.4131	2.2989	0.9497	0.2272	0.3733	0.0470
0.44	45.1	0.0725	1.4495	0.6378	0.0881	0.4214	2.2727	0.9577	0.2320	0.3833	0.0489
0.445	44.7	0.0724	1.4720	0.6550	0.0914	0.4297	2.2472	0.9656	0.2368	0.3933	0.0509
0.45	44.3	0.0722	1.4946	0.6726	0.0948	0.4381	2.2222	0.9735	0.2417	0.4035	0.0529
0.455	43.9	0.0721	1.5174	0.6904	0.0982	0.4464	2.1978	0.9812	0.2466	0.4137	0.0550
0.46	43.5	0.0720	1.5405	0.7086	0.1018	0.4549	2.1739	0.9889	0.2515	0.4239	0.0571
0.465	43.1	0.0719	1.5637	0.7271	0.1054	0.4633	2.1505	0.9964	0.2565	0.4343	0.0593
0.47	42.7	0.0718	1.5872	0.7460	0.1091	0.4718	2.1277	1.0039	0.2615	0.4446	0.0615
0.475	42.3	0.0717	1.6109	0.7652	0.1130	0.4804	2.1053	1.0113	0.2666	0.4550	0.0638
0.48	41.9	0.0716	1.6348	0.7847	0.1169	0.4889	2.0833	1.0186	0.2717	0.4655	0.0661
0.485	41.5	0.0715	1.6590	0.8046	0.1209	0.4975	2.0619	1.0259	0.2768	0.4760	0.0685
0.49	41.1	0.0713	1.6834	0.8248	0.1250	0.5062	2.0408	1.0330	0.2819	0.4865	0.0709
0.495	40.7	0.0712	1.7080	0.8455	0.1293	0.5148	2.0202	1.0400	0.2871	0.4970	0.0734
0.5	40.3	0.0711	1.7329	0.8664	0.1336	0.5235	2.0000	1.0470	0.2924	0.5076	0.0759
0.505	39.9	0.0710	1.7580	0.8878	0.1380	0.5322	1.9802	1.0539	0.2977	0.5181	0.0785
0.51	39.5	0.0709	1.7834	0.9095	0.1426	0.5409	1.9608	1.0606	0.3030	0.5286	0.0812
0.515	39.1	0.0707	1.8090	0.9316	0.1472	0.5497	1.9417	1.0673	0.3083	0.5391	0.0839
0.52	38.7	0.0706	1.8349	0.9542	0.1520	0.5584	1.9231	1.0739	0.3137	0.5496	0.0866
0.525	38.3	0.0705	1.8611	0.9771	0.1569	0.5672	1.9048	1.0804	0.3191	0.5601	0.0894
0.53	37.9	0.0703	1.8876	1.0004	0.1619	0.5760	1.8868	1.0868	0.3245	0.5705	0.0923
0.535	37.5	0.0702	1.9143	1.0241	0.1670	0.5848	1.8692	1.0931	0.3300	0.5809	0.0952
0.54	37.1	0.0701	1.9413	1.0483	0.1723	0.5936	1.8519	1.0993	0.3355	0.5912	0.0981
0.545	36.7	0.0700	1.9686	1.0729	0.1776	0.6024	1.8349	1.1054	0.3410	0.6014	0.1011
0.55	36.3	0.0698	1.9963	1.0979	0.1831	0.6113	1.8182	1.1114	0.3465	0.6115	0.1042

z	y^+	u	$f(z)$	$zf(z)$	$\int zf(z)$	$-\phi(z)$	$1/z$	$-\psi(z)$	$-\int\psi(z)$	$\chi(z)$	$\int\chi(z)$
0.555	35.9	0.0697	2.0242	1.1234	0.1887	0.6201	1.8018	1.1173	0.3521	0.6216	0.1073
0.56	35.5	0.0696	2.0525	1.1494	0.1945	0.6289	1.7857	1.1231	0.3577	0.6315	0.1105
0.565	35.1	0.0694	2.0810	1.1758	0.2004	0.6377	1.7699	1.1287	0.3634	0.6414	0.1137
0.57	34.7	0.0693	2.1099	1.2027	0.2064	0.6466	1.7544	1.1343	0.3691	0.6510	0.1169
0.575	34.3	0.0691	2.1392	1.2300	0.2125	0.6554	1.7391	1.1398	0.3748	0.6606	0.1202
0.58	33.8	0.0690	2.1688	1.2579	0.2188	0.6642	1.7241	1.1451	0.3805	0.6700	0.1236
0.585	33.4	0.0688	2.1987	1.2862	0.2252	0.6730	1.7094	1.1504	0.3862	0.6792	0.1270
0.59	33.0	0.0687	2.2290	1.3151	0.2318	0.6817	1.6949	1.1555	0.3920	0.6883	0.1304
0.595	32.6	0.0686	2.2597	1.3445	0.2385	0.6905	1.6807	1.1605	0.3978	0.6971	0.1339
0.6	32.2	0.0684	2.2907	1.3744	0.2454	0.6992	1.6667	1.1654	0.4036	0.7057	0.1374
0.605	31.8	0.0683	2.3222	1.4049	0.2524	0.7080	1.6529	1.1702	0.4095	0.7142	0.1410
0.61	31.4	0.0681	2.3540	1.4360	0.2596	0.7167	1.6393	1.1749	0.4154	0.7223	0.1446
0.615	31.0	0.0679	2.3863	1.4676	0.2670	0.7253	1.6260	1.1794	0.4213	0.7302	0.1483
0.62	30.6	0.0678	2.4190	1.4998	0.2745	0.7340	1.6129	1.1838	0.4272	0.7378	0.1520
0.625	30.2	0.0676	2.4521	1.5325	0.2821	0.7426	1.6000	1.1881	0.4331	0.7452	0.1557
0.63	29.8	0.0672	2.5477	1.6050	0.2901	0.7509	1.5873	1.1920	0.4391	0.7350	0.1594
0.635	29.4	0.0668	2.6157	1.6610	0.2984	0.7592	1.5748	1.1955	0.4451	0.7317	0.1630
0.64	29.0	0.0665	2.6847	1.7182	0.3070	0.7672	1.5625	1.1988	0.4511	0.7275	0.1666
0.645	28.6	0.0662	2.7546	1.7767	0.3159	0.7751	1.5504	1.2017	0.4571	0.7223	0.1703
0.65	28.2	0.0658	2.8255	1.8366	0.3251	0.7829	1.5385	1.2044	0.4631	0.7162	0.1738
0.655	27.8	0.0655	2.8975	1.8978	0.3346	0.7904	1.5267	1.2067	0.4691	0.7090	0.1774
0.66	27.4	0.0651	2.9704	1.9605	0.3444	0.7978	1.5152	1.2088	0.4752	0.7007	0.1809
0.665	27.0	0.0648	3.0445	2.0246	0.3545	0.8050	1.5038	1.2105	0.4812	0.6913	0.1843
0.67	26.6	0.0644	3.1197	2.0902	0.3650	0.8120	1.4925	1.2119	0.4873	0.6807	0.1877
0.675	26.2	0.0640	3.1961	2.1573	0.3758	0.8187	1.4815	1.2129	0.4933	0.6689	0.1911
0.68	25.8	0.0637	3.2736	2.2260	0.3869	0.8253	1.4706	1.2137	0.4994	0.6558	0.1944
0.685	25.4	0.0633	3.3523	2.2963	0.3984	0.8316	1.4599	1.2141	0.5055	0.6414	0.1976
0.69	25.0	0.0629	3.4323	2.3683	0.4102	0.8378	1.4493	1.2141	0.5116	0.6256	0.2007
0.695	24.6	0.0625	3.5136	2.4420	0.4224	0.8436	1.4388	1.2139	0.5176	0.6084	0.2038
0.7	24.2	0.0621	3.5963	2.5174	0.4350	0.8493	1.4286	1.2132	0.5237	0.5896	0.2067
0.705	23.8	0.0617	3.6803	2.5946	0.4480	0.8546	1.4184	1.2123	0.5298	0.5693	0.2095
0.71	23.4	0.0613	3.7658	2.6737	0.4614	0.8597	1.4085	1.2109	0.5358	0.5474	0.2123
0.715	23.0	0.0609	3.8527	2.7547	0.4751	0.8646	1.3986	1.2092	0.5419	0.5238	0.2149
0.72	22.6	0.0604	3.9412	2.8377	0.4893	0.8691	1.3889	1.2071	0.5479	0.4984	0.2174
0.725	22.2	0.0600	4.0313	2.9227	0.5039	0.8734	1.3793	1.2047	0.5539	0.4712	0.2198
0.73	21.8	0.0596	4.1231	3.0098	0.5190	0.8773	1.3699	1.2018	0.5599	0.4421	0.2220
0.735	21.4	0.0591	4.2165	3.0991	0.5345	0.8810	1.3605	1.1986	0.5659	0.4111	0.2240

z	y^+	u	$f(z)$	$zf(z)$	$\int zf(z)$	$-\phi(z)$	$1/z$	$-\psi(z)$	$-\int\psi(z)$	$\chi(z)$	$\int\chi(z)$
0.74	21.0	0.0587	4.3118	3.1907	0.5504	0.8843	1.3514	1.1950	0.5719	0.3779	0.2259
0.745	20.6	0.0582	4.4089	3.2846	0.5668	0.8872	1.3423	1.1909	0.5778	0.3426	0.2276
0.75	20.1	0.0577	4.5079	3.3809	0.5838	0.8898	1.3333	1.1865	0.5838	0.3051	0.2291
0.755	19.7	0.0572	4.6089	3.4797	0.6012	0.8921	1.3245	1.1816	0.5897	0.2653	0.2305
0.76	19.3	0.0567	4.7120	3.5811	0.6191	0.8940	1.3158	1.1763	0.5956	0.2230	0.2316
0.765	18.9	0.0562	4.8173	3.6852	0.6375	0.8955	1.3072	1.1705	0.6014	0.1783	0.2325
0.77	18.5	0.0557	4.9248	3.7921	0.6564	0.8965	1.2987	1.1643	0.6072	0.1309	0.2331
0.775	18.1	0.0552	5.0347	3.9019	0.6760	0.8972	1.2903	1.1577	0.6130	0.0808	0.2335
0.78	17.7	0.0546	5.1470	4.0147	0.6960	0.8974	1.2821	1.1505	0.6188	0.0279	0.2337
0.785	17.3	0.0541	5.2620	4.1307	0.7167	0.8972	1.2739	1.1429	0.6245	-0.0280	0.2335
0.79	16.9	0.0535	5.3796	4.2499	0.7379	0.8965	1.2658	1.1348	0.6302	-0.0871	0.2331
0.795	16.5	0.0529	5.5001	4.3726	0.7598	0.8953	1.2579	1.1262	0.6358	-0.1493	0.2324
0.8	16.1	0.0523	5.6236	4.4989	0.7823	0.8937	1.2500	1.1171	0.6414	-0.2149	0.2313
0.802	16.0	0.0521	5.6738	4.5504	0.7914	0.8929	1.2469	1.1133	0.6436	-0.2421	0.2308
0.804	15.8	0.0518	5.7246	4.6026	0.8006	0.8921	1.2438	1.1095	0.6458	-0.2699	0.2303
0.806	15.6	0.0516	5.7759	4.6554	0.8099	0.8911	1.2407	1.1056	0.6480	-0.2983	0.2297
0.808	15.5	0.0513	5.8277	4.7088	0.8193	0.8901	1.2376	1.1017	0.6502	-0.3273	0.2290
0.81	15.3	0.0511	5.8801	4.7628	0.8288	0.8890	1.2346	1.0976	0.6524	-0.3569	0.2283
0.812	15.2	0.0508	5.9330	4.8176	0.8385	0.8879	1.2315	1.0934	0.6546	-0.3871	0.2275
0.814	15.0	0.0506	5.9864	4.8730	0.8482	0.8866	1.2285	1.0892	0.6568	-0.4179	0.2267
0.816	14.8	0.0503	6.0405	4.9290	0.8581	0.8852	1.2255	1.0848	0.6590	-0.4494	0.2258
0.818	14.7	0.0501	6.0951	4.9858	0.8681	0.8838	1.2225	1.0804	0.6611	-0.4815	0.2248
0.82	14.5	0.0498	6.1504	5.0433	0.8781	0.8822	1.2195	1.0759	0.6633	-0.5143	0.2238
0.822	14.3	0.0495	6.2063	5.1015	0.8883	0.8806	1.2165	1.0713	0.6654	-0.5478	0.2227
0.824	14.2	0.0492	6.2628	5.1605	0.8987	0.8788	1.2136	1.0665	0.6676	-0.5820	0.2215
0.826	14.0	0.0490	6.3199	5.2202	0.9091	0.8770	1.2107	1.0617	0.6697	-0.6168	0.2203
0.828	13.9	0.0487	6.3777	5.2807	0.9197	0.8750	1.2077	1.0568	0.6718	-0.6524	0.2190
0.83	13.7	0.0484	6.4362	5.3420	0.9304	0.8730	1.2048	1.0518	0.6739	-0.6888	0.2176
0.832	13.5	0.0481	6.4954	5.4041	0.9412	0.8708	1.2019	1.0467	0.6760	-0.7259	0.2162
0.834	13.4	0.0478	6.5552	5.4671	0.9521	0.8686	1.1990	1.0415	0.6781	-0.7637	0.2146
0.836	13.2	0.0475	6.6158	5.5308	0.9632	0.8662	1.1962	1.0362	0.6802	-0.8023	0.2130
0.838	13.1	0.0472	6.6772	5.5955	0.9743	0.8638	1.1933	1.0307	0.6822	-0.8418	0.2113
0.84	12.9	0.0469	6.7393	5.6610	0.9857	0.8612	1.1905	1.0252	0.6843	-0.8820	0.2096
0.842	12.7	0.0466	6.8022	5.7275	0.9971	0.8585	1.1876	1.0196	0.6863	-0.9231	0.2077
0.844	12.6	0.0463	6.8659	5.7948	1.0087	0.8557	1.1848	1.0139	0.6883	-0.9650	0.2058
0.846	12.4	0.0460	6.9304	5.8631	1.0204	0.8528	1.1820	1.0080	0.6903	-1.0078	0.2038
0.848	12.3	0.0457	6.9958	5.9324	1.0323	0.8497	1.1792	1.0021	0.6923	-1.0515	0.2017

z	y^+	u	$f(z)$	$zf(z)$	$\int zf(z)$	$-\phi(z)$	$1/z$	$-\psi(z)$	$-\int\psi(z)$	$\chi(z)$	$\int\chi(z)$
0.85	12.1	0.0454	7.0620	6.0027	1.0443	0.8466	1.1765	0.9960	0.6943	-1.0961	0.1995
0.852	11.9	0.0451	7.1291	6.0740	1.0565	0.8433	1.1737	0.9898	0.6963	-1.1416	0.1972
0.854	11.8	0.0447	7.1971	6.1464	1.0688	0.8399	1.1710	0.9835	0.6983	-1.1881	0.1948
0.856	11.6	0.0444	7.2661	6.2198	1.0812	0.8364	1.1682	0.9771	0.7002	-1.2356	0.1924
0.858	11.4	0.0441	7.3360	6.2943	1.0938	0.8327	1.1655	0.9705	0.7022	-1.2840	0.1898
0.86	11.3	0.0437	7.4070	6.3700	1.1065	0.8289	1.1628	0.9639	0.7041	-1.3335	0.1871
0.862	11.1	0.0434	7.4789	6.4468	1.1194	0.8250	1.1601	0.9571	0.7060	-1.3840	0.1844
0.864	11.0	0.0430	7.5519	6.5248	1.1325	0.8209	1.1574	0.9502	0.7079	-1.4356	0.1815
0.866	10.8	0.0427	7.6260	6.6041	1.1457	0.8168	1.1547	0.9431	0.7098	-1.4883	0.1785
0.868	10.6	0.0423	7.7012	6.6846	1.1590	0.8124	1.1521	0.9360	0.7117	-1.5421	0.1754
0.87	10.5	0.0419	7.7775	6.7664	1.1726	0.8079	1.1494	0.9287	0.7135	-1.5971	0.1722
0.872	10.3	0.0416	7.8550	6.8496	1.1863	0.8033	1.1468	0.9212	0.7154	-1.6533	0.1689
0.874	10.2	0.0412	7.9338	6.9341	1.2001	0.7986	1.1442	0.9137	0.7172	-1.7107	0.1655
0.876	10.0	0.0408	8.0138	7.0201	1.2142	0.7936	1.1416	0.9060	0.7190	-1.7693	0.1620
0.878	9.8	0.0404	8.0951	7.1075	1.2284	0.7886	1.1390	0.8981	0.7208	-1.8292	0.1583
0.88	9.7	0.0400	8.1777	7.1964	1.2428	0.7833	1.1364	0.8901	0.7226	-1.8905	0.1545
0.882	9.5	0.0396	8.2618	7.2869	1.2574	0.7779	1.1338	0.8820	0.7244	-1.9531	0.1506
0.884	9.3	0.0392	8.3472	7.3789	1.2721	0.7724	1.1312	0.8737	0.7261	-2.0171	0.1466
0.886	9.2	0.0388	8.4342	7.4727	1.2871	0.7667	1.1287	0.8653	0.7278	-2.0825	0.1424
0.888	9.0	0.0383	8.5227	7.5681	1.3022	0.7608	1.1261	0.8567	0.7296	-2.1495	0.1381
0.89	8.9	0.0379	8.6128	7.6654	1.3175	0.7547	1.1236	0.8480	0.7313	-2.2180	0.1337
0.892	8.7	0.0375	8.7045	7.7644	1.3331	0.7485	1.1211	0.8391	0.7329	-2.2880	0.1291
0.894	8.5	0.0370	8.7980	7.8654	1.3488	0.7420	1.1186	0.8300	0.7346	-2.3597	0.1244
0.896	8.4	0.0366	8.8932	7.9683	1.3647	0.7354	1.1161	0.8208	0.7362	-2.4331	0.1195
0.898	8.2	0.0361	8.9903	8.0733	1.3809	0.7286	1.1136	0.8114	0.7379	-2.5083	0.1145
0.9	8.1	0.0356	9.0893	8.1804	1.3972	0.7216	1.1111	0.8018	0.7395	-2.5852	0.1093
0.902	7.9	0.0351	9.1903	8.2897	1.4138	0.7144	1.1086	0.7921	0.7410	-2.6640	0.1040
0.904	7.7	0.0346	9.2934	8.4013	1.4306	0.7070	1.1062	0.7821	0.7426	-2.7448	0.0985
0.906	7.6	0.0341	9.3987	8.5152	1.4476	0.6994	1.1038	0.7720	0.7441	-2.8275	0.0929
0.908	7.4	0.0336	9.5062	8.6317	1.4649	0.6916	1.1013	0.7617	0.7457	-2.9124	0.0870
0.91	7.3	0.0331	9.6161	8.7507	1.4824	0.6836	1.0989	0.7512	0.7472	-2.9994	0.0810
0.912	7.1	0.0325	9.7285	8.8724	1.5002	0.6754	1.0965	0.7405	0.7487	-3.0887	0.0749
0.914	6.9	0.0320	9.8434	8.9969	1.5182	0.6669	1.0941	0.7296	0.7501	-3.1803	0.0685
0.916	6.8	0.0314	9.9611	9.1244	1.5364	0.6582	1.0917	0.7185	0.7516	-3.2744	0.0620
0.918	6.6	0.0308	10.0816	9.2549	1.5549	0.6492	1.0893	0.7072	0.7530	-3.3710	0.0552
0.92	6.4	0.0302	10.2050	9.3886	1.5737	0.6400	1.0870	0.6957	0.7544	-3.4702	0.0483
0.922	6.3	0.0296	10.3316	9.5258	1.5927	0.6306	1.0846	0.6839	0.7557	-3.5723	0.0411

z	y^+	u	$f(z)$	$zf(z)$	$\int zf(z)$	$-\phi(z)$	$1/z$	$-\psi(z)$	$-\int\psi(z)$	$\chi(z)$	$\int\chi(z)$
0.924	6.1	0.0290	10.4615	9.6664	1.6121	0.6208	1.0823	0.6719	0.7571	-3.6773	0.0338
0.926	6.0	0.0284	10.5949	9.8108	1.6317	0.6109	1.0799	0.6597	0.7584	-3.7853	0.0262
0.928	5.8	0.0277	10.7318	9.9592	1.6516	0.6006	1.0776	0.6472	0.7597	-3.8965	0.0184
0.93	5.6	0.0270	10.8727	10.1116	1.6718	0.5901	1.0753	0.6345	0.7610	-4.0111	0.0104
0.932	5.5	0.0263	11.0176	10.2684	1.6924	0.5792	1.0730	0.6215	0.7622	-4.1293	0.0021
0.934	5.3	0.0256	11.1669	10.4299	1.7132	0.5681	1.0707	0.6082	0.7634	-4.2512	-0.0064
0.936	5.2	0.0249	11.3208	10.5962	1.7344	0.5566	1.0684	0.5947	0.7646	-4.3770	-0.0151
0.938	5.0	0.0241	11.4767	10.7651	1.7560	0.5449	1.0661	0.5809	0.7658	-4.5050	-0.0241
0.94	4.8	0.0233	11.6379	10.9396	1.7778	0.5328	1.0638	0.5668	0.7669	-4.6375	-0.0334
0.942	4.7	0.0225	11.7991	11.1147	1.8001	0.5203	1.0616	0.5524	0.7680	-4.7707	-0.0430
0.944	4.5	0.0218	11.9603	11.2905	1.8226	0.5076	1.0593	0.5377	0.7691	-4.9045	-0.0528
0.946	4.4	0.0210	12.1215	11.4669	1.8456	0.4945	1.0571	0.5227	0.7701	-5.0391	-0.0628
0.948	4.2	0.0202	12.2826	11.6439	1.8689	0.4811	1.0549	0.5075	0.7711	-5.1742	-0.0732
0.95	4.0	0.0194	12.4438	11.8216	1.8925	0.4673	1.0526	0.4919	0.7721	-5.3100	-0.0838
0.952	3.9	0.0187	12.6050	12.0000	1.9165	0.4532	1.0504	0.4761	0.7731	-5.4463	-0.0947
0.954	3.7	0.0179	12.7662	12.1790	1.9409	0.4388	1.0482	0.4600	0.7740	-5.5833	-0.1059
0.956	3.5	0.0171	12.9274	12.3586	1.9656	0.4240	1.0460	0.4436	0.7749	-5.7208	-0.1173
0.958	3.4	0.0163	13.0886	12.5389	1.9907	0.4089	1.0438	0.4269	0.7757	-5.8589	-0.1290
0.96	3.2	0.0155	13.2498	12.7198	2.0161	0.3935	1.0417	0.4099	0.7766	-5.9975	-0.1410
0.962	3.1	0.0148	13.4110	12.9014	2.0419	0.3777	1.0395	0.3926	0.7773	-6.1366	-0.1533
0.964	2.9	0.0140	13.5722	13.0836	2.0681	0.3616	1.0373	0.3751	0.7781	-6.2762	-0.1658
0.966	2.7	0.0132	13.7334	13.2664	2.0946	0.3451	1.0352	0.3572	0.7788	-6.4163	-0.1787
0.968	2.6	0.0124	13.8946	13.4499	2.1215	0.3283	1.0331	0.3391	0.7795	-6.5568	-0.1918
0.97	2.4	0.0117	14.0557	13.6341	2.1488	0.3111	1.0309	0.3207	0.7801	-6.6977	-0.2052
0.972	2.3	0.0109	14.2169	13.8189	2.1764	0.2936	1.0288	0.3020	0.7807	-6.8390	-0.2189
0.974	2.1	0.0101	14.3781	14.0043	2.2044	0.2757	1.0267	0.2831	0.7813	-6.9807	-0.2328
0.976	1.9	0.0093	14.5393	14.1904	2.2328	0.2575	1.0246	0.2638	0.7818	-7.1228	-0.2471
0.978	1.8	0.0086	14.7005	14.3771	2.2616	0.2389	1.0225	0.2443	0.7823	-7.2652	-0.2616
0.98	1.6	0.0078	14.8617	14.5645	2.2907	0.2200	1.0204	0.2245	0.7828	-7.4079	-0.2764
0.982	1.5	0.0070	15.0229	14.7525	2.3202	0.2007	1.0183	0.2044	0.7832	-7.5508	-0.2915
0.984	1.3	0.0062	15.1841	14.9411	2.3501	0.1811	1.0163	0.1840	0.7835	-7.6940	-0.3069
0.986	1.1	0.0054	15.3453	15.1304	2.3803	0.1611	1.0142	0.1634	0.7839	-7.8375	-0.3226
0.988	1.0	0.0047	15.5065	15.3204	2.4110	0.1407	1.0121	0.1424	0.7841	-7.9811	-0.3385
0.99	0.8	0.0039	15.6676	15.5110	2.4420	0.1200	1.0101	0.1212	0.7844	-8.1249	-0.3548
0.991	0.7	0.0035	15.7482	15.6065	2.4576	0.1096	1.0091	0.1105	0.7845	-8.1969	-0.3630
0.992	0.6	0.0031	15.8288	15.7022	2.4733	0.0990	1.0081	0.0998	0.7846	-8.2690	-0.3713
0.993	0.6	0.0027	15.9094	15.7981	2.4891	0.0884	1.0070	0.0890	0.7847	-8.3410	-0.3796

z	y^+	u	$f(z)$	$zf(z)$	$\int zf(z)$	$-\phi(z)$	$1/z$	$-\psi(z)$	$-\int\psi(z)$	$\chi(z)$	$\int\chi(z)$
0.994	0.5	0.0023	15.9900	15.8941	2.5050	0.0777	1.0060	0.0781	0.7848	-8.4131	-0.3880
0.995	0.4	0.0019	16.0706	15.9903	2.5210	0.0669	1.0050	0.0672	0.7848	-8.4853	-0.3965
0.996	0.3	0.0016	16.1512	16.0866	2.5371	0.0559	1.0040	0.0562	0.7849	-8.5574	-0.4051
0.997	0.2	0.0012	16.2318	16.1831	2.5533	0.0450	1.0030	0.0451	0.7849	-8.6296	-0.4137
0.998	0.2	0.0008	16.3124	16.2798	2.5695	0.0339	1.0020	0.0339	0.7850	-8.7017	-0.4224
0.999	0.1	0.0004	16.3930	16.3766	2.5859	0.0227	1.0010	0.0227	0.7850	-8.7739	-0.4312
1	0.0	0.0000	16.4736	16.4736	2.6024	0.0114	1.0000	0.0114	0.7850	-8.8461	-0.4400

APPENDIX E

CORRECTIONS TO PARK AND GOMEZPLATA (1971) EXPERIMENTAL DATA

Park and Gomezplata (1971) performed experiments on setups consisting of short straight pipe sections connected by 90^o elbows. The data obtained from these experiments cannot be directly used for validation purposes as the dispersion coefficient reported would not be at steady state conditions. The data reported by Park and Gomezplata (1971) can be approximated to their steady state values using the technique outlined below. The experimental data reported for a setup with three bends at a Reynolds number of 3840 is used to illustrate the calculations.

The experimental setup consisted of an initial straight section 149" in length. Park and Gomezplata (1971) reported experimental data for this initial straight section at seven different Reynolds number. The values of axial dispersion coefficient reported are much lower than the values predicted using Equation (3.24). Assuming no major error in the experimental procedure, the data can be considered for short pipe systems. The reported data along with the steady state axial dispersion data (Equation 3.24) can be substituted in Equation (3.29) to calculate the time required to attain steady state (T). Park and Gomezplata (1971) reported a dimensionless axial dispersion coefficient value of 2.45 for the initial straight section at a Re = 3840. Substituting this in Equation (3.29) along with the dimensionless steady state value of 8.47 gives T = 65.65 sec. Table E.1 lists the values of T for the different Reynolds numbers reported.

Table E.1: Steady state time (T) estimations for Park and Gomezplata (1971) experimental data on a 0.824" diameter, 149" long tube.

Reynolds Number	Velocity (ft./sec)	$K/\bar{U}\,d$ Equation (3.24)	$K/\bar{U}\,d$ Reported	T (sec)
3840	0.17	8.7	2.45	65.65
5120	0.23	6	1.6	52.51
6400	0.29	4.3	1.2	39.82
7680	0.35	3.3	1.02	29.36
8960	0.41	2.9	0.85	26.83
10240	0.47	2.3	0.8	19.05
11520	0.53	2.02	0.785	14.71

The value of T thus obtained is independent of the pipe length. It can therefore be employed to estimate the straight pipe axial dispersion coefficients for other pipe lengths. The total length of the system with three bends is 250.5". Substituting this value in Equation (3.29) along with the value of T listed above gives a value of 3.67 for the dimensionless dispersion coefficient in the straight section of the setup. The reported value of the dimensionless dispersion coefficient minus the estimated straight pipe dispersion coefficient comes to 0.29. This number represents the enhanced dispersion on account of the three bends. Assuming the contribution of the bends to be independent of the straight section lengths, the effective dispersion at steady state can be estimated by adding 0.29 to the dimensionless steady state dispersion value of 8.7. The effective dimensionless dispersion coefficient for the experiment at steady state is therefore estimated to be 8.99.

VITA

Patrachari, Anirudh Ramanujan

Candidate for the Degree of

Doctor of Philosophy

Thesis: DETERMINISTIC MODELS TO EXPLAIN THE PHENOMENON OF INTERFACIAL MIXING IN REFINED PRODUCTS PIPELINES

Major Field: Chemical Engineering

Biographical:

Education:

Completed the requirements for the Doctor of Philosophy in Chemical Engineering at Oklahoma State University, Stillwater, OK in December 2012.

Master of Science in Chemical Engineering, Oklahoma State University, Stillwater, OK, December 2008.

Bachelor of Engineering in Chemical Engineering, University of Mumbai, Mumbai, India, May 2006.

Experience:

Graduate Assistant, School of Chemical Engineering, Oklahoma State University; January 2010 to July 2012.

Teaching Assistant, School of Chemical Engineering, Oklahoma State University; August 2007 to May 2012.

Professional Memberships:

American Institute of Chemical Engineers

International Society of Automation

Honor Society of Omega Chi Epsilon

Honor Society of Phi Kappa Phi

Chemical Engineering Graduate Student Association

Name: Patrachari, Anirudh Ramanujan Date of Degree: December, 2012

Institution: Oklahoma State University Location: Stillwater, Oklahoma

Title of Study: DETERMINISTIC MODELS TO EXPLAIN THE PHENOMENON OF INTERFACIAL MIXING IN REFINED PRODUCTS PIPELINES

Pages in Study: 161 Candidate for the Degree of Doctor of Philosophy

Major Field: Chemical Engineering

Scope and Method of Study:

Understanding the processes governing axial dispersion of contaminants in a flowing system is one of the unsolved classical problems in fluid mechanics. Taylor (1953; 1954) provided a robust methodology to model such systems in their ideal laminar and turbulent flow conditions. The current study reveals that both viscous and turbulent aspects need to be considered simultaneously in order to accurately model axial dispersion in real systems. Theoretical and phenomenological analyses are carried out to show that the viscous sublayer, long believed to be a major influence on axial dispersion, has a significant role in the axial dispersion phenomenon. The axial dispersion model proposed in the current study has been validated using laboratory, pilot, and field experimental data. The higher mixing rates at lower Reynolds number turbulent flows have been explained by the effects of the viscous sublayer. A straight forward technique to incorporate the influence of bends has also been included in this work.

Findings and Conclusions:

A robust phenomenological model has been developed for estimating the axial dispersion coefficient for flow of liquids through straight pipes. The proposed model employs the viscous sublayer thickness as a parameter to combine the convective-diffusion equation with the boundary layer theory. The mathematical formulations developed using Reynolds analogy, in concurrence with the characteristic turbulent bursting events observed in the near-wall regions of the flow, have been shown to be applicable even for non-ideal low Reynolds numbers conditions. This hints at the possibility of a universal theory governing all mass, momentum, and heat transport processes. Furthermore, theoretical and empirical concepts used in pressure drop estimations for flow through straight and bent pipes have been demonstrated to be applicable to axial dispersion estimations. The analyses presented in this work provide a physical backing to Taylor's theory, while providing new conceptual visualizations of the processes governing axial dispersion. The proposed concepts could be used in identifying novel techniques to help reduce interfacial contamination in petroleum pipelines and other similarly affected processes. This work is also expected to lead to improved models and theories that broaden our understanding of the axial dispersion process.

ADVISER'S APPROVAL: Dr. Arland H. Johannes